Wire Explosion in Vacuum

Vladimir I. Oreshkin and Rina B. Baksht, *Member, IEEE*

***Abstract*— This article presents a review of experimental and theoretical studies devoted to the processes that occur during explosions of wires in vacuum when the current densities in the wire are of the order of 10^8 A/cm^2 and the current density rise rates are no less than 10^{15} A/(cm^2 · s). The theoretical background is focused on the transformation of the wire metal into ionized plasma. In particular, the basic physical notions used to describe wire explosions (WEs; state diagram, current action integral, and metal conductivity changes in phase transitions) are given; magnetohydrodynamic equations are described which are used to simulate WEs, and the simulation predictions are discussed together with their reliability. Extensive experimental data on WEs in vacuum are presented which made it possible to describe the corona and core formation and the development of electrothermal instabilities in the core. The data on the energy deposited in a wire exploding in vacuum reported by different authors are compared. In conclusion, problems are discussed that require additional experimental investigations, namely, the role of metastable states in a WE and the mechanism by which the core is shunted.**

***Index Terms*— Electrothermal instabilities (ETIs), exploding wires, magnetohydrodynamic (MHD) equations, transport coefficients.**

Nomenclature

$\mathbf{B}$	Magnetic induction.
$\mathbf{E}$	Electric field.
$\mathbf{j}$	Current density.
$\mathbf{W}$	Energy flux.
$\mathbf{v}$	Material velocity.
μ_0	Permeability of vacuum.
k	Boltzmann's constant.
$\hbar$	Plank's constant.
e	Electron charge.
ρ	Material density.
p	Material pressure.
ε	Material internal energy.
T	Material temperature.
$\bar{h}$	Specific current action integral.
k	Wave vector.
σ	Conductivity.
δ	Resistivity.
κ	Thermal conductivity.
S	Material entropy.
μ	Chemical potential.
F	Material free energy.
H_{atom}	Atomization enthalpy.
ε_{vap}	Vaporization energy.
$\varepsilon_{\text{atom}}$	Atomization energy.
ε_{cr}	Critical point energy.
ε_{dep}	Deposited energy.
τ_{ex}	Explosion time.
τ_{melt}	Melting time.
t_{res}	Joule heating time.
$(dI/dt)_{\text{av}}$	Pulser current rate.

Manuscript received June 5, 2019; revised January 28, 2020; accepted March 20, 2020. Date of publication April 17, 2020; date of current version May 8, 2020. This work was supported by the Russian Science Foundation under Project 19-08-01004 and Project 17-08-00131. The review of this article was arranged by Senior Editor S. J. Gitomer. *(Corresponding author: Rina B. Baksht.)*

The authors are with the Institute of High Current Electronics SB RAS, 634055 Tomsk, Russia (e-mail: oreshkin@ovpe.hcei.tsc.ru; bakshtrina@gmail.com).

Color versions of one or more of the figures in this article are available online at http://ieeexplore.ieee.org.

Digital Object Identifier 10.1109/TPS.2020.2985100

I. Introduction

THE wire explosion (WE) phenomenon has attracted the interest of researchers for many years [1]–[4]. On the one hand, the WE is intriguing as an object of basic research; on the other hand, exploding wires are widely used in various technical applications. The WE was first described as a phenomenon at a meeting of the Royal Society of London in 1773 [5]. Since then, researchers repeatedly returned to this phenomenon; however, its technological application was found only in the 40s–50s of the twentieth century, when exploding wires began to be used in rocket technology as detonators for igniting propellants in rocket motors [5].

The attractiveness of the WE as an object of basic research is due to the fact that the thermodynamic parameters of the material of an exploding wire reach extreme values. WE is a dramatic change in the physical state of the wire metal as a result of an intense energy release caused by a high-density pulsed current passed through the metal. The state of the metal goes through all phases from condensed matter to plasma. From the point of view of fundamental research, the WE is of interest as an object convenient for studying the thermophysical and transport properties of dense nonideal plasmas [6]–[10], in particular, the conductivity of metals in the vicinity of the critical point, that is, the point of the phase diagram at which the liquid, the gas, and the two-phase region touch one another.

There is a huge variety of electrical explosion regimes, which are different in a large number of parameters. For instance, according to the nature of the current flow, the skinned current mode [11]–[14] is different from the regime of uniform current flow through the conductor cross section [15]–[19]. The electrically exploding conductors also vary in geometry: these can be microwires [15], [16], crossed wires (X-pinch assemblies) [20]–[24], plane conductors (foils) [25]–[29], wire arrays, both cylindrical [30], [31] and

planar [32], [33], solenoids [34], etc. According to the environment in which an explosion occurs, it is customary to distinguish the WEs in vacuum [11]–[15] and in a dielectric medium (in a gas [35], [36] or in a liquid [37], [38]), and the explosion of dielectric-coated wires [39]. And this is not a complete list of the parameters by which various WE regimes can be classified.

Different explosion regimes dictate different technological applications of WEs. For instance, the explosion of wires in a medium is used to increase electric power in pulse power technology [2], [40] and to produce nanopowders [35], [36], [41]–[44], and the WE underlies the operation of X-ray sources used in microelectronics [45]. The interest in the skinned-current WE is also related to various applications [11]–[14], [46]–[48]. Some of them are noteworthy. First, this is the creation of strong magnetic fields by using imploding metal shells [49]–[52] and exploding single-turn solenoids [34], [53]. Second, this is the use of heavy metal liners imploding in Z-pinch geometries to achieve extreme states of matter with pressures of 1–100 Mbars [50], [54], [55]. Third, this is the electromagnetic acceleration of bodies [56], in particular, the acceleration of metal plates in experiments on studying shock waves [57]–[60]. Finally, this is electromagnetic energy transport through vacuum transmission lines in currently being developed multiterawatt generators capable of producing currents of 30–50 MA [61]–[65], which are supposed to be used in Z-pinch-based controlled fusion schemes. Increased attention to the WE phenomenon is associated with the research on the controlled thermonuclear fusion in the Z-pinch geometry, both in experiments on imploding wire arrays [66]–[70] and in the framework of the MAGO/magnetized target fusion (MTF, [71], [72]) and Magnetized Liner Inertial Fusion (MagLIF, [55], [73]) concepts in which the compression of an initially heated deuterium-tritium mixture by a metal shell is used.

In this introduction, we describe some general characteristics and physical notions that refer not only to the WE in vacuum but also to a WE in any environment.

A. Specific Current Action Integral

The most important characteristic of a WE is the explosion time. The explosion time τ_{ex} is usually defined as the time at which the electrical resistance of an exploding wire reaches a maximum [2]. The typical current and voltage waveforms measured during a WE show an initial increase in current with the voltage smoothly increasing due to the wire heating and melting and a subsequent sharp increase in voltage accompanied by a decrease in current. The time at which the wire resistance is a maximum corresponds quite well to the time the voltage across the wire reaches a maximum [2], [74], which we consider the explosion time.

The explosion time τ_{ex} can be defined in terms of a quantity called the specific current action integral [40], [74], [75], which is a characteristic of a particular metal. The expression for the specific current action integral $\bar{h}$ derived from the energy conservation law is

$$\bar{h} = \int_0^{\tau_{ex}} j^2 dt = \int_C \frac{\rho d\varepsilon}{\delta} \tag{I-1}$$

where j is the current density, ρ is the material density, ε is the internal energy, and δ is the resistivity. The right-hand integral in (I-1) is taken along the phase trajectory $\tilde{N}$ that represents how the state of the wire metal changes during the explosion.

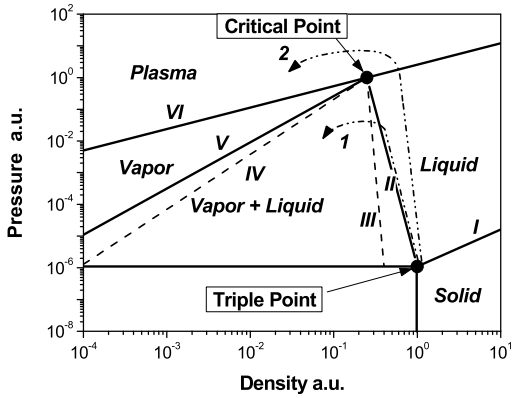

Fig. 1. Phase diagram and phase trajectories of the metal of an exploding wire: *I*—melting curve, *II*—binodal liquid branch (boiling curve), *III*—spinodal liquid branch (dashed line), *IV*—spinodal gas branch (dashed line), *V*—binodal gas branch, and *VI*—critical isotherm (isotherm at a temperature equal to the critical point temperature); dash-and-dot lines *1* and *2* represent the phase trajectories of the exploding wire metal.

Fig. 1 shows a schematic phase diagram typical of most metals with the phase trajectories of the metal of an exploding wire marked with arrows. Consider briefly what happens when a metal is heated at pressures $p \geq p_{triple}$ and densities $\rho \leq \rho_{triple}$. When a metal is heated under these conditions, its density decreases and it transforms into a mixture of liquid and vapor, so that a two-phase region is formed. The line in the phase diagram that separates the two-phase region and the liquid-phase region is called the binodal. For slow temperature and density changes, with characteristic times longer than the decay time of a metastable liquid, there is only a two-phase region to the left of the binodal. For fast temperature and density changes, which are typical of WEs, the material may exist in the form of a metastable liquid corresponding to the phase diagram region lying to the left of the binodal [76], [77]. In the phase diagram given earlier, the region of existence of this metastable phase is bounded by a curve called the spinodal (curve *III* in Fig. 1).

The most typical of the phase trajectories, represented by curve *I* which corresponds to the state of molten metal, passes along the binodal (curve *II*). The pressure is low to the left of the binodal, either in the two-phase region or in the metastable region. If the metal in this region is a liquid-vapor mixture, the pressure does not depend on density and it is equal to the saturated metal vapor pressure at a given temperature. If the metal is in the metastable state of a superheated, stretched liquid, the pressure may be negative. The pressure increases rapidly with density in the liquid region to the right of the binodal because of the low compressibility of liquids.

When heated by electric current, the wire material expands and enters the two-phase region, where the magnetic pressure, which is greater than the saturated vapor pressure, compresses it again to a liquid state. The explosion of the metal occurs near the critical point (the point of the phase diagram at which the gas, liquid, and two-phase regions come in touch), when the magnetic pressure is no longer able to hold the expanding material. Thus, the phase trajectory of an exploding metal (see Fig. 1, curve *I*) is actually fixed and, therefore, the specific current action integral can well be considered an invariant for a given metal. Deviations from the phase trajectory occur when the current density rise time is so short, such that the metal does not have time to expand during heating [74], [78]–[80], that is, the matter is held by inertial forces (see Fig. 1, curve *II*). In this case, the energy deposited in a wire can be significantly greater than the atomization energy of the wire metal; however, to a good approximation, the specific current action integral remains an invariant characterizing the explosion of the metal [74].

When describing WEs, it is customary to distinguish two types of specific action integrals [40], [75]

$$\bar{h} = h_1 + h_2 \tag{I-2}$$

where h_1 and h_2 describe the specific current action for heating the metal, respectively, from room temperature to the melting point and from the melting point to the explosion temperature. The values of these quantities, which can be determined experimentally [35], are given for a number of metals in [40] and [75]. It should be noted that the assumption of constancy of the value of h_1 holds quite well for all explosion regimes, whereas the value of h_2 increases, though insignificantly, with current density. When the current density changes from 10^6 to 10^8 A/cm^2, the specific current action changes by a factor of 1.5–2 [40], [75].

The times from the onset of current flow through a wire to its explosion, τ_{ex}, and to its melting, τ_{melt}, and the time interval between the melting and the explosion can be expressed in terms of the specific action integrals as follows:

$$\tau_{\text{ex}} \approx A\frac{\bar{h}}{j^2}, \quad \tau_{\text{melt}} \approx A\frac{h_1}{j^2}, \quad (\tau_{\text{ex}} - \tau_{\text{melt}}) \approx A\frac{h_2}{j^2} \tag{I-3}$$

where τ_{melt} is the melting time and A is a dimensionless factor determined by the current pulse waveform: $A = 1$ for a constant current, $A = 2$ for a sinusoidal current, and $A = 3$ for a linearly rising current. For the two latter cases, j in (3) is the maximum current density.

The explosion time (the time at which the voltage across the wire is a maximum) depends on various factors. A WE in a (liquid or gas) medium occurs in conditions corresponding to the critical point, such that the magnetic pressure is no longer able to keep the material from expanding. For a WE in vacuum, the time of the voltage maximum is determined by the time of occurrence of a shunting breakdown along the wire surface [81], [82]. Therefore, a WE in vacuum is in some sense an incomplete, interrupted explosion. In this case, the value of the dimensionless factor A in (3) is slightly lower than that for an explosion in a medium, but still remains of the order of unity [83]. The breakdown time depends on the time derivative of the current density: the greater the dj/dt, the further the phase trajectory of the metal moves toward the critical point (see Fig. 1) and the greater the energy deposited in the wire material.

The values of the specific current action integrals for various metals are presented in Table I. In addition, the table presents the values of melting energy $\varepsilon_{\text{melt}}$, vaporization energy ε_{vap}, and the critical point parameters for the metals. It should be noted that in the literature, various interrelated energy characteristics are used to describe the final stage of a WE. These are: first, the internal energy at the critical point, ε_{cr}; second, the sublimation (vaporization) energy $\varepsilon_{\text{vap}} = \varepsilon_{\text{cr}} - \varepsilon_0$, where ε_0 is the internal energy of the metal under normal conditions, and, finally, the atomization energy $\varepsilon_{\text{atom}} = \varepsilon_{\text{cr}}$ and the atomization enthalpy $H_{\text{atom}} = \varepsilon_{\text{cr}} + m_a p_{\text{cr}}/\rho_{\text{cr}}$, where p_{cr} and ρ_{cr} are, respectively, the critical point pressure and density of the metal, and m_a is its atomic mass. All these quantities are close in value to each other: ε_{cr} coincides with ε_{vap} to within parts of a percent because $\varepsilon_{\text{cr}} \gg \varepsilon_0$, and the atomization enthalpy is greater than ε_{cr} by no more than 10%, which, in estimating the energy deposited in the wire, is generally within the experimental error.

B. Classification of WE Modes

In an exploding wire, various processes occur in the metal, each developing during a certain period of time (characteristic time). The proportions between the characteristic times of these processes underlie any classification of WE modes; the first one was performed by Chace and Levine [84]. The main time scales of WEs are determined by the following times.

First, this is the characteristic time of energy deposition into a wire, or the explosion time τ_{ex} determined by expression (3) (here, we assume that the dimensionless factor $A = 1$).

Second, this is the characteristic time of development of magnetohydrodynamic (MHD) sausage instabilities, τ_{inst}, which determines the time during which the magnetic field pressure generated by the current flowing through the wire is able to change the wire shape. The time of development of MHD instabilities of the sausage type (mode $m = 0$) [88], [89] depends on the wire radius r_0 and on the velocity of propagation of MHD perturbations in the wire material

$$\tau_{\text{inst}} \approx \frac{r_0}{c_A} = \frac{2}{j}\sqrt{\frac{\rho}{\mu_0}} \tag{I-4}$$

where $c_A = (B/\sqrt{\mu_0\rho})$ is the Alfven velocity [90], B is the magnetic induction, and μ_0 is the permeability of vacuum. Note that in writing relation (I-4), we assumed that the current is uniformly distributed over the wire cross section and the magnetic field is equal to that at the wire surface, $B = (\mu_0 I/2\pi r_0)$, where $I = \pi r_0^2 j$ is the current flowing through the wire.

Third, this is the skin-effect time τ_{skin}, which is determined by the diffusion of the magnetic field into the wire and depends on the wire radius and resistivity δ [90]

$$\tau_{\text{skin}} \approx \frac{\mu_0 r_0^2}{\delta}. \tag{I-5}$$

TABLE I
CHARACTERISTICS OF METALS

Metal	Cu	Au	Al	Ag	Ni	Fe	W	Ti	Mo	Zn
$\overline{h}$, 10^9 A^2·s/cm^4	4.1	1.8	1.8	2.8	1.9	1.4	1.85*	0.8	-	-
h_1, 10^9 A^2·s/cm^4	1.07	0.56	0.41	0.77	0.28	0.15	0.35	-	0.36	-
Melting energy, kJ/g	0.205	0.06	0.4	0.1	0.3	0.25	0.19	0.32	0.37	0.11
Atomization enthalpy, kJ/g	4.75	1.69	10.85	2.33	6.3	6.27	4.2	8.56	6.06	1.76
ρ_{cr}, g/cm^3	2.39	5.68	0.64	2.93	2.19	2.03	4.85**	1.13**	3.18	2.29
T_{cr}, eV	0.72	0.77	0.69	0.61	0.89	0.83	1.38**	0.75**	1.39	0.275
p_{cr}, kbar	7.46	6.1	4.47	4.5	9.12	8.25	11.8**	4.78**	12.63	2.63

Note: The data on the specific current action integral and on the critical point parameters not marked with asterisks were taken from [40, 75], and the values of atomization and melting energies were borrowed from [85].

* data from [86]

** data from [87].

If the characteristic time for the development of MHD instabilities during a WE is much less than the time of loss of metallic conductivity ($\tau_{inst} \ll \tau_{ex}$), then the WE occurs in a slow mode, and in the opposite case, a fast mode of WE takes place. According to expressions (3) and (I-4), for a twofold difference between τ_{inst} and τ_{ex}, so that a WE occurs in a fast mode, the current density must satisfy the condition

$$j > \frac{\bar{h}}{4}\sqrt{\frac{\mu_0}{\rho}}. \tag{I-6}$$

A slow WE and a fast WE are essentially different in nature. A slow WE is accompanied by the development of sausage instabilities with mode number $m = 0$ caused by magnetic pressure, which distorts the wire shape. The wire takes the shape of a sausage and its cross section becomes variable along the z-axis. In this case, the wire is heated nonuniformly, and until it is destroyed, only a small part of the metal evaporates, and it mostly splashes and breaks up into droplets. In a fast WE, the shape of the wire does not have time to change significantly during heating, and the liquid-to-gas transition of the material occurs more uniformly. In this case, the explosion is due to the loss of metallic conductivity during the metal-insulator transition [91], [92]. In a fast WE, electrothermal instabilities (ETIs), which are due to the temperature dependence of resistivity, prevail [86], [93].

In addition to the slow and fast WE modes, it is customary to distinguish the skinned current mode, or the superfast mode that occurs when the magnetic field does not have time to penetrate the inner layers of the wire and is localized in its surface layers. This mode takes place if the characteristic skin-effect time is greater than the explosion time ($\tau_{skin} > \tau_{ex}$). For this case, (3) and (5) yield the following condition for the current density:

$$j > \frac{1}{r_0}\sqrt{\frac{\bar{h}\delta}{\mu_0}}. \tag{I-7}$$

Note that in the skinned current mode, the magnetic pressure acting on the surface of the wire is greater than the thermal pressure of the wire material. For a WE, the thermal pressure is the critical point pressure p_{cr}. If the magnetic pressure is dominant, we have $(B^2/2\mu_0) > p_{cr}$, where B is the magnetic induction at the conductor surface used in writing (I-4). This inequality yields the following condition for the current density, similar to condition (7):

$$j > \frac{1}{r_0}\sqrt{\frac{8p_{cr}}{\mu_0}}. \tag{I-8}$$

However, relation (8) is valid only for a fast explosion. In a slow explosion, sausage instabilities develop due to magnetic pressure. The sausage instabilities start growing immediately after the meltdown of the wire [90], when the thermal pressure is significantly lower than p_{cr}.

It should also be noted that in a pronounced skinned current mode, the explosion time is determined not by expression (I-1), but by the time at which the magnetic energy density at the surface of the wire reaches a value approximately equal to the atomization energy density for the metal [48], that is, when $(B^2/2\mu_0) \approx \rho\varepsilon_{atom}$. This yields the magnetic induction at which the conductor explodes: $B_s \approx \sqrt{2\mu_0\rho\varepsilon_{atom}}$. For various metals, B_S varies between 2 and 4 MGs [48].

In addition, the high-temperature explosion regime can be distinguished in which the energy that can be deposited into the wire is greater than the atomization energy of the wire metal, and not only in an explosion occurring in a gas medium [10], [35], [42], [93], but it may be possible in an explosion occurring in vacuum [94]. There are two different points of view on the reasons for such a behavior of the material of an exploding wire. The first one assumes the decisive role of the magnetic pressure [95], which balances the gas-kinetic pressure and, hence, inhibits the expansion of the metal. The second one suggests the influence of inertia forces, which keep the wire from expanding substantially within a short time [78]. More convincing evidence, both experimental [79], [96] and theoretical [74], [95], has been found for the second point of view.

Based on the assumption of the key role played by inertial forces, let us estimate the radius of an exploding wire at which these forces begin to affect the expansion of the wire. To do this, we use the law of conservation of momentum $\rho(d\mathbf{v}/dt) = -\nabla p$, where $\mathbf{v}$ is the wire expansion velocity. As the explosion of a wire occurs at nearly critical point parameters, the law of conservation of momentum can be written approximately as

$$\rho_{\rm cr}\frac{v}{\tau_{\rm ex}} \approx \frac{p_{\rm cr}}{r_0}. \tag{I-9}$$

On the other hand, as the critical point density $\rho_{\rm cr}$ is three to five times lower than the normal density ρ_0, the wire should expand to about twice its radius before it explodes. Thus, the explosion time can be estimated as

$$\tau_{\rm ex} \approx \frac{r_0}{v}. \tag{I-10}$$

If the effect of inertia forces is significant, the left side of relation (9) is greater than the right one. Then, eliminating the wire expansion velocity v from (9) and (10), we obtain a condition which relates the explosion time and the wire radius

$$\tau_{\rm ex} < r_0\sqrt{\frac{\rho_{\rm cr}}{p_{\rm cr}}}. \tag{I-11}$$

This relation, in view of (3), yields the condition for the occurrence of an explosion regime in which the inertial forces play a dominant part (being also a high-temperature explosion regime) [74]

$$j > \sqrt{\frac{\bar{h}}{r_0}\left(\frac{p_{\rm cr}}{\rho_{\rm cr}}\right)^{1/2}}. \tag{I-12}$$

Fig. 2 shows a current-density–radius diagram illustrating different explosion modes for aluminum wires. The solid lines represent conditions (6) and (7), and the dashed line represents condition (12).

These lines were plotted using the values of ρ and δ for the molten material. As can be seen from the diagram, the fast WE mode occurs at current densities close to and higher than $\sim 10^8$ A/cm^2. The diagram region corresponding to the fast WE mode can be subdivided into two regions. The first one refers to the low-temperature explosion regime (occurring at comparatively low current densities), and the second one refers to the high-temperature regime (occurring when inertia forces prevail). The fast explosion mode is just the central issue of this review. The studies of this explosion mode are focused on the initial stage of a WE that includes the solid-to-plasma transition of the wire metal, the formation of a low-density plasma corona surrounding a dense core, and the formation of strata, alternating high-density and low-density core layers. Note that, in this review, we do not consider the phenomena directly related to wire array implosions.

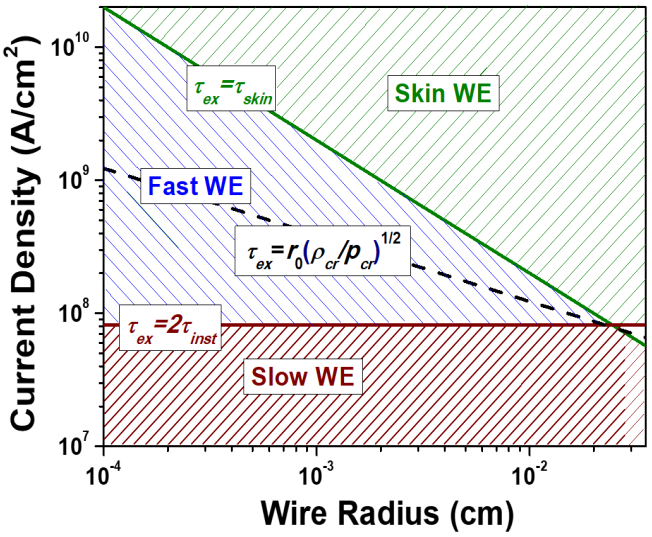

Fig. 2. Diagrammatic sketch illustrating WE modes for aluminum wires.

The review is focused on the fast modes of the explosion of wires in vacuum in which skin-effect processes are not essential. This type of explosion mode is typically like the explosion of microwires in wire arrays. Interest in studying nanosecond explosions of wires has increased in the last 15–20 years since the successful experiments carried out on the Z facility [67] in which record soft X-ray yields (over 1.5 MJ/pulse) were achieved. A wire array is a cylindrical structure designed as a "squirrel wheel" [66]–[70], [97] with the wires spaced by $(2\pi R_{wa}/N_{wa})$, where $R_{\rm wa}$ is the radius of the wire array and $N_{\rm wa}$ is the number of wires in the array. The (maximum) magnetic induction at the surface of an individual wire is given by $B_w = (\mu_0 I_{wa}/2\pi r_w N_{wa})$, where $I_{\rm wa}$ is the current through the wire array and r_w is the wire radius, and the maximum induction of the collective field of the wire array is given by $B_{wa} \approx (\mu_0 I_{wa}/2\pi R_{wa})$. Thus, the collective field of a wire array is greater than the field of an individual wire, if the following condition is fulfilled:

$$r_w > \frac{R_{wa}}{N_{wa}}. \tag{I-13}$$

In the experiments [67], the number of tungsten wires was 120–300, the initial wire radius was 3.75–7.5 μm, and the wire array radius was 0.9–2 cm. That is, before the individual wires exploded, condition (13) was obviously not fulfilled. This situation was typically observed in other experiments with wire arrays. This suggests that the processes that occur in the dense core of an individual conductor of a wire array, such as the heating and explosion of the metal and the formation of strata, proceed similar to those occurring in single conductors.

However, when condition (13) becomes valid for the radius of an individual wire during the expansion of the low-density plasma corona, consisting of desorbed gas and vaporized metal, the collective field of the wire array begins to play a decisive part. This occurs even before the coronas of adjacent wires come into contact, as the distance between the wires in a wire array is greater than the value of r_w determined by condition (13). The collective field changes the topology of the expanding corona. The corona of a single wire expands uniformly in azimuth, whereas the expansion of an individual wire of a wire array is strongly nonuniform azimuthally. The collective field strengthens the field of an individual wire on the outer side of the wire array and reduces it on the inner side. As a result, the vaporizing wire material flows to the center of the wire array.

Using the data of Z-pinch experiments [67] as an example, let us estimate the characteristic times at which WEs in wire arrays occur. In [67], it is noted that in the experiments, the explosion of microconductors occurred within a prepulse, the current in which could be approximated as linearly increasing with a rate $(dI_{wa}/dt) \approx (4–6) \cdot 10^{12}$ A/s. Estimating the rise rate of the current density in an individual wire as $(dj/dt) \approx (3–5) \cdot 10^{16}$ A/(cm^2·s) and using (3), we obtain the following estimate for the explosion time: $\tau_{\text{ex}} \approx [3\bar{h}(dj/dt)^{-2}]^{1/3} \approx 15–20$ ns.

The outline of this review is as follows: Section II describes the physical principles that underlie the interpretation of phenomena arising in a WE, namely, the MHD equations are discussed that make it possible to simulate a WE, the now available equations of state of metals are described, and the temperature dependence of the electrical conductivity of metals is discussed. In addition, Section II considers the principal mechanisms of the development of ETIs. Section III describes the features of current and voltage measurements at load currents rising at rates of 1–100 A/ns typically like WEs in vacuum. An extensive database on the explosion of thin wires in vacuum is given in Section IV. It includes the data on the energy deposition into wires exploded in vacuum and on the behavior of the parameters of the wire material during a WE in vacuum, obtained experimentally using laser and soft X-ray backlighting diagnostics.

II. Theoretical Background

The WE process is conventionally simulated using MHD approximation [90]. To perform numerical calculations in this approximation, it is necessary to know the equations of state of matter (EOS) for a wide range of thermodynamic parameters and the transport coefficients of the wire material, the most important of which is electrical conductivity. There are a number of semiempirical models and various databases that can be used for describing the thermodynamic properties of metals. However, the issues related to the transport coefficients in the metal–insulator transition region and near the critical point have received much less study.

The MHD approximation that is generally used for numerical simulation of WEs includes the following.

1) The hydrodynamic equations that represent the conservation of mass, momentum, and energy.
2) Maxwell's equations and Ohm's law.
3) The equations of state that relate the thermodynamic functions (pressure and internal energy) to the thermodynamic parameters of the wire material (temperature and density).
4) A model or tables of conductivity.
5) Equations of radiative transfer.

The choice of a specific model for MHD simulation of a WE is dictated by the fact that one has to deal, as a rule, with the dense and relatively low-temperature matter. MHD models are generally based on the following assumptions. First, it is assumed that the ion temperature is equal to the electron temperature, that is, a one-temperature approximation is used. Second, displacement currents are not taken into account as the metal conductivity is high, and a quasi-stationary approximation is used to solve Maxwell's equations. Third, the conductivity is considered a scalar quantity and the Hall effects, which are significant in a rarefied plasma, are not taken into account. Fourth, radiative processes are not considered if the plasma temperature during an explosion is low (not higher than 5 eV), as in this case, the radiated energy is small compared with the energy deposited in the wire. Boundary conditions for the system of MHD equations are specified according to a given problem. They are determined by both the geometry of the load and the equations of the circuit in which the exploding wire is connected.

The WE experiments and MHD simulations, on the one hand, provide information on the electrical conductivity of materials used in this field of research and, on the other hand, they allow one to judge whether a particular conductivity model is correct [6], [8], [10], [98]. From this point of view, of most interest are WEs in liquid dielectrics, in particular, in water [10], [98], [99], rather than in vacuum, where phenomena occur which are not directly related to the transport properties of the wire material, such as gas desorption from the metal surface, metal evaporation, etc. In addition, the dielectric medium in which a wire explodes impedes its expansion, which leads to a more uniform heating of the metal. Therefore, the higher the density of the dielectric, the more reliable is the information on the properties of the metal obtained in the experiment. For instance, to determine the electrical conductivity of aluminum, a metal foil was placed between two thick polished silica glass plates [8].

The key diagnostic information on the processes occurring in the material of an exploding wire is obtained from oscilloscope measurements of the current flowing in the circuit and the voltage across the wire. Usually, several stages of a WE in a medium are distinguished: the heating of the wire by electric current, the explosion of the wire, the current pause, and the resumption of current flow. However, the resumed current has no direct relation to the WE [2], and the current pause may be absent. The WE in a medium may occur in the so-called "optimal" regime [100]–[102], in which almost all the energy stored in the capacitor bank are delivered to the wire during the first half-period of the discharge. This regime may result from a sharp increase in the resistance of the wire during its heating. It occurs if the explosion time coincides with the time during which the electric energy of the capacitor bank is

converted into the magnetic energy of the circuit inductance. The relationship between the parameters of the electric circuit and the parameters of the exploding wire, which must be known to realize the optimal regime, is considered in [42] and [102]. This relationship can be expressed in terms of the specific current action integral defined by relation (I-1). To achieve the optimal regime of a WE, in which almost all the energy stored in the capacitor bank are delivered to the load, is quite desirable in various applications. This regime is used, for instance, to produce nanopowders [41] and to initiate intense shock waves in a liquid dielectric in exploded nested wire arrays [103], [104].

To perform an MHD simulation of a WE in a dielectric medium, it is necessary to simulate the processes occurring not only in the exploding wire but also in the medium, which requires knowledge of the equations of state of the medium and its transport properties. In general, by using models of a WE in a medium which describe adequately the equations of state of the metal and its transport properties, it is possible to achieve a good agreement between experimental data and simulation predictions [10], [98], [99].

A. Equations of State of Matter

In exploding wires, the parameters of the wire metal vary over a very wide range, and the phase trajectory of the material (see Fig. 1) passes through several regions corresponding to different phase states, such as a crystalline state (solid), a liquid, a two-phase state (a mixture of liquid and vapor), gas, and plasma.

To perform MHD calculations for a WE, the relations between the thermodynamic variables (density and temperature) and the thermodynamic functions (pressure, internal energy, free energy, entropy, etc.) must be specified. This can be done only based on wide-range equations of state. These equations, in virtue of their universality, are semiempirical, that is, they contain fitting coefficients to be determined from experimental data. The well-known EOS databases are available at the Los Alamos National Laboratory (SESAME Database) [105], at the Joint Institute for High Temperatures (Moscow and Chernogolovka) [87], [106], and at two Russian Federal Nuclear Centers (Arzamas [107] and Snezhinsk [108]). In wide-range EOSs, the thermodynamic functions are represented as the sums of three components [109], which describe the elastic properties of a cold body, the thermal motion of atoms (nuclei), and the thermal excitation of electrons.

When constructing an EOS as the thermodynamic potential of a solid (or liquid, or gas) phase, the free energy $F(V, T)$ is written as the sum of three terms [87], [109]

$$F(V,T) = F_{\text{cold}}(V) + F_i(V,T) + F_e(V,T)$$

where $V = m_i/\rho$ is the specific volume of the material and m_i is its atomic mass. The terms in the expression for the thermodynamic potential describe the cold (elastic) energy at absolute zero temperature $T = 0$ K, F_{cold}, the thermal energy of atoms, F_i, and the thermal energy of electrons, F_e. To determine the components of the thermodynamic potential, semiempirical formulas are used which are different for different regions of the phase plane. The fitting parameters contained in the semiempirical formulas are estimated from the conditions for the best description of the available experimental data. As the effective range of each of the fitting parameters is limited, this makes it possible to select their values in a largely independent manner.

Once the thermodynamic potential has been constructed for the entire phase plane, the remaining thermodynamic functions are calculated using well-known thermodynamic relations, in particular

$$p = -\left(\frac{\partial F}{\partial V}\right)_S; \quad \varepsilon = F + TS$$

where $S = -(\partial F/\partial T)_V$ is the entropy of the material and ε is its internal energy.

For instance, the EOS models developed at the Joint Institute for High Temperatures [87], [106], [110] contain about 50 fitting parameters that determine the type of functional relation for the free energy of a metal in wide ranges of densities and temperatures. Therefore, in a simulation, EOSs tabulated as functional relations $p\ (V, T)$, $\varepsilon\ (V, T)$, and the like, are used. These EOSs take into account the effects of high-temperature melting and evaporation and, in addition, imply the possibility of the existence of metastable states near the liquid and gas regions of the phase diagram.

B. Transport Properties of Metals

There are various theoretical, semiempirical, and empirical models for determining the electrical conductivity of metals in the metal–insulator transition region [111]–[117]. However, two of them [111]–[113] give the best agreement with the experimental results obtained for different explosion regimes.

First, this is the LMD (Lee–More–Desjarlais) model, being developed by Desjarlais [111] at the Sandia National Laboratories, USA, who compiled tables of electrical conductivity and thermal conductivity for various metals by using the Lee–More model [112] modified based on experimental data. Central to the Lee–More model is the Boltzmann kinetic equation in the relaxation time approximation, which is valid for low-temperature and electric-field gradients. This model takes into account the electron degeneracy, the Debye screening, the ion-ion interaction, and the electron scattering by neutrals. For the solid and liquid phases, the average electron range is calculated using the Thomas–Fermi model taking account of melting effects.

In this model, the thermal conductivity is calculated using the Bloch–Grüneisen formula for monovalent metals and the electrical conductivity is calculated using the expression

$$\sigma = A(\mu/kT, \omega\tau)\frac{e^2\tau n_e}{m_e}$$

where e and m_e are the electron charge and mass, respectively; k is Boltzmann's constant; ω and τ are the electron cyclotron frequency and the momentum relaxation time, respectively, and μ is the chemical potential. The factor A is a function of the chemical potential and the electron magnetization $(\omega\tau)$. For a completely magnetized plasma $(\omega\tau \to \infty)$ or a completely degenerate plasma $(\mu/kT \to \infty)$, it is equal to

unity. The maximum A is $32/3\pi$ in the limits $\omega\tau \to 0$ and $\mu/kT \to -\infty$.

The second model used to determine the electrical conductivity of a metal, the Bakulin–Kuropatenko–Luchinskii (BKL) model, is based on a computational–experimental procedure [113] assuming that the conductivity depends parametrically on the equation of state. In the framework of this procedure, the conductivity is tabulated as follows. The initial data are: 1) the temperature dependence of conductivity for the normal density of the metal, which is a tabulated quantity; and 2) the temperature dependence of conductivity in the gas-plasma region, which is calculated by classical formulas [118], [119]. The conductivity in the transition region, near the critical point, is specified in the parametric form [98], [113]

$$\lg \frac{\sigma\,(T,\xi)}{\sigma_1\,(T,\xi=1)} = \Phi\,(T,\xi)\lg\frac{\sigma_{\rm cr}}{\sigma_1}\left(\frac{\lg\xi}{\lg\xi_{\rm cr}}\right)$$

where $\sigma_{\rm cr}$ is the critical point conductivity, $\xi = \rho/\rho_0$ is the relative density of the material, ρ_0 is the normal density of the material, $\xi_{\rm cr}$ is the critical point relative density of the material, and $\Phi(T,\xi)$ is a function of the order of unity depending on the position of the phase mixture boundary. When compiling conductivity tables, $\sigma_{\rm cr}$ is a variable parameter, which is assumed to be independent of temperature. The critical point conductivity is selected so that the results of the MHD simulation would give the best fit to the available experimental data. This approach supposes that the metal–insulator transition occurs when the material density becomes equal to the critical point density; that is, at this density, the temperature dependence of conductivity changes qualitatively. At a density greater than the critical one, the conductivity decreases with increasing temperature, which is characteristic of metals in condensed states. When the density is below the critical point density, the conductivity increases with temperature, which is characteristic of gases and plasmas.

A comparison of the tabulated conductivity of aluminum [111] with the conductivity calculated by the method proposed in [113] shows that the tabulated values obtained by these two methods are consistent both qualitatively and quantitatively. Fig. 3 presents the plots of the electrical conductivity of aluminum versus its density at various temperatures, constructed using the Desjarlais tables [111] and the computational–experimental procedure [113].

As can be seen from Fig. 3, at low densities, the electrical conductivity obtained by both methods is consistent with the classical Spitzer and Braginskii formulas [118], [119]: the conductivity increases with temperature, and, as it becomes metallic in the high-density region, it starts decreasing with increasing temperature. In both methods, the change in the behavior of electrical conductivity with a change in temperature occurs at densities close to the critical point density. In both approaches, the temperature dependence of electrical conductivity changes at near-critical densities.

The authors of this review used the BKL method and experimental data on WEs in water to compile conductivity tables for aluminum, copper, and tungsten [18], [38], [98]. The procedure of compiling these tables is described in detail in [18].

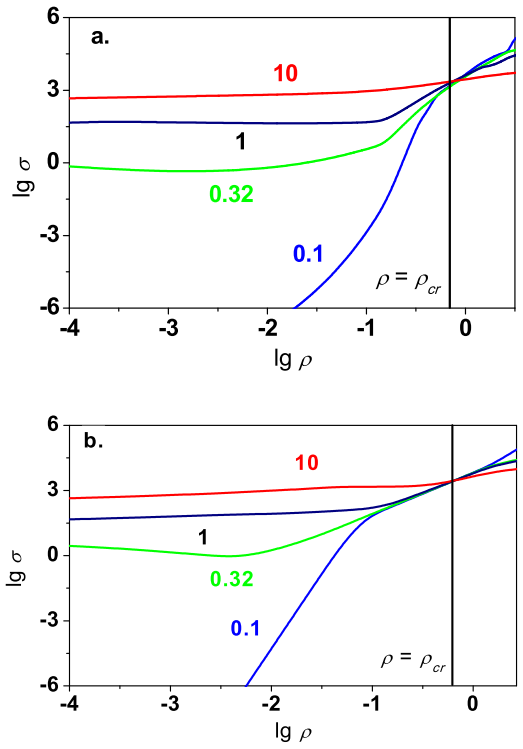

Fig. 3. Plots of the electrical conductivity σ ($\Omega^{-1}\cdot$cm^{-1}) of Al versus density ρ (g/cm^3) at different temperatures constructed using (a) LMD method and (b) BKL method. The numerals at the curves denote the temperature in electron-volts.

As noted earlier, in the BKL method, the critical point conductivity, $\sigma_{\rm cr}$, serves as the main, essentially fitting, parameter. In an MHD simulation, the current–voltage characteristic of a WE strongly depends on the critical point conductivity. The value of $\sigma_{\rm cr}$ determines the explosion time (the time at which the voltage across the wire reaches a maximum) and the variation in wire resistance during the explosion. Despite the fact that aluminum, copper, and tungsten have significantly different thermodynamic and electrical properties (the conductivity of copper at room temperature is three times higher than that of tungsten), the values of the critical point conductivity for these metals turned out to be close to each other. The BKL method gave $\sigma_{\rm cr}^{Al} = 2.8\cdot 10^3\ \Omega^{-1}\cdot{\rm cm}^{-1}$ for aluminum, $\sigma_{\rm cr}^{Cu} = 2\cdot 10^3\ \Omega^{-1}\cdot{\rm cm}^{-1}$ for copper, and $\sigma_{\rm cr}^{W} = 2.6\cdot 10^3\ \Omega^{-1}\cdot{\rm cm}^{-1}$ for tungsten; that is, the values of $\sigma_{\rm cr}$ for these metals are different to within about 20%. Let us discuss, relying on the ideas presented in [120], the reasons for such a coincidence of the conductivities in the vicinity of the critical point.

According to the classical Drude–Lorenz theory, the conductivity due to the motion of electrons can be described by the following formula (see [121]):

$$\sigma = \frac{e^2 n_e l_e}{m_e \upsilon_e}$$

where l_e and υ_e are the electron mean free path and velocity, respectively. As the electrical conductivity in the conduction band of a metal is determined by the motion of quasi-free electrons, the real part of the wave function of which is a

sinusoid, the electron momentum can be related to the de Broglie wavelength as $m_e v_e = \hbar k_w$, where $\hbar$ is Plank's constant and k_w is the wavevector. For metals, the de Broglie wavelength of electrons is related to the radius of the curvature of the Fermi surface [120]. In the approximation of a spherical Fermi surface, the wavevector can be expressed in terms of the density of quasi-free electrons as

$$k_w = \left(3\pi^2 n_e\right)^{1/3}.$$

Then, with these assumptions, the formula for the conductivity becomes [120]

$$\sigma = \frac{e^2 n_e l_e}{\hbar k_w} = \frac{e^2 n_e^{1/3}}{\left(3\pi^2\right)^{2/3}\hbar}\left(k_w l_e\right).$$

For strongly disordered media, the free path of electrons in the metal–insulator transition region is limited from below. This is the so-called Ioffe–Regel limit [122], which is defined as $k_w l_e \geq 1$.

This inequality is justified by the following statement [120]: a segment of a sinusoid whose length is less than the wavelength cannot be considered a sinusoid. The Ioffe–Regel limit specifies a certain minimum conductivity of a material being in a state in which it can still be considered a metal.

If $k_w l_e = 1$, we may speak of a minimum metallic conductivity, which is defined as [120]

$$\sigma^* \approx A^* \frac{e^2 a}{\hbar} \tag{II-1}$$

where $a \approx (n_e)^{1/3}$ is the average distance between the metal atoms, approximately equal to the average distance between the charge carriers (quasi-free electrons), and A^* is a dimensionless constant. For a condensed metal, the density of quasi-free electrons can be estimated as $n_e \approx 4 \cdot 10^{22}$ cm^{-3} [120]. Then, relation (II-1) with $A^* = (3\pi^2)^{-2/3} \approx 0.1$ yields the minimum conductivity $\sigma^* \approx 8.7 \cdot 10^2$ $\Omega^{-1}\cdot$ cm^{-1}. However, as noted in [120], the best fit to experimental data is obtained with $A^* \approx 0.3$–0.5. For our case, assuming that the critical point conductivity equals the minimum metallic conductivity, $\sigma_{\rm cr} = \sigma^*$, we have $A^* \approx 0.2$–0.3, determined by the BKL method.

C. Features of the MHD Simulation of the Explosion of Wires in Vacuum

The main feature of the electrical explosion of wires in vacuum is that during the heating of the wire material, a low-density corona is formed at the metal–vacuum interface, in which a shunting discharge develops as the voltage across the wire increases. The low-density corona can be formed due to the desorption of gases from the wire surface and evaporation of the metal. A comparative analysis of the discharge along the surface of tungsten wires exploded at current densities ranged from $2 \cdot 10^7$ to $5 \cdot 10^7$ A/cm^2 and the breakdown of a 6-mm gap filled with hydrogen is presented in [123]. This analysis was supported by the fact that a tungsten surface usually contains about 10^{15} adsorbed hydrogen atoms per square centimeter [123], [124]. Of course, tungsten also adsorbs atoms of other gases, but as hydrogen is the lightest element, it is most responsible for the expansion of the low-density corona. The comparison showed that the discharge characteristics for both cases were in good agreement with each other, which made it possible to formulate a criterion for the development of a shunting discharge for the given explosion regime [123].

For a preheated exploding wire [125], [126], the shunting discharge in the metal vapor produced due to the evaporation of an exploding wire material occurs in its pure form, that is, in the absence of gas desorbed from the metal surface. The evaporation of the metal of an exploding wire from its surface was theoretically investigated by Rakhel [127] and Vorobev [128]. Anisimov *et al.* [129] have shown that in the gas produced as a result of a WE, a thin layer is formed near the condensed material boundary in which local thermodynamic equilibrium is disturbed. The thickness of this layer is comparable to the free path of the vapor particles. The sharp boundary between the liquid and the gas phase disappears as the surface temperature of the condensed material increases to the critical point temperature of the liquid–vapor phase transition. The evaporation of the wire metal plays an important part in wire array implosions driven by megaampere current pulses [66]–[70]. In this case, the metal vapor formed on the wire surface is compressed toward the axis of the array, forming a precursor, and the cores of the wires remain on the periphery, continuing to evaporate. Simplified models of such a pattern of plasma generation in exploding wire arrays are described in [130] and [131].

The evaporation from the surface of an exploding wire creates conditions at the interface between the condensed phase and the vapor under which metastable liquid states may occur in the bulk of the wire subject to heating [106], [127], [132]. Note that the formation of a metastable superheated liquid is also possible when a wire explodes in a medium. However, in this case, the wire expansion is hindered by the counterpressure of the medium; therefore, a possible effect of the metastable states is not so significant. The question of which of the possible states (metastable liquid or liquid plus vapor, see Fig. 1) will occur in a WE is related to the rate of decay of the metastable states. Experimental studies of the explosion of metal foils [27], [83] showed that when the energy deposited in the foil metal was about half the sublimation energy, the time of decay of the superheated liquid was about 100 ns. However, this time should decrease with an increase in energy input [76].

When using the MHD approach, numerical calculations are more convenient to perform assuming the existence of metastable states. This is due to the fact that the pressure in a liquid-vapor mixture does not depend on density, and, hence, the velocity of sound, which is defined as $c_s = \sqrt{\partial p/\partial \rho}$, is formally equal to zero. Therefore, taking account, or not taking account, of metastable states while simulating a WE significantly affects the density distribution of the wire material, as shown in Fig. 4, which represents the results of calculations for a tungsten wire of diameter 7.5 μm at a current density of about $5 \cdot 10^7$ A/cm^2 [132]. In this case, two different types of EOS were used for MHD calculations. The first EOS did not take into account the possibility of the existence of metastable states; that is, it was assumed that in

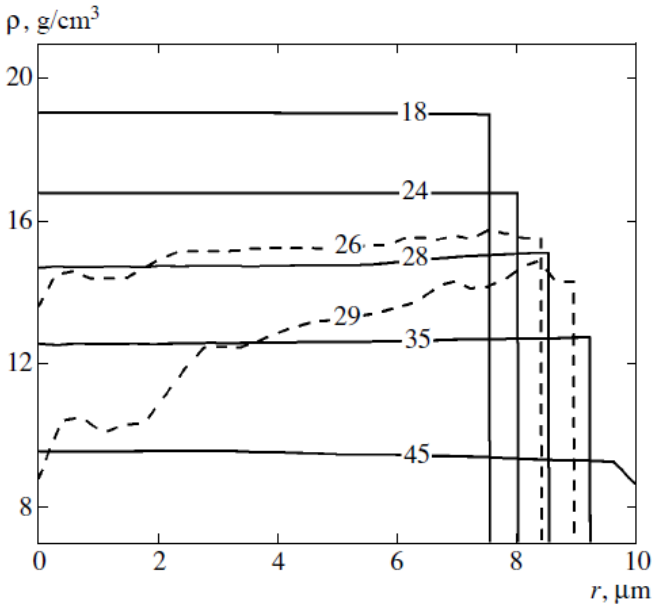

Fig. 4. Radial distribution of the wire material density ρ in a condensed state at different points of time: the solid and dashed lines represent the results of calculations performed with account and with no account of metastable states, respectively; the numerals at the curves denote the time in nanoseconds [132]. Copyright 2001, Springer Nature.

the region between the liquid bimodal (curve *II*, Fig. 1) and the gas binodal (curve *V*, Fig. 1), the material is in the form of a vapor-droplet mixture. Under this assumption, the dashed lines in Fig. 4 were obtained. The second EOS, on the contrary, took into account the possibility of the existence of metastable states. In this case, it was assumed that in the region between the liquid binodal (curve *II*, Fig. 1) and the liquid spinodal (curve *III*, Fig. 1), the material is in a metastable state, namely, in the form of a superheated liquid. Under this assumption, the solid lines in Fig. 4 were obtained. It seems that the use of the first type of EOS, excluding metastable states, is justified for slow explosions (with explosion times longer than 100 ns). For fast explosions, it is better to use the second type of EOS, which takes into account the possibility of the existence of metastable states.

Let us return to the shunting discharge along the surface of an exploding wire. The initiation of this discharge was investigated experimentally [133]. In the experiment of [133], luminescence was observed in a thin layer of the near-surface plasma, which propagated from the cathode to the anode at a velocity of $(1.5–3.5) \cdot 10^8$ cm/s. Sarkisov *et al.* [133] associate this luminescence with the propagation of an ionization wave. It should be noted that such a high propagation velocity is characteristic of streamers formed at the initial stage of the development of gas discharges [134]. However, the initial discharge stage (breakdown), even in gas discharges, having been the subject of investigation for many decades, still remains not fully understood and debatable [134], [135]. At this stage, both the radiation of the plasma and the runaway electrons that occur at the streamer head can play a significant part [134]–[136]. Naturally, the breakdown along the surface of an exploding wire cannot be described in the context of the MHD model, and the theory of this breakdown is to be developed in the future research.

The absence of a theory of the breakdown along the surface of an exploding wire restricts the use of the MHD approach to simulate a WE in vacuum. In this situation, reliable information can be obtained only for the initial stage of the wire heating that precedes the development of a shunting discharge. To simulate the later WE stages, semiempirical models of the development of a shunting discharge [82], [123] can be used in which the equations that describe the equivalent discharge circuit contain a time-dependent resistor connected in parallel with the exploding wire. The shunting resistance value depends on time. The initial shunting resistance is large, and as the breakdown develops, it decreases, in 5–10 ns, to values much lower than the resistance of the wire, and the generator current starts flowing through the shunting resistor. The use of this approach is justified by the observation that as soon as a shunting breakdown occurs, the current is drawn by the low-density corona, and a high-temperature plasma is generated in the corona and expands radially at a velocity of up to 10^7 cm/s [81].

The MHD simulation of a WE in vacuum gives a good agreement with experimental results in cases where the gas desorption and the evaporation of the metal have little effect on the processes occurring during the explosion. Such a situation may arise, first, in the explosion of conductors in the skinned current mode [14], [137], when the magnetic pressure impedes the expansion of the desorbed gas, and, second, in the explosion of wires at high energy deposition rates [96], [138]–[140], that is, at high current densities and high dj/dt. In this case, the explosion occurs in a time shorter than that required for the development of a shunting breakdown in the gas desorbed from the wire surface.

The latter case, that is, the explosion of wires at high current densities, is essentially the same as the explosion of micropoints on the surface of a cathode that initiates explosive electron emission [40], [75], [141]. Cathode micropoints are metal protrusions about 1 μm in diameter extended toward the anode, and their explosion occurs within several nanoseconds. Expression (11) indicates that cathode micropoints explode in the high-temperature regime described in Section I-B.

Explosive electron emission arises on the surface of a cathode at high electric field strengths, and it is accompanied by explosions of the metal in cathode microregions. High energy is concentrated in small volumes due to Joule heating, and electrons are emitted from the cathode surface in bunches, called ectons [40], [75], [142], [143]. The occurrence of an ecton is due to overheating of the metal during a microexplosion, and the cessation of ecton formation is due to the cooling of the emission zone. The operation of an ecton is a complex and multifactorial process, the details of which are yet not clearly understood. It should, however, be noted that as the formation of an ecton is related to the electrical explosion of a microprotrusion, the specific current action integral defined by expression (I-1) plays an important part in the theory of ectons. The operation of an ecton is accompanied, besides electron emission, by generation of multiply charged ions, droplets of liquid metal, etc. When an ecton stops

operating, it leaves a micrometer-size crater on the cathode surface. Explosive electron emission plays an important part in a variety of pulsed processes such as the operation of the cathode spot of a vacuum arc [40], [134], the formation of high-current electron beams in vacuum X-ray diodes [144], the establishment of a magnetic self-isolation mode in vacuum transmission lines [145], etc.

The MHD simulation of the explosion of a cathode microprotrusion based on a quasi-2-D model was first performed by Loskutov *et al.* [146], who showed that the explosion occurs at current densities of the order of 10^9 A/cm^2. Subsequently, relevant MHD calculations were carried out in 2-D cylindrical geometry. Fig. 5 presents the results of an MHD simulation of the explosion of a cylindrical microprotrusion of radius 0.3 μm on a copper cathode [147], [148]. The current through the protrusion was set equal to 3.2 A, which is the current carried by an individual cell (ecton) of the cathode spot of a copper cathode vacuum arc [75]. Under these conditions, the current density was $1.1 \cdot 10^9$ A/cm^2, which is close to the threshold current density of field emission [149]. The MHD simulations have shown that the electrical explosion of a cathode microprotrusion having parameters typical of an ecton should result in the formation of a crater on the cathode surface whose dimensions are close to those observed in experiments [40], [75].

D. Formation of Strata in a Fast WE (ETI)

According to experimental data [16], [150]–[154], the explosion of a wire in vacuum is accompanied by the formation of a low-density plasma corona surrounding a dense core and by the occurrence of strata, alternating layers of increased and decreased density, in the core. As shown earlier, under the conditions of a fast WE, to which this review is devoted, the cause of the formation of strata, which was considered, for instance, in [9], [16], [86], and [155], is the development of ETIs. The structure of ETI is determined by the behavior of the resistivity of the wire material as a function of temperature. If the resistivity decreases with increasing temperature, as is the case of classical plasma, ETIs lead to the formation of current channels. Otherwise, if the resistivity increases with temperature, as is the case of most metals in the liquid and condensed states, ETIs lead to the formation of layered structures with the layers arranged normal to the direction of current flow. For metals, the change in the behavior of the resistivity with a change in temperature that results in the transition from metallic to plasma conductivity occurs at densities close to the critical point density. This is demonstrated by Fig. 3, which shows the conductivity of aluminum as a function of density at different temperatures. Thus, the development of ETI in a WE occurs at the initial stage of the explosion, that is, at the stage of heating of the metal, which is already at least in a liquid phase.

The formation of strata in a fast WE was numerically simulated using a 2-D MHD code [18], [98], [154], [156]. Fig. 6 presents the results of a simulation of the explosion of an aluminum wire of diameter 15 μm at a current density of about

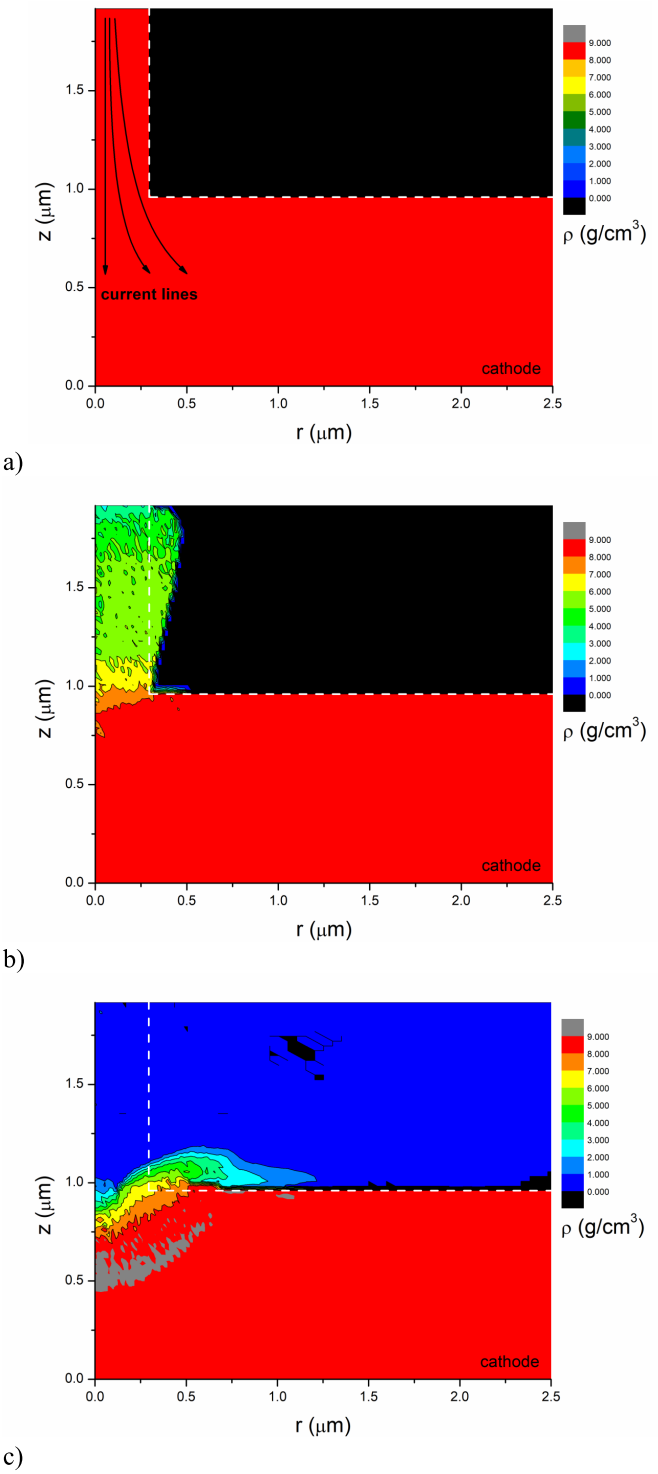

Fig. 5. Radial distribution of the material density during the explosion of a cylindrical copper cathode microprotrusion of radius 0.3 μm carrying a current of 3.2 A. (a) Initial distribution, t= 0. (b) Microprotrusion explosion, t= 2 ns after the onset of current flow. (c) Formation of a crater on the cathode surface, t= 3 ns after the onset of current flow. Adapted from [148].

10^8 A/cm^2 that occurred at the point of time when the energy deposited in the wire material became approximately equal to the atomization energy of aluminum. Analysis of the results shows that strata develop after melting of the wire, when its material is in the liquid and two-phase states. The strata

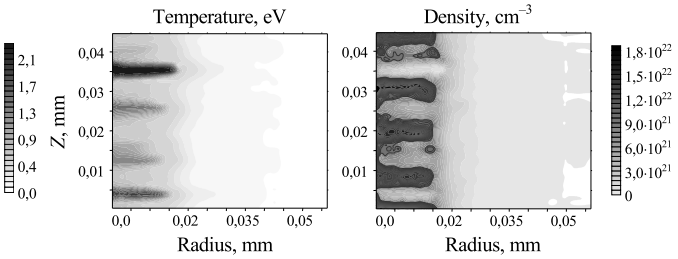

Fig. 6. Spatial distributions of the thermodynamic parameters of the metal obtained in a simulation of the explosion of an aluminum wire of diameter 15 μm [156]. Copyright 2004, AIP Publishing LLC.

consist of alternating regions with high temperature and low density and regions with lower temperature and higher density. The striation wavelength in this simulation was about 10 μm, which coincides with the wavelengths observed in experiments conducted under similar conditions [150]–[153].

The main physical mechanisms responsible for the development of ETI in a WE can be investigated using a small perturbation theory [80], [86], [155]–[158]. Consider the simplest case. Let there be a wire of constant cross section which carries a current of constant cross-sectional density j, and let the wire material be at rest. For this case, the law of energy variation is written as

$$\frac{\partial \varepsilon}{\partial t} = j^2\delta - \nabla \mathbf{W} \tag{II-2}$$

where δ is the resistivity, $\mathbf{W} = -\kappa \nabla T$ is the heat flux, and κ is the thermal conductivity.

Define the internal energy as $\varepsilon = \rho c_V$, where c_V is the heat capacity of the metal, which we consider to be a constant.

Suppose that in the unperturbed state there are no gradients of thermodynamic quantities, hence, we have the following equation to describe the behavior of temperature:

$$\rho c_V \frac{\partial T_0}{\partial t} = j^2\delta \tag{II-3}$$

where T_0 is the unperturbed value of temperature. To find an equation for small temperature perturbations, represent the material temperature and density as $T(t,z) = T_0(t) + T_1(t,z)$ and $\delta(T) = \delta(T_0) + T_1(\partial\delta/\partial T)$ (T_1 is the small temperature perturbation), respectively. Given these assumptions, we obtain the following equation for the temperature perturbation [86]:

$$\rho c_V \frac{\partial T_1}{\partial t} = j^2 \frac{\partial \delta}{\partial T} T_1 + \kappa \Delta T_1. \tag{II-4}$$

We will seek a solution to (17) in the form $T_1(t,z) = \text{const} \cdot \exp(\int_0^t \gamma\, dt^* + ik_z z)$, where γ is the instantaneous instability growth rate, $k_z = 2\pi/\lambda$ is the axial component of the wavevector, and λ is the wavelength. In this case, the dispersion equation describing the relationship between the instantaneous growth rate and the axial component of the wavevector will have the following form:

$$\gamma = \frac{1}{\rho c_V}\left(j^2 \frac{\partial \delta}{\partial T} - k_z^2 \kappa\right). \tag{II-5}$$

For most metals in the solid and liquid states, the temperature derivative of resistivity is positive: $(\partial\delta/\partial T) > 0$ (see Fig. 3).

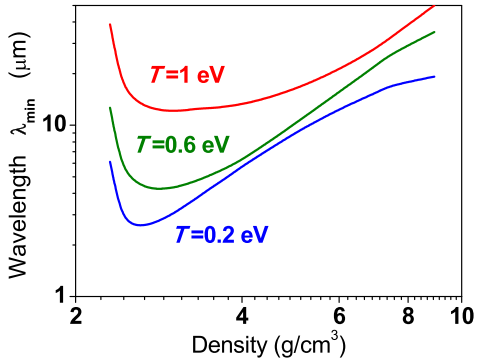

Fig. 7. Characteristic scale of thermal instabilities $\lambda_{\min}$ versus density at different temperatures for a copper wire.

Therefore, the modes with wavelengths

$$\lambda > \lambda_{\min} = \frac{2\pi}{j}\sqrt{\kappa\left(\frac{\partial \delta}{\partial T}\right)^{-1}} \tag{II-6}$$

are unstable and the modes with wavelengths $\lambda < \lambda_{\min}$ are damped by heat conduction. The instantaneous instability growth rates have maximum limiting values for $k_z \to 0$, defined as

$$\gamma_m = \frac{j^2}{\rho c_V}\frac{\partial \delta}{\partial T}. \tag{II-7}$$

However, because of the square dependence of γ on k_z, the instantaneous growth rate of a mode whose wavelength is only three times $\lambda_{\min}$ is different from $\gamma_{\rm m}$ only by 10%. Therefore, $\lambda_{\min}$ can be considered a characteristic scale of ETI.

Fig. 7 presents $\lambda_{\min}$ as a function of density at different temperatures for Cu, calculated with the resistivity tabulated using the BKL method [18], [113] and the thermal conductivity estimated using the Wiedemann–Franz relation [159]. As can be seen from the plots, the characteristic scale of thermal instabilities is about 10 μm, which is close to the initial wavelength of strata found in experiments [150]–[153] and predicted by simulations [18], [156].

The temperature derivative of resistivity can be approximately expressed in terms of the specific current action integral $\bar{h}_2$ defined by relation (I-1). To do this, we represent the resistivity as $\delta \approx T(\partial\delta/\partial T)_{av}$, where $(\partial\delta/\partial T)_{av}$ is an average value of the temperature derivative of resistivity. Substituting this relation in the second integral of (I-1) and integrating the resulting relation from the melting temperature $T_{\rm melt}$ to the critical temperature $T_{\rm cr}$ (the temperature interval in which ETI develops), we obtain

$$\bar{h}_2 \approx \rho c_V \left(\frac{\partial \delta}{\partial T}\right)_{av}^{-1} \ln\frac{T_{\rm cr}}{T_{\rm melt}}. \tag{II-8}$$

In view of (21), the relation for estimating the instantaneous instability growth rate becomes

$$\gamma_m \approx \frac{j^2}{\bar{h}_2}\ln\frac{T_{\rm cr}}{T_{\rm melt}}. \tag{II-9}$$

The growth of instabilities over the entire interval of their development is characterized by the integrated growth rate

$\Gamma(k_z) = \int_{\tau_{\text{melt}}}^{\tau_{\text{ex}}} \gamma(k_z)dt$. Integrating relation (22) from the melting time to the explosion time, we obtain [86], [157]

$$\Gamma_m \approx \ln \frac{T_{\text{cr}}}{T_{\text{melt}}}. \tag{II-10}$$

Thus, under the assumptions made [see (21)], the integrated growth rate of ETIs in an exploding material does not depend of the explosion regime and is determined only by the constants of the material. Steiner *et al.* [160] investigated experimentally how the growth of ETI depends on the critical-to-melting temperature ratio and argued the validity of relation (23). It should be noted that expression (20) assumes a constant specific current action integral; however, this assumption is not always valid. For instance, in a high-temperature explosion regime, $\bar{h}_2$ increases [74], in contrast to that in a slow explosion mode, and in a skinned current mode, the explosion time is determined not by expression (I-1), but by the time at which the magnetic induction at the surface of the conductor reaches a certain value [48], [137] (see Section I-B).

Comparing the characteristic time of growth of ETIs, $\tau_{\text{ther}} \approx 1/\gamma_m$, with the explosion time τ_{ex}, we obtain

$$\frac{\tau_{\text{ex}}}{\tau_{\text{ther}}} \approx \frac{\bar{h}}{\bar{h}_2} \ln \frac{T_{\text{cr}}}{T_{\text{melt}}}. \tag{II-11}$$

Relation (II-11) indicates that the time of growth of ETI is comparable to (but always less than) the explosion time. This suggests that the ETIs that inevitably occur in an electrical explosion of a metal do not depend of the explosion regime.

Comparing the time τ_{ther} with the characteristic time of growth of MHD sausage instability, τ_{inst}, defined by relation (I-4), we obtain an expression for the threshold current density [86], [157]

$$j_{\text{cr}} \approx \frac{\bar{h}_2}{2 \ln \frac{T_{\text{cr}}}{T_{\text{melt}}}} \sqrt{\frac{\mu_0}{\rho}}. \tag{II-12}$$

At current densities lower than j_{cr}, sausage instabilities grow faster than electrothermal ones, and at current densities higher than j_{cr}, ETIs prevail. The values of j_{cr} are close to the current density values determined by inequality (6); that is, they are of the order of $\sim 10^8$ A/cm^2. It follows that in a fast explosion mode, ETIs are most dangerous, and in a slow mode, they develop in parallel with the (more rapidly growing) sausage instabilities.

More detailed information on the mechanisms of development of ETIs, in particular, on the effect of the phase state of the material, can be obtained by considering not only the equation describing temperature variations but also the equations that describe the variations of density and momentum. In this case, the dispersion equation in γ is a cubic algebraic equation of the form [86], [161]

$$\gamma = \frac{j^2 \left(\frac{\partial \delta}{\partial T} + \frac{\delta}{T^*} - \frac{\rho}{T^*} \frac{\partial \delta}{\partial \rho} \right) - k_z^2 \kappa}{\rho c_V + \frac{p}{T^*}} \tag{II-13}$$

where $T^* = \rho((\partial p/\partial \rho) + \gamma^2/k_z^2)(\partial p/\partial T)^{-1}$ is a function expressed in units of temperature.

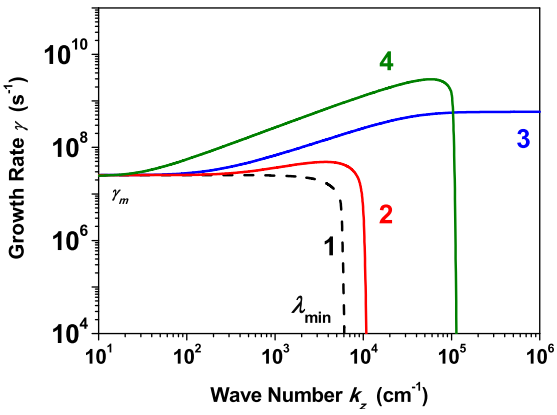

Fig. 8. Dispersion curves showing the relationship between the instantaneous instability growth rate γ and the wavevector axial component k_z calculated with no account of pressure (curve *1*), for a liquid phase (curve *2*), for a liquid-vapor mixture (curve *3*), and for a superheated metastable liquid (curve *4*).

Let us discuss the effect of the phase state of the material on the growth of ETIs by the example of an exploding aluminum wire [158], [161]. To do this, we consider the dispersion curves for the liquid, two-phase, and metastable regions, separated by the binodal, in which each of these phase states may exist. The instantaneous growth rates were calculated based on wide-range semiempirical equations of state [106] providing for the existence of metastable states (both a superheated liquid and a supercooled vapor). The resistivity of aluminum and its derivatives with respect to temperature and density were determined using tabulated data [111].

Fig. 8 presents the dispersion curves obtained for an exploding aluminum wire. The curves show the relationship between the instantaneous instability growth rate γ and the wavevector axial component k_z calculated for the current density $j = 10^8$ A/cm^2, temperature $T = 0.4$ eV, and the material density close to that on the binodal, $\rho_{bin} \approx 1.6$ g/cm^3. The calculations were performed for a pressure equal in absolute value to the saturated vapor pressure $p = \pm 156$ atm (the pressure in the region of metastable superheated metal states is negative). The dashed line in Fig. 8 refers to γ calculated by relation (20), that is, with no account of pressure, and the solid lines correspond to a liquid, a droplet-vapor mixture, and a superheated liquid metal. Note that when the metal being heated goes over into a liquid state, the instability modes with wavelengths less than λ_{min} are damped (see Fig. 8). Hence, it is quite probable that in exploding wires, the perturbations with $\lambda \approx \lambda_{\text{min}}$ are most unstable.

Analysis of the calculation results shows that the growth of ETIs is mainly affected by three destabilizing factors: first, the existence of a positive temperature derivative of resistivity, $(\partial \delta/\partial T) > 0$; second, the existence of a negative density derivative of resistivity, $(\partial \delta/\partial \rho) < 0$; and, third, the existence of a positive time derivative of temperature, $(\partial T/\partial t) > 0$. The values of instantaneous growth rates in the long-wavelength part of the spectrum are determined mainly by the derivative $(\partial \delta/\partial T)$. In this spectrum part, the values of γ for all phase diagram regions are close to each other. In the short-wavelength part of the spectrum, the values of γ

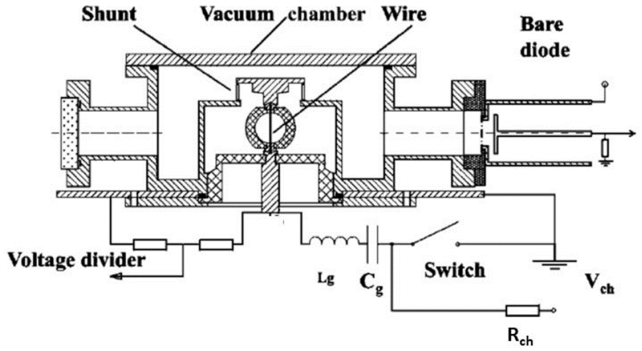

Fig. 9. Schematic of a setup containing a vacuum chamber with a WE load and an *LC* pulser. $L_g = 730$ nH and $C_g = 67$ nF are the pulser inductance and capacitance, respectively; V_{ch} and R_{ch} are the charge voltage and resistance, respectively. The current in the pulser circuit, the voltage across the load, and the discharge radiation were measured using a shunt, a RVD, and a BD. Adapted from [82].

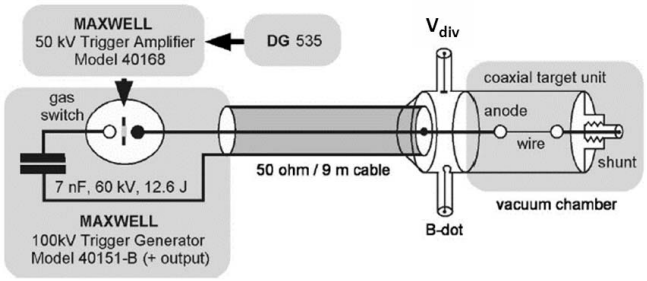

Fig. 10. Electrical diagram of an LC pulser and a vacuum chamber with an exploding wire load. The shunt and the B-dot probe are used for measuring currents; V_{div} is a CVD. Adapted from [94].

are determined by the derivatives $(\partial\delta/\partial\rho)$ and $(\partial T/\partial t)$, and the behavior of the instantaneous growth rate as a function of the wavenumber is essentially different in different regions of the phase diagram. Calculations [158] show that in the two-phase and metastable regions, the amplitude values of γ may be greater than their maximum values in the liquid region by more than two orders of magnitude. Therefore, in an exploding wire, the growth rate of ETIs increases substantially if the phase trajectory of the metal falls into a two-phase or a metastable region.

III. Experimental Arrangements for Studying the WE in Vacuum

An experimental setup intended to study the WE phenomenon should provide pulsed currents of density 10^8–10^9 A/cm^2 in the test wire that would rise at rates reaching 10^{10}–10^{12} A/s. It is also important to have reliable instruments and methods for measuring currents and voltages at these current rates. This section of the review briefly describes the equipment and diagnostics typically used in WE experiments. To become aware of the basics of pulse power technology, the reader may refer to the monographs by Bluhm [162] and Mesyats [40].

The simplest way to produce a current rate of 10^{10}–10^{12}A/s is to discharge a capacitor of capacitance C into the test wire. In this type of circuit, the current rate is limited by the inductance of the discharge circuit, L, which is the sum of the inductances of the capacitor, the switch, and the chamber in which the test wire is placed. The electric circuit of a typical *LC* driver (*LC* pulser) is shown in Fig. 9 [82].

When driving a short-circuit (SC) low-inductance load, the pulser produced a damped sinusoidal current pulse. When wire loads were used, the wire current was measured with a shunt and the voltage across the wire was measured with a resistive voltage divider (RVD). The pressure in the chamber was maintained at 10^{-4}–10^{-5} torr [82], which is typical of the majority of WE experiments.

An important characteristic of the electric circuits used in WE experiments is the average current rate $(dI/dt)_{av}$ that can be provided by a given driver in an SC load. The usual SC load is a copper rod of diameter 1–2 cm and length 2–3 cm (see [19]. The short-circuit value of $(dI/dt)_{av}$ is conventionally estimated as $(dI/dt)_{av} = \Delta I/t_{rt}$, where t_{rt} is the current rise time, which is typically measured between the 10% and 90% levels of the amplitude current value I_{max}, and ΔI is the difference between the 10% and 90% values of I_{max}. In an *LC* pulser, I_{max} is determined by the charge voltage V_{ch}. In the WE experiments reported in [4], [81], [82], [123], [125], [126], [150], [151], and [163]–[171], I_{max} was in the 3–5 kA range and the quarter period of the (sinusoidal) current pulse was in the 300–500 ns range; hence, the *LC* pulser provided $(dI/dt)_{av}$ that ranged between 10 and 70 A/ns. The use of *LC* pulsers with low-inductance, low-capacitance (0.2–1 nF) capacitors made it possible to increase $(dI/dt)_{av}$ to 100–170 A/ns [19], [172]–[175]. However, in these cases, the intrinsic impedance of the driver became comparable to the resistance of the exploded wire, and the actual rate of the wire current is decreased. For instance, Wu *et al.* [174] report that for $(dI/dt)_{av} = 100$ A/ns, the rate of the current in an exploded 13-μm tungsten wire was 47 A/s.

Sarkisov *et al.* [94], [152], [176]–[179] proposed a driver for WE experiments which combines an off-the-shelf voltage pulse generator capable of producing nanosecond-rise time currents and a segment of coaxial cable. An experimental arrangement containing this type of driver [94] is exemplified in Fig. 10.

In the circuit shown in Fig. 10, the pulser is connected to the coaxial target unit via a piece of cable of impedance $Z = 50\ \Omega$. The duration of the current first "wave" passing through the low-resistance load ($R_{load} \ll Z$) equals the doubled electric length of the cable, and the current amplitude is $2V_{ch}/Z$ (V_{ch} is the charge voltage of the pulser capacitor). By the duration of the current first "wave," we mean, in this context, the time from the onset of current flow to the time when the current changes its direction. In general, the duration of damped oscillations in the circuit shown in Fig. 10 is determined by the losses due to the circuit resistance. If the inductance of the coaxial target unit is not greater than 50 nH, the rise time of the current pulse passing through the circuit with the SC load is approximately equal to the rise time of the pulser current. Using circuits containing a cable generator, Sarkisov *et al.* [94], [152], [176]–[179] obtained $(dI/dt)_{av} =$ 150–170 kA/ns.

In conducting WE experiments, it is important to provide reliable contacts between the wire and the electrodes. In the experiments reported in [170], the wire–electrode contacts were modified by soldering the cathode ends of the wires to the electrodes. According to [170], "laser shadowgraphic images showed that nonsoldered wires had a tapered expansion at each electrode" at $(dI/dt)_{\text{av}} = 15$ A/ns for wires of length 1–2 cm. Despite the difference in expansion uniformity between soldered and nonsoldered wires, the single wire experiments [170] showed insignificant difference in the peak resistive voltage and, therefore, in the deposited energy. In these experiments, the length of the expanded region was 1–2 mm. Therefore, it is very likely that for shorter wires, there would be a marked difference in the deposited energy between soldered and nonsoldered wires. However, no relevant data have been published thus far.

Soft metal (indium and silver) gaskets were used to reduce the contact resistance between the wire and the electrodes in an aluminum wire array [171]. In the WE experiments [81], [82], [123], the wire was placed in a dielectric holder mounted between the electrodes. The wire was soldered to auxiliary electrodes mounted inside the holder. After soldering, the wire-containing holder was placed in the vacuum chamber.

A key metric in WE experiments is the energy deposited in the exploding wire, ε_{dep}. This energy is estimated from measurements of the voltage across and the current through the wire. The design features and equivalent circuits of the proper voltage and current sensors can be found in [162], [180], and [181]. In this review, we only dwell on the sources of errors that may occur in particular conditions of measuring currents and voltages in WE experiments.

In the experimental arrangements intended for WE studies, two types of voltage sensors are used: RVDs and capacitive voltage dividers (CVDs). In general, any voltage divider is a two-port network. The voltage to be measured is applied to the high-voltage (HV) input, and the low-voltage output signal is fed to an oscilloscope through a cable. A nondistorting measuring device faithfully reproduces the input voltage waveform at the output. This is possible in the only case that the HV arm of the divider is quite similar to the low-voltage arm from which the measured signal is taken off. Unfortunately, such a perfect voltage divider is impracticable. In actual devices of this type, stray inductances and stray capacitances are inevitable. The response function of a voltage divider is generally defined as the response of the divider to a unit pulse.

In what follows, we consider several simple formulas that indicate how the stray inductance affects the transfer functions of a voltage divider and discuss how these formulas can be used to predict measurement errors in WE experiments under vacuum conditions.

In these experiments, an RVD, because of the low vacuum flashover strength, is always placed outside the vacuum chamber. At expected voltages of 40–70 kV, the resistance of its HV arm is of the order of kiloohms; therefore, the stray inductance for the HV arm can be neglected. For this case, the RVD response function can be approximately described as [181]

$$V_2 = \frac{1}{K} V_1 \left[1 - \exp\left(-t/\tau\right)\right] \qquad \text{(III-1)}$$

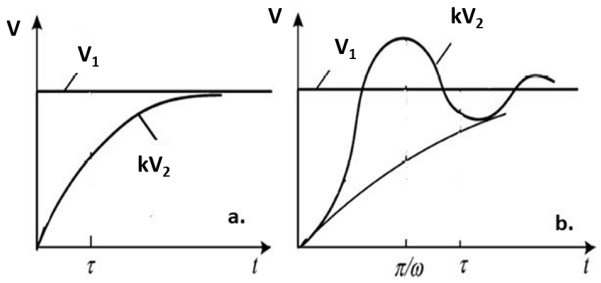

Fig. 11. Unit pulse responses of (a) RVD (increased voltage pulse rise time and smoothed sharp voltage fluctuations) and (b) CVD (voltage bursts and decaying oscillations during the pulse rise time). Adapted from [181].

where V_1 is the amplitude of the test unit pulse, V_2 is the amplitude of the signal arrived at the oscilloscope, $K = V_1/V_2$ is the step-down ratio of the divider, and $\tau = \sim (L/R_2)$, where L is the stray inductance of the divider low-voltage arm and R_2 is its resistance. In deriving (III-1) it was assumed that the cable connecting the voltage divider and the oscilloscope contains a matching resistor at the oscilloscope input. As follows from (III-1), an RVD distorts an input signal by increasing the voltage pulse rise time and smoothing sharp voltage fluctuations. Fig. 11(a) illustrates a typical response of an RVD to a unit pulse.

In experiments on WEs in vacuum, the RVD is structurally located inside a steel cylinder with the HV and low-voltage arm resistors located along the cylinder axis. As mentioned earlier, the RVD is outside the vacuum chamber. In WE experiments, as a rule, the RVD, if calibrated at τ no greater than 1 ns, does not distort the input signal.

In voltage measurements on the nanosecond scale, a CVD of special design, which sometimes is called a capacitive voltage probe [182], is used (see [162, Ch. 9]). In this device, the HV arm is the "capacitor" formed by the HV electrode and the plate of the capacitor that represents the low-voltage arm. This type of voltage divider was proposed by Fletcher [183]. Voltage dividers of this type were used in the WE experiments reported in [19], [174], [175], and [184]. For a capacitive voltage probe, the response to a unit pulse can be described approximately as

$$V_2 = \frac{1}{K} V_1 \left[1 - \exp\left(-t/\tau\right) \times \cos\left(\omega t\right)\right] \qquad \text{(III-2)}$$

where V_1 is the amplitude of the test unit pulse; V_2 is the amplitude of the signal at the oscilloscope input; $K = V_1/V_2$ is the step-down ratio of the divider; $\tau = \sim (L/R)$, where L is the stray inductance of the divider and R is its resistance; and $\omega \sim 1/\sqrt{LC_1}$, where C_1 is the capacitance of the HV arm. The value of R, estimated with consideration of the skin effect in leads and the dielectric losses in the divider capacitors, is of the order of several ohms. At the same time, the wave impedance of the divider may reach hundreds of ohms. Therefore, when CVDs are used in experiments on WE in vacuum, the measured pulse waveform is most probably distorted when resonance oscillations occur at the natural frequencies of the LC_1 circuit [see Fig. 11(b)]. In some cases, the resonance oscillations may cause doubling the measured

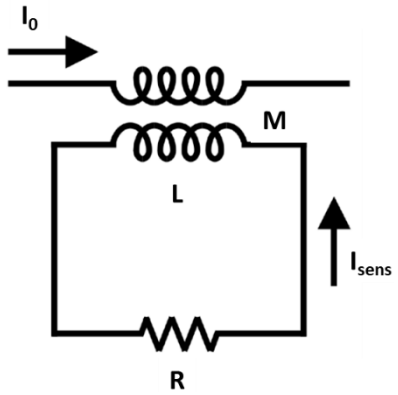

Fig. 12. Sketch of the circuit of a model current sensor containing a B-dot probe or a self-integrating RC. M is the mutual inductance between the HV electrode and the current sensor, L is the sensor inductance, and R is the resistance of the coil terminating resistor. Adapted from [180].

pulse amplitude. Resonance oscillations can be avoided by calibrating CVDs with rectangular voltage pulses.

In WE experiments, three types of current sensors are used: B-dot probes, self-integrating Rogowski coils (RCs), and shunts. The principle of operation of the first two types of sensors is based on Faraday's law. A variation in magnetic flux at the location of a loop consisting of one or several turns (for a B-dot probe) or a multiturn coil (for a self-integrating RC) determines the current in the loop or coil. The circuit diagram of a self-integrating RC is sketched in Fig. 12. The signal V_{sens} that occurs when a current flows through the coil terminating resistor of resistance R is used to estimate the measured current I_0.

For these sensors, the measured current I_0 is related to the voltage V_{sens} as [181]

$$I_0(t) = \frac{1}{M}\left(\frac{L}{R}V_{\text{sens}}(t) + \int_0^t V_{\text{sens}}(t)\,dt\right) \qquad \text{(III-3)}$$

where M is the mutual inductance between the HV electrode and the B-dot probe, L is the sensor inductance, and R is the resistance of the coil terminating resistor, i.e., the resistor through which the sensor current flows. When the first term on the right-hand side of (III-3) is much greater than the second one, the output voltage of the current sensor, V_{sens}, is approximately proportional to I_0. In this limit, the sensor is said to be a self-integrating RC. When the first term is much smaller than the second one, the output voltage of the sensor is approximately proportional to dI_0/dt, and the sensor is said to be a B-dot probe.

A B-dot probe measures the time derivative of a current-induced magnetic field. A detailed description of the design and calibration features of this type of sensor for $(dI/dt) = 10^9$–10^{11} A/s is given in [180]. The B-dot probe signal is numerically integrated to reconstruct the current signal. A conventional B-dot probe consists of a single loop of copper wire whose ends are connected to a coaxial cable. The inductance of the loop, L, is generally 40–60 nH [185]. The coaxial cable acts as a terminating resistor for the probe; that is, we have $R = Z$, where Z is the impedance of the probe output cable. In measuring the rise time of a rectangular current pulse, the 10%–90% rise time of the B-dot current is determined as

$$\tau_{10\%-90\%} = \frac{2.2L}{Z} \qquad \text{(III-4)}$$

where Z is the cable impedance ($Z = 50\ \Omega$ for conventionally used cables). Thus, (III-4) yields $\tau_{10\%-90\%} = 1.76$–2.64 ns. In some cases, two B-dot probes are used to suppress common mode noise [180]. In this type of sensor, the opposite-polarity signals pass through a balun, which suppresses high-frequency noise.

When experimenting with exploding wires, it is highly undesirable to place a B-dot probe at the entrance to the load unit. The displacement current flows through the stray capacitance between the HV electrode and the return current rods, C_{HV}. The capacitance C_{HV} appears to be connected in parallel with the load. Therefore, the current I_0 recorded using the B-dot probe is

$$I_0(t) = I_{\text{wire}}(t) + I_{C_{\text{HV}}}(t) \qquad \text{(III-5)}$$

where I_{wire} is the current flowing through the exploding wire and $I_{C_{\text{HV}}}$ is the displacement current in the circuit containing C_{HV}. For a coaxial entrance to the vacuum chamber, C_{HV} may be several and even tens of picofarades. The time derivative of the current $I_{C_{\text{HV}}}$ can be found as

$$\left(\frac{dI}{dt}\right)_{C_{\text{HV}}} = \frac{\exp(-t/R_{\text{dr}}C_{\text{HV}})}{R_{\text{dr}}} \times \left\{\frac{dV(t)}{dt} - \frac{V(t)}{R_{\text{dr}}C_{\text{HV}}}\right\} \qquad \text{(III-6)}$$

where R_{dr} is the impedance of the driver and $V(t)$ is the load input voltage. For a voltage pulse of amplitude 20 kV and rise time 2 ns arriving at the input of the load unit, according to (III-6), we have $(dI/dt)_{C_{\text{HV}}} = 140$ A/ns at $R_{\text{dr}} = 50\ \Omega$ and $C_{\text{HV}} = 4$ pF and 460 A/ns at $R_{\text{dr}} = 50\ \Omega$ and $C_{\text{HV}} = 6$ pF, respectively. It follows that placing a B-dot probe at the entrance to the load unit may introduce a significant measurement error. Therefore, in WE experiments, it seems more reasonable to place a B-dot probe at the outlet of the load unit, although even with this arrangement, the possibility of occurrence of a stray capacitance should be considered.

A self-integrating RC is a toroidal multiturn coil containing a terminating resistor of resistance $R = 0.1$–$0.3\ \Omega$. The operation of a self-integrating RC is discussed in detail in [186]. As mentioned, the voltage drop across the coil terminating resistor of resistance R is proportional to the current I_0. In measuring the rise time of a rectangular current pulse, the 10%–90% rise time of the current flowing through the RC, $\tau_{10\%-90\%}$, is determined by the stray capacitance and inductance of the coil terminating resistor. According to [186], it is equal to several nanoseconds. It is more reasonable to place a RC, like a B-dot probe, at the outlet of the load unit.

A shunt is a low-resistance device connected in series with the exploded conductor. Conventionally, the shunt is connected to the grounding point of the circuit. The voltage drop across the shunt is proportional to the circuit current. As the shunt resistance is low (tens of milliohms), the stray inductance, even small, increases the time $\tau_{10\%-90\%}$. It may also increase the impedance of the shunt.

To calibrate current and voltage sensors at current rates of 10^9–10^{11} A/s, it seems reasonable to use a pulse generator with a mercury-wetted reed-relay switch. This type of switch is capable of providing a rectangle voltage pulse with rise time of several hundreds of picoseconds and voltage amplitude of about 750 V [182]. A detailed description of the calibration procedure is given in [180], [182], and [185].

IV. Experimental Data on the Explosion of Fine Wires in Vacuum

A. Deposited Energy

As mentioned earlier, the studies on the generation of soft X-ray pulses by the plasma shell formed from an exploded wire array gave impetus to experiments on WE in vacuum. When using wire arrays in experiments with imploding plasma shells, it is desirable to have a plasma shell uniform in the radial, axial, and azimuthal directions. The initial idea of using wire arrays [97] was to attain a situation in which the material of individual wires would completely go into a gas–plasma phase just before the arrival of a high-power (terawatt) pulse. It was supposed that a plasma shell might be formed due to the wire expansion and plasma formation initiated by a 50–100 ns, 0.1–1-kA wire current ramp (prepulse). However, the first experiments performed at Cornel University [4], [126], [150], [151], [168], [169] showed that the energy deposition to an exploded fine wire stopped much earlier than the specific deposited energy ε_{dep} became equal to the specific atomization energy $\varepsilon_{\text{atom}}$. Assuming that the greater the energy deposited in an exploded wire, the more efficient is the radiation production by the wire array, it is important to understand what are the mechanisms that limit the energy deposition. In this section, we will consider, first, the results of the WE experiments that made it possible to understand why ε_{dep} is lower (sometimes much lower) than $\varepsilon_{\text{atom}}$. Second, we will discuss some methods which can be used to ensure complete vaporization of an exploded wire, that is, to fulfill the condition $\varepsilon_{\text{dep}} \geq \varepsilon_{\text{atom}}$.

In terawatt pulse generators loaded with a wire array, the cathode is always a HV electrode. This is why most of the experiments on the WE in vacuum were performed with the HV electrode having negative polarity, although, from the viewpoint of increasing the energy deposited in the exploded wire, it would be reasonable that the HV electrode would be of positive polarity [15]. When discussing the experimental data in the following, we will assume by default that the HV electrode is the cathode. For the data obtained with the HV electrode of positive polarity (anode), special notes will be made.

Fig. 13 presents the current and voltage waveforms and the time-varying deposited energy $\varepsilon_{\text{dep}}(t)$ typical of WEs in vacuum. The voltage waveform represents an inductively corrected voltage across the wire, which is defined as

$$V = V_{\text{div}} - L\frac{dI}{dt} \tag{IV-1}$$

where V_{div} is the measured divider voltage and L is the load inductance. The inductance L is the net inductance of the vacuum chamber and the exploded wire. The energy $\varepsilon_{\text{dep}}(t)$ was estimated as

$$\varepsilon_{\text{dep}}(t) = \frac{1}{\pi r_0^2 \rho l}\int_0^t V I dt \tag{IV-2}$$

where r_0 is the wire radius, ρ is the wire material density, l is the wire length, I is the current through the wire, and V is the inductively corrected voltage across the wire.

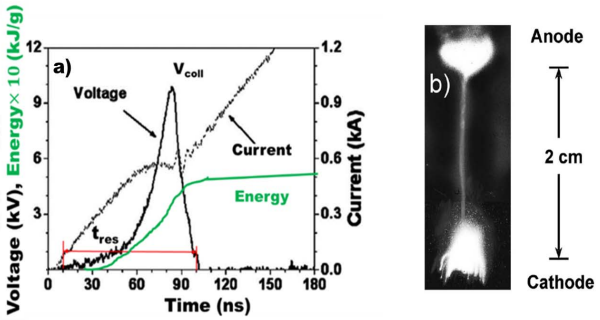

Fig. 13. (a) Current and inductively corrected voltage waveforms and the time-varying deposited energy for the explosion of a 30.48-μm-diameter, 2-cm-long W wire (t_{res} is the time at which $R_{\text{wire}} = 0.1\ R_{\text{wiremax}}$) and (b) image of the self-radiation of the discharge channel taken at $t \sim t_{\text{coll}}$ with an exposure time of 10 ns. The melting energy for tungsten $\varepsilon_{\text{melt}} = 0.8$ kJ/g. Adapted from [82].

The voltage and current waveforms shown in Fig. 13 indicate that the wire goes through a short resistive heating phase during which it is heated by the Joule mechanism. The wire resistance R_{wire} increases with temperature, and so does the resistive voltage across the wire, $V(t)$. We define the duration of the resistive phase as the time from the onset of current flow to $t = t_{\text{res}}$ (t_{res} is the time at which $R_{\text{wire}} = 0.1\ R_{\text{wiremax}}$). The value of ε_{dep} at $t = t_{\text{res}}$ estimated by relation (IV-2) is somewhat greater than the actual energy deposited in the wire material. This is due to the fact that during the formation of the corona (see Section IV-C), the energy delivered to the discharge is deposited, for a certain time, not only into the core but also into the surrounding plasma corona. The energy deposited in the corona makes 5%–10% of that deposited in the core. At $t = t_{\text{coll}}$, when the voltage peaks at $V(t) = V_{\text{coll}}$, a so-called voltage collapse occurs: shunting of the wire core begins and a plasma corona is formed around the core. Note that in some studies (see [151], [165]), t_{res} is determined as the time from the onset of current flow to the beginning of corona formation. The different approaches in determining t_{res} give values of the energy deposited in the wire which are within the dispersion limits. After $t = t_{\text{res}}$, the discharge current flows completely through the corona surrounding the core.

The time in which the voltage falls from V_{coll} to zero, t_{fall}, depends on the wire length and surface condition. The characteristic times of a WE in vacuum (t_{coll}, t_{res}, and t_{fall}) are significantly determined by the processes responsible for the initiation and development of a discharge in the gas layer in which the corona is formed. It is precisely due to the stochastic nature of the processes involved in the gas breakdown [134] that there is a large shot-to-shot variability in both the energy deposition time and the deposited energy ε_{dep} (Table II and Fig. 17). Framing photography [see Fig. 13(b)] shows bright

TABLE II

RELATIVE ENERGY INPUT VALUES FOR EXPLODED 25-μM BARE WIRES MADE OF VARIOUS METALS. THE MELTING AND BOILING POINTS AND THE ATOMIZATION ENERGY ε_{atom} ARE TAKEN FROM [190], AND THE RESISTIVITY IS TAKEN FROM [191]

Wire materials	$\varepsilon_{dep}/\varepsilon_{atom}$, %	Resistivity, nΩ·m	Melting point, K	Boiling point, K	Atomization enthalpy, kJ/g
Ag	55–81	16	1235	2435	2. 6
Cu	37–47	17	1358	3200	5.3
Au	45–53	22	1337	3129	2.2
Al*	51	26	933	2792	12.1
Mo	16	50	2896	4912	6.2
Zn	67–90	59	692	1180	2.1
Fe(SS)	24	70	1811	3134	7.4
W	8–14	55	3695	5828	4.3
Nb	17	152	2750	5017	8.2
Ti	9	420	1941	3560	9.8

*The data are taken from [165].

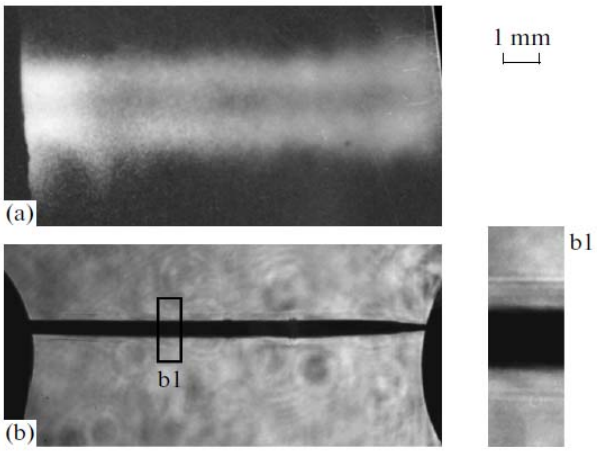

Fig. 14. Explosion of a 25-μm-diameter, 1.2-cm-long Al wire, $(dI/dt)_{av}$ = (10–20 A/ns), $t_{res} \sim 120$ ns. (a) UV image of the discharge channel obtained 155 ns after the onset of current flow at an exposure time of 5 ns. (b) Shadow image of the core obtained 155 ns after the onset of current flow with the use of the second harmonic of a YAG:Nd +3 laser with $\lambda = 532$ nm. Reprinted with permission from [187]. Copyright 2012, Springer Publishing.

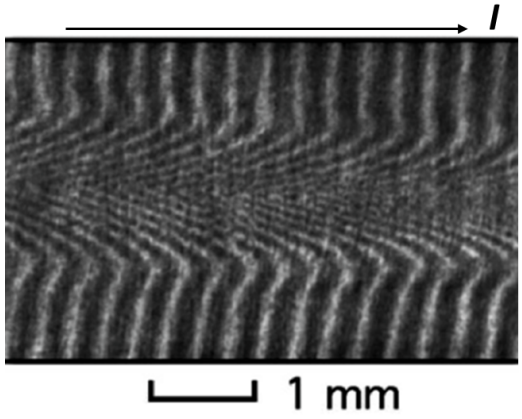

Fig. 15. Laser interferometry image of an exploded 25-μm-diameter, 1-cm-long Ag wire ($t = 313$ ns); $(dI/dt)_{av} = 15$ A/ns, $t_{res} \sim 80$ ns; the arrow shows the direction of current I. Adapted from [151].

luminous regions at the electrodes in addition to the luminous channel around the wire. Sarkisov *et al.* [133] performed an experiment with fast-exploding 25.4-μm nickel (Ni) and stainless-steel (SS) wires. The anode served as the HV electrode. The ionization wave propagated in the gas medium from the cathode along the wire surface; its velocity for Ni and SS-304 wires was measured to be $(1–4)\cdot 10^6$ m/s [133]. Using a two-frame intensified charge-coupled device imaging system with a 2-ns exposure time, Sarkisov *et al.* [133] detected luminous regions at the electrodes 1–2 ns ahead of the occurrence of the ionization wave.

The corona and the core of an exploded wire can be clearly seen in Fig. 14 [187]. Figure 14(a) presents an image of the discharge channel radiating in the UV range during the explosion of a 25-μm, 1.2-cm-long Al wire. Fig. 14(b) shows a shadow image of the same discharge channel obtained with the use of a YAG:Nd +3 laser ($\lambda = 532$ nm). Both images were taken 155 ns after the onset of current flow through the wire (the energy deposition to the wire proceeded within $t_{res} \sim 120$ ns). The image shown in Fig. 14(a) clearly demonstrates that a bright luminous corona surrounds the wire core that does not radiate in the UV range. At the same time, the corona is poorly visible in the shadow image, and we see a dense core opaque to the laser radiation.

The core and the corona of an exploded 25-μm Ag wire can well be seen in the interferogram presented in Fig. 15 [151], which was taken 313 ns after the onset of current flow, that is, about 220–230 ns after the shunting of the wire core. We see that the interference fringes are shifted in different directions. At the center of the pattern, the fringe shifts are directed opposite to the current. The shifting is due to the refraction of the laser light by neutral Ag atoms that have appeared during the expansion of the core. In the corona region, the fringes are shifted in the opposite direction, and the shifting is due to the refraction of the laser light by free electrons. The radius within which the refraction by neutral atoms goes to the refraction by free electrons is approximately equal to the radius of the

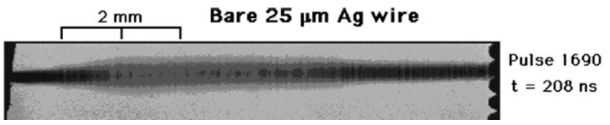

Fig. 16. Radiograph of an exploding 25-μm Ag wire taken at $t = 208$ ns after the onset of current flow through the wire; $(dI/dt)_{\text{av}} = 15$ A/ns, $t_{\text{res}} \sim 80$ ns. Reprinted with permission from [151]. Copyright 2001, AIP Publishing LLC.

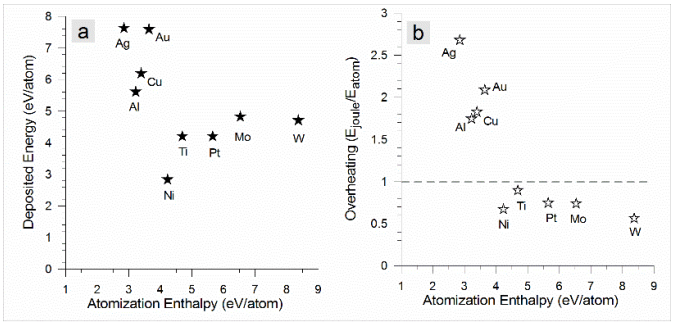

Fig. 17. (a) Deposited energy averaged over several shots and (b) $\varepsilon_{\text{dep}}/\varepsilon_{\text{atom}}$ versus atomization enthalpy of metals for fast (150 A/ns) and slow (20 A/ns) explosions of 20-μm wires. Positive polarity. Reprinted with permission from [152]. Copyright 2001, AIP Publishing LLC.

core. According to the measurements [151], at the 313th ns, the neutral particle density in the core was $\sim 8 \cdot 10^{19}$ cm^{-3}, whereas the electron density in the corona was not greater than $5 \cdot 10^{16}$ cm^{-3}. Note that the core radius varied even within a small segment of the interference pattern shown in Fig. 15.

The first experiments utilizing X-ray backlighting for fast WEs in vacuum were performed by a team from Cornel University [4], [126], [150], [151], [168], [169]. X-ray backlighting also revealed the presence of a corona and a core for wires exploded in vacuum. Fig. 16 shows a radiograph of an exploding 25-μm Ag wire [151]. The radiograph was taken with an exposure time of 0.25 ns at the 208th ns after the onset of current flow, which approximately corresponded to the 80th ns after the shunting of the wire.

In contrast to laser shadow imaging, X-ray backlighting makes it possible to see the internal structure of the wire core. In particular, in Fig. 16, we can see striations, whose formation mechanism was discussed in Section II-D. Both the laser shadow image and the radiograph (see Figs. 14(b) and 16, respectively) indicate that the core expands nonuniformly: its diameter at the electrodes is noticeably smaller than that at the center of the image.

Axial nonuniformity in expanding wire cores was also observed in other experiments (see [176], [178]). In the experiments described in [163] and [170], the nonuniform core expansion was caused by the electrode plasma that shunted part of the wire. This electrode plasma was generated by the arcs that occurred between the electrodes and the wires due to poor contacts. Soldering the wire to the cathode reduced the plasma expansion at this electrode, presumably because it mitigated arcing. However, single wire experiments [170], despite the difference in expansion uniformity, showed insignificant differences in collapse voltage and, therefore, in deposited energy between soldered and nonsoldered wires. The axial nonuniformity adds ambiguity in estimating the specific energy deposited in an exploded wire, ε_{dep}, as follows from relation (IV-2). However, this ambiguity is difficult to quantify, and so it is generally ignored.

Sinars *et al.* [151] performed a series of WE experiments with different wire materials, including Al, Ti, Fe, Cu, Zn, Nb, Mo, Ag, W, Au, and Pt. In the experiments, the current rate $(dI/dt)_{\text{av}}$ was 15 A/ns, the peak current was 4.5 kA, the wire diameter was varied from 7.5 to 25 μm, and the wire length was 1 cm. Sinars *et al.* [151] used unsoldered wires. Using X-ray backlighting and laser diagnostics, they observed the formation of a corona and a core for all the bare wire materials used. They also investigated the explosion of insulated wires; preliminary results of that experiment are reported in [150]. Let us first discuss the experimental results for bare wires.

Note that the energy deposited in a wire exploded in vacuum is proportional to the wire length. Sinars *et al.* [151] compared the results obtained for bare 25-μm Ag wires of different lengths: 1, 2, and 3 cm. It turned out that the electric field along the wire at the time of voltage collapse, E_{coll}, and the energy deposited in the wire per unit length, ε_{dep}, were nearly invariant with wire length (see [152, Table II]). At the same time, the experiments performed by Shi *et al.* [19], [188], [189] for bare Al and Cu wires of different lengths: 0.5, 1, and 2 cm, showed that both E_{coll} and ε_{dep} decreased with increasing wire length. The contradiction between these two results is related to the different impedances of the drivers that were used for the WE experiments described in [151] and in [19], [188], and [189]. In the experiments of Sinars *et al.* [151], the driver impedance, estimated from short-circuit waveforms, was close to 100 Ω, that is, it was significantly greater than the wire resistance under Joule heating (about 8–15 Ω). However, in the experiments of Shi *et al.* [19], [188], [189], the driver impedance was about 10–15 Ω, which is comparable to the resistance of a wire under Joule heating. As a result, in the experiments [19], [188], [189], the current decreased with increasing wire length. It follows that the current rate for a wire of length 0.5 cm will be considerably higher than that for a wire of length 3 cm. Therefore, in the experiments [19], [188], [189], ε_{dep} should be maximum for wires of length 0.5 cm, as was just observed.

For metals, the energies of vaporization, ε_{vap}, and atomization, $\varepsilon_{\text{atom}}$, are different by 5%–10%. The differences in the absolute values of ε_{vap} and $\varepsilon_{\text{atom}}$ between different metals are in the range of ambiguity. In this review, when discussing experimental data presented in an article, we will use the value of specific vaporization energy ensuring a complete solid-to-gas transition that is used by the authors of the cited article. If the authors of a cited article do not indicate the absolute value of vaporization energy that they use to estimate the relative energy input $\varepsilon_{\text{dep}}/\varepsilon_{\text{atom}}$, we will use the relevant data of the National Institute of Standards and Technology (NIST) [190].

Table II gives the values of relative energy input $\varepsilon_{\text{dep}}/\varepsilon_{\text{atom}}$, expressed in percentage, which were obtained for exploded 25-μm bare wires made of various metals. All the data were taken from [151], except for the data for Al wires, which were

taken from [164]. Table II also lists the values of resistivity at 393 K, melting and boiling points, and atomization energy $\varepsilon_{\text{atom}}$ for the respective metals.

The data given in Table II show a certain trend in the dependence of $\varepsilon_{\text{dep}}/\varepsilon_{\text{atom}}$ on material properties: the value of $\varepsilon_{\text{dep}}/\varepsilon_{\text{atom}}$ decreases with increasing resistivity. However, this is not the case for all materials; we see that the relative energy input for Zn ($\delta = 55$ nΩ·m) is much greater than that for low-resistivity metals (Ag, Cu, Al, and Au). As Sinars *et al.* [151] rightly suggest, the anomalous behavior of the Zn wires is associated with the low atomization energy of Zn. The small relative energy input for Ti wires also attracts attention. A possible reason for the anomalously low energy input is the unique ability of Ti to absorb hydrogen. Indeed, the concentration of hydrogen dissolved in Ti under normal conditions is $4 \cdot 10^{21}$ cm^{-3} [192], whereas for other metals, it is not above 10^{15} cm^{-3}. As a result, at a comparatively low energy input, most of the hydrogen dissolved in titanium is desorbed even at a comparatively low temperature (≈1000 K), resulting in the development of a shunting discharge along the wire in about 30 ns.

As can be seen from the data of Table II, when $(dI/dt)_{\text{av}} <$ 15 A/ns, it is impossible to vaporize a bare wire by exploding it in vacuum, regardless of the wire material. Moreover, for some materials (W, Nb), the energy deposited in the wire is insufficient even to melt it. An effective way to increase the energy input is to explode conductors having insulating coatings, which was first described in [169]. In the experiment [151] performed with insulated Ag wires (25-μm Ag wire + 1- or 5-μm polyester), $\varepsilon_{\text{dep}}/\varepsilon_{\text{atom}}$ was 225%–304% (13 shots) and 82%–120% (seven shots), respectively. Sinars *et al.* [151] believe that the 5-μm insulated Ag wires absorbed less energy than the 1-μm insulated wires because of poor initial electrical contact. For 1-μm insulated W wires (25-μm W wire + 1-μm polyester), $\varepsilon_{\text{dep}}/\varepsilon_{\text{atom}}$ was 28%–49% in contrast to 8%–14% attained for 25-μm bare W wires.

To increase $\varepsilon_{\text{dep}}/\varepsilon_{\text{atom}}$ for exploded bare wires, Sarkisov *et al.* [152], [176]–[179] proposed to increase the rate of the current flowing in the wire.

Increasing the current rate to 150–170 A/ns with the HV electrode being positive made it possible to obtain $\varepsilon_{\text{dep}}/\varepsilon_{\text{atom}} =$ 200% –300% for low-resistivity materials (Ag, Cu, Al, Au) and 0.5–0.9 for high-resistivity metals (Ti, Mo, Pt, W) [176]. The experiments [19], [123], [172]–[175], [184] also demonstrated the effectiveness of increasing $(dI/dt)_{\text{av}}$ as a means of increasing the energy input into the wire. Table III shows the experimentally obtained values of $\varepsilon_{\text{dep}}/\varepsilon_{\text{atom}}$ reported by various authors for W wires exploded at different values of $(dI/dt)_{\text{av}}$.

According to the data given in Table III, for W wires exploded with the HV electrode being positive, ε_{dep} is almost twice that attained with the HV electrode being negative. The effect of the electrode polarity on deposited energy ε_{dep} was first demonstrated in the experiment performed by Sarkisov *et al.* [15], where ε_{dep} increased by a factor of 1.3–1.8 for all test metals when the polarity of the HV electrode was changed from negative to positive.

TABLE III

EXPERIMENTALLY MEASURED DEPOSITED ENERGY ε_{dep} EXPRESSED AS A PERCENTAGE OF THE ATOMIZATION ENERGY $\varepsilon_{\text{atom}}$ FOR W WIRES EXPLODED AT DIFFERENT VALUES OF CURRENT RATE $(dI/dt)_{\text{av}}$ AND DIFFERENT DIAMETERS d

$\left(\frac{dI}{dt}\right)_{\text{av}}$ A/ns	d, μm	$\varepsilon_{\text{dep}}/\varepsilon_{\text{atom}}$, %	Notes	Refs
10	30	7	Bare wire	[82]
10	30	18	Heating of bare wire	
15	7.5	21–28	Bare wire	[152]
	11.5	13–21		
	25	8–14		
20	20	25	Bare wire	[177]*
40	30	12	Bare wire	[82]
40	30	30	Heating of bare wire	
50	25	20–24	Bare wire	[167]
47	13	15	Bare wire	[176]
100	15	40	Bare wire	[189]
150	20	75	Bare wire	[177]*
W wire with insulating coating				
15	25	28–49	5 μm**	[152]
60	12.5	20–25	3.5 μm**	[176]
100	15	140	2 μm**	[189]
170	12.5	38–52	3.5 μm**	[176]

*Positive polarity (HV electrode is anode).
**Thickness of the insulating coating.

Subsequently, this effect was confirmed in the experiments reported in [19] and [193]. The polarity effect is associated with the mechanism of the discharge development during a WE in vacuum. Optical imaging showed that in a WE in vacuum, the surface of the electrodes is completely covered with plasma several nanoseconds ahead the voltage collapse (see Fig. 13(b) and [153, Fig. 4] and [193, Fig. 5], respectively).

As shown in [194], plasma may occur at the cathode due to the surface breakdown and at the anode due to the electron flow. When the HV electrode is negative (cathode), the cathode plasma is a source of an intense electron flow due to the presence of an electric field. According to the measurements reported in [193], the electron emission current may reach 100–200 À.

In general, the mechanism underlying the polarity effect can be described as follows [15], [193]. The electrons emitted by the cathode plasma enter the region of crossed electric and magnetic fields. The magnetic field is produced by the current flowing through the wire.

As a result, under the action of the Lorentz force, the electrons arrive at the surface of the wire and ionize the desorbed gas, which intensifies the phase transition from a neutral gas to a plasma and leads to a voltage collapse at $V = V_{\text{coll}}$. With the HV electrode being positive (or at a low magnetic field), there is no external ionizer on the wire surface, and thus conditions arise which provide an increase in V_{coll}, and, hence, in ε_{dep}, compared with their values obtained with the HV electrode being negative.

According to the data presented in Table III, the relative energy deposited in an exploding wire, $\varepsilon_{\text{dep}}/\varepsilon_{\text{atom}}$, increases with current rate $(dI/dt)_{\text{av}}$ both for bare wires and for wires with insulating coatings. Shi *et al.* [188] were able to increase the energy input into an insulated W wire to values greater than the vaporization energy by increasing the current rate $(dI/dt)_{\text{av}}$ to about 100 A/ns. In the experiment, they used 15-μm W wires coated with 2-μm polyimide (PI); the wire length was 0.5 cm. In addition, special measures were taken to ensure good contact between the wire and the electrodes: the metallic oxide on the surface of the electrodes was removed with sandpaper, and then both ends of the wire were soldered with soldering tin to the electrodes in holes drilled in them. As a result, $\varepsilon_{\text{dep}} = 6.76$ kJ/g was obtained which is considerably greater than $\varepsilon_{\text{atom}} = 4.6$–$4.34$ kJ/g. It seems that this is the maximum energy input into a W wire exploded in vacuum that was reliably attained by the time of writing this review.

The energy input into a bare W wire can also be increased if conditions are provided in which the wire surface is free from contaminants. In the experiment performed by Pikuz *et al.* [126], W wires were cleaned by preheating them to about 2000 K for several minutes immediately before the application of pulsed voltage in order to eliminate adsorbed gases. The experiment was performed with 7.5-μm-diameter, 1.04-cm-long W wires at $(dI/dt)_{\text{av}} = 15$ A/ns. It was found that t_{res} was 10 ns for unheated wires and 20–23 ns for preheated wires. This allowed Sinars *et al.* [151] to state the following: "Assuming the voltage collapse indicates the development of a coronal plasma around the wire, the fact that this occurs earlier for the wire that is the one not preheated is consistent with the idea that preheating delays breakdown by eliminating easily desorbed gases." Measurements of the energy input in exploding 30-μm-diameter, 2-cm-long W wires [82], [125] showed that when a wire was heated to 1900 K, the energy deposited in the wire increased by a factor of 2–3 compared with an unheated wire at the same value of $(dI/dt)_{\text{av}}$ (see Table III).

B. Core Structure (Core Expansion and Stratification, and Microdrop Formation)

Once an exploding wire is shunted with the coronal plasma, the wire core starts expanding, as illustrated in Fig. 18, which presents the results of measuring the core diameter during an Ag WE at various points in time after the onset of current flow through the wire [151]. The core expansion velocity was measured for exploding 25-μm Ag bare wires and 25-μm Ag wires coated with polyester. The graph in Fig. 18 combines data from two different diagnostics: X-ray backlighting and laser interferometry. In the case of X-ray backlighting, the diameter of the wires was measured by scanning the radiographs into a computer and plotting the optical density profile to evaluate the full width of the wire core profile. In the case of laser interferometry, the plasma–neutral boundary seen in the image was assumed to be the outside edge of the wire core. Namely, Sinars *et al.* [151] used the point of zero net fringe shift between the negative refractive index shift caused by the plasma and the positive shift caused by the neutral metal vapor (see Fig. 15).

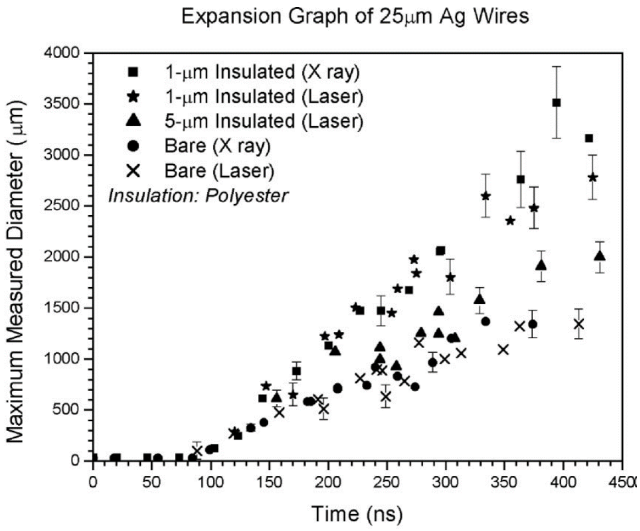

Fig. 18. Graph of the maximum measured wire core diameter versus time for 25-μm bare Ag wires and 25-μm Ag wires coated with polyester. The data points were extracted from radiographs and interferometric images. Reprinted with permission from [151]. Copyright 2001, AIP Publishing LLC.

According to Fig. 18, the values of the wire core diameter determined using X-ray backlighting and interferometry are the same within the measurement error. Note that the X-ray backlighting diagnostics showed that the core did not expand until it was shunted. The expansion velocity estimated from the data of Fig. 18 was $\sim 0.2 \cdot 10^6$ and $\sim 0.5 \cdot 10^6$ cm/s for 25-μm bare Ag wires and for 25-μm Ag wires with insulating coatings, respectively. The core expansion velocity v_{core} was determined by the values of radius obtained by the x-ray backlighting diagnostics.

As expected, the increase in expansion velocity for wires coated with polyester was associated with an increase in energy input: in the experiment [151], the energy input was 0.416 kJ/g for bare Ag wires and 6.5 kJ/g for Ag wires with polyester insulating coatings. In general, according to [151], the core expansion velocity at $(dI/dt)_{\text{av}} = (10$–$20)$ A/ns was in the range $(0.05$–$0.5) \cdot 10^6$ cm/s for bare wires made of various materials and in the range $(0.1$–$0.5) \cdot 10^6$ cm/s for wires with insulating polyester coatings. As mentioned in Section IV-A, the energy input into the core of a wire can be

increased not only by using insulating coatings; for bare wires, it can be increased by increasing the rate of the current flowing through the wire. Sarkisov and McCrorey [178] determined the core expansion velocity at current rates of 150–170 A/ns by using laser diagnostics (shadow images). In particular, for 20-μm bare Ag wires exploded at $(dI/dt)_{\text{av}} = 150$ A/ns, the energy input was 7.3 ± 0.6 kJ/g and the expansion velocity was $0.34 \cdot 10^6$ cm/s [178]. According to [178], the core expansion velocity at $(dI/dt)_{\text{av}} = 150$ A/ns was $(3–6) \cdot 10^5$ cm/s for bare wires made of Au, Cu, Ag, and Al and $(0.4–1) \cdot 10^5$ cm/s for bare wires made of W, Mo, and Pt. Shi *et al.* [19], Rousskikh *et al.* [123], Zhao *et al.* [172], Wu *et al.* [173], [174], and Li *et al.* [184] measured v_{core} values similar to those reported in [168] and [178].

In studies of the WE in vacuum, the question still remains open as to the specific energy that must be deposited in the wire core in order to completely transform the wire material into gas. For estimating the proportion of the wire material transformed into gas, Hamilton *et al.* [195] proposed to use the atomization coefficient $K_{\text{atom}} = N_{\text{lin}}/N_{\text{lin0}}$, where N_{lin} is the linear number density at the probing time and N_{lin0} is the initial linear number density of the wire material. Obviously, when $K_{\text{atom}} = 1$, the entire wire material is transformed into gas. The difference between N_{lin}, measured during the core expansion, and the initial linear number density of the wire material, N_{lin0}, was first detected by Sinars *et al.* [169] based on X-ray backlighting images of the exploded wires. In particular, for 25-μm bare Al wires, they found that 250 ns after the onset of current flow through a wire, the detectable wire core diameter was 250 μm, but the core contained only about 30% of the initial wire material. Pikuz *et al.* [126] do not indicate the value of energy input; however, based on the known $(dI/dt)_{\text{av}} = 15–20$ A/ns, it can be speculated that in their experiment, ε_{dep} was substantially lower than $\varepsilon_{\text{atom}}$.

Pikuz *et al.* [126] observed that part of the wire material did not transform into gas and persisted in the form of (X-ray opaque) microparticles. Eventually, the microparticles settled on the walls of the vacuum chamber. The fact that microparticles are formed during the explosion of a wire is well confirmed by the radiographs shown in Fig. 19 which were taken 2.32 and 10.75 μs after the onset of current flow through the wire ($t_{\text{res}} \approx 100$ ns). Romanova *et al.* [196] performed experiments with Ag wires 25 μm in diameter exploded at $(dI/dt)_{\text{av}} = 100$ A/ns. They observed that even when a considerable energy (equal to several atomization energies) was deposited into the wire material at the resistive stage of the discharge, part of the material remained condensed.

The detected microparticles may be both "coarse" undestroyed fragments of the wire and submicrometer-size droplets. Karakhanov [197] reports that in his experiment with exploding W wires, coarse fragments were observed when the energy deposited in the wire made 7% of the vaporization energy. When the percentage of the deposited energy was increased to 21%, droplets were detected [197]. A possible mechanism of the droplet formation for a wire with a liquid current-carrying core is proposed in [198] and [199]. The material of the liquid core does not reach its boiling point because of the compression caused by the self-magnetic field,

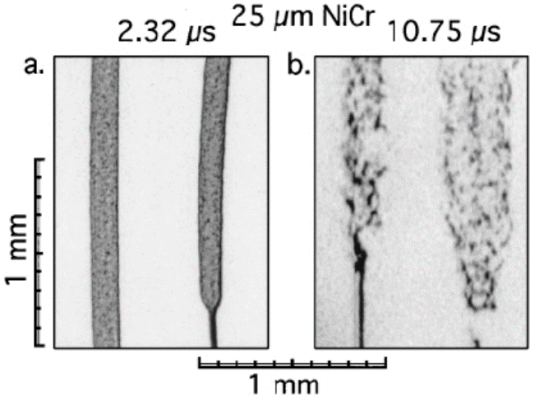

Fig. 19. Radiographs of exploding NiCr wires (two-wire loads) taken (a) 2.32 and (b) 10.75 μs after the onset of current flow. $t_{\text{res}} \sim 100$ ns, $(dI/dt)_{\text{av}} = 15$ A/ns. Reprinted with permission from [126]. Copyright 2000, AIP Publishing LLC.

whereas the equilibrium pressure of the vapor coexisting with the liquid core exceeds the saturation vapor pressure. The loss of thermodynamic equilibrium of the two-phase system is accompanied by the formation of liquid-phase nuclei in the metal vapor. According to the estimates of Tkachenko *et al.* [199], for the relative energy input $\varepsilon_{\text{dep}}/\varepsilon_{\text{atom}} = 50\%–100\%$, the average size of the microdrops is several tens of micrometers.

Wu *et al.* [174] and Hamilton *et al.* [195] investigated the process of atomization of Al wires exploded in vacuum at $(dI/dt)_{\text{av}} = 100$ and 160–200 A/ns, respectively. In both experiments, the linear density of Al particles in the discharge channel was estimated based on interferograms obtained using laser radiation ($\lambda = 532$ nm). The interferograms were taken 200–300 ns after the onset of current flow through the wire. Wu *et al.* [174] and Hamilton *et al.* [195] used the dynamic polarizability of neutral Al atoms $\alpha = 10.8 \cdot 10^{-24}$ cm^3 for $\lambda = 532$ nm [200]. In the experiment [195], the diagnostics was arranged so that the fringes in the interference pattern were parallel to the axis of the discharge channel. This made it possible to evaluate N_{lin} during a WE even when there was no axial symmetry.

Hamilton *et al.* [195] measured $K_{\text{atom}} = N_{\text{lin}}/N_{\text{lin0}}$ for exploding Al wires of diameter 16, 21, and 26 μm. According to [200], K_{atom} is related to the phase shift of interference fringes, $\delta(y)$, as

$$K_{\text{atom}} = \frac{\lambda}{2\pi N_{\text{lin0}} \alpha} \int \delta(y)\, dy$$

where λ is the probing wavelength and α is the dynamic polarizability of Al atoms at the wavelength λ (in cm^3).

According to the measurements [195] (see Table IV), for the relative energy input $\varepsilon_{\text{dep}}/\varepsilon_{\text{atom}} = 100\%–200\%$, the atomization coefficient was significantly less than unity; that is, 50%–70% of the wire material turned into gas. At the same time, Wu *et al.* [174] report that in their experiment with Al wires, at least 87% of the wire material turned into gas when the energy deposited in the wire was approximately equal to the atomization energy. Perhaps, such a large

TABLE IV

ATOMIZATION COEFFICIENT $K_{atom} = N_{lin}/N_{lin0}$ FOR EXPLODING AL WIRES [174], [195] WITH $\varepsilon_{atom} = 3.2$ EV/ATOM (12.1 KJ/G)

Wire diameter d, μm	Deposited energy ε_{dep}, eV/atom	Core expansion velocity v_{core}, 10^5 cm/s	Atomization coefficient, K_{atom}
16*	9–11	9.2–9.7	0.98
21*	4.5	4.6–6.2	0.5–0.8
15**	3–4	5.2	0.87–0.93

* Hamilton *et al*. [196], current rate 160 A/ns.
** Wu *et al*. [175], current rate 100 A/ns.

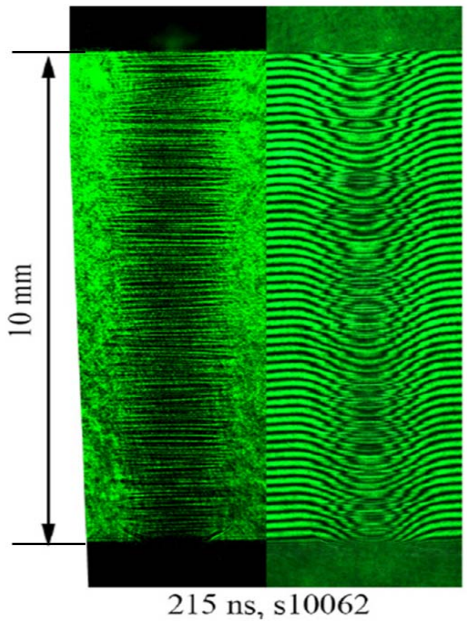

Fig. 20. Laser shadow and interferometric images of an exploding 25-μm-diameter, 1-cm-long Ag wire. The resistive phase duration is 20 ns; $\varepsilon_{dep}/\varepsilon_{atom} \sim 250\%$–$300\%$. Reprinted with permission from [173]. Copyright 2017, AIP Publishing LLC.

discrepancy between the results of different experiments can be accounted for by the difficulties in measuring energy inputs at high current rates. Note that, following Wu *et al.* [174] and Hamilton *et al.* [195], we give the values of ε_{dep} in Table IV measured in eV/atom.

The main goal of most studies of the WE in vacuum aimed at increasing the energy input was to produce a homogeneous vapor-plasma column. However, as can be seen in Figs. 20 and 21, even a twofold or threefold excess of the deposited energy over the vaporization energy does not provide axially uniform explosion.

Fig. 20 shows a shadow and an interferometric image of an exploding 25-μm-diameter, 1-cm-long Ag wire which were taken 215 ns after the onset of current flow. According to the data given in [173], the energy deposition time was about 20 ns and the deposited energy was 7.5–8 kJ/g with the

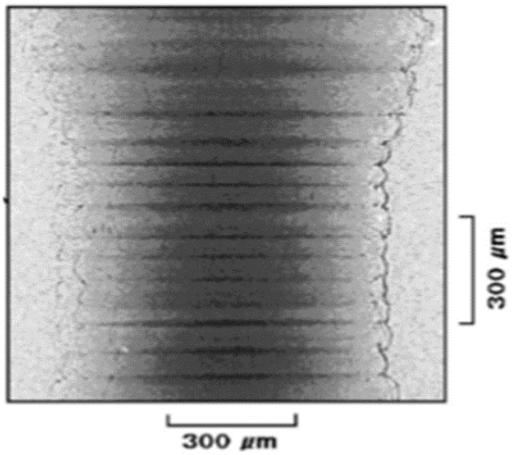

Fig. 21. Radiograph of an exploding 1-μm polyester-insulated 25-μm Ag wire taken 318 ns after the onset of current flow, the only one among the 14 exploded wires of this type that exhibited striation. $\varepsilon_{dep}/\varepsilon_{atom} \sim 225\%$–$304\%$. Reprinted with permission from [151]. Copyright 2001, AIP Publishing LLC.

atomization energy of Ag equal to 2.6 kJ/g. The shadow and interferometric images were taken using a Nd:YAG laser (532 nm, 30 ps). The shadow image shows strata (alternating transparent and opaque layers of the wire material). Some interference fringes in the central part of Fig. 20 are lost, which is associated with the occurrence of wire material layers opaque to laser radiation. Striation also occurred in exploded wires with insulating coatings, as it can clearly be seen in the radiograph presented in Fig. 21 [151].

As mentioned in Section II-D, the striation in WEs is accounted for by ETIs. If the local increase of the wire resistivity occurs within a small volume $\mathbf{V}'$ (e.g., at a grain boundary), the temperature at this place increases, resulting in a further increase in resistivity within the volume $\mathbf{V}'$. This leads to a decrease in current density within $\mathbf{V}'$ and, hence, an increase in current density near the region of increased resistivity. The increased current density intensifies the energy release and increases the temperature in the region adjacent to the volume $\mathbf{V}'$, and this inevitably leads to an increase in resistivity. Thus, the high-resistivity region propagates normal to the current flow, which also follows from (18). As a result, a high-resistivity layer is formed. The temperature in the high-resistivity layer becomes higher than that in the low-resistivity layer. After the voltage collapse, the core material in "hot" and in "cold" layers will expand adiabatically with different velocities. Indirect evidence of high temperatures in low-density, transparent layers subject to ETIs is a clear correlation between the periodicity of the striation layers and the perturbations in the insulating coating, which are seen in the right-hand image of Fig. 21. It can be speculated that the breaks in the micrometer-width insulating coating occur under the pressure of the vapor propagating from the high-temperature layers.

The problem with the experimental observation of stratification is that the initial wavelength λ_{min} at which ETIs start developing is about 10 μm [86], [156]. On the other hand, in WE experiments, only strata with a wavelength of 40–50 μm

TABLE V
COMPARISON BETWEEN THE EXPERIMENTAL VALUES OF THE WAVELENGTH $\lambda_{collapse}$ AND THE VALUES OF $\lambda_{collapse}$ ESTIMATED USING (II-12)

Wire diameter d, μ	Current rate $\frac{dI}{dt_{av}}$, A/ns	Collapse time $t_{collapse}$, ns	Deposited energy ε_{dep}, kJ/g	Core velocity v_{core}, 10^5 cm/s	Minimal wavelength $\lambda_{collapse}$	
					Exper.	Model.
20	7	77	4.2–5.3	0.8	8 ± 1.5	8
35	14	114	6.3–7.7	1.2	7.5 ± 1.3	8.5
50	18	120	6.2–8.1	1.3	5 ± 1	8.9

were observed (see Figs. 20 and 21). This discrepancy can be primarily explained by the fact that stratification occurs when the wire material is in a liquid or a liquid-vapor phase (see Section II-D). Therefore, at the onset of stratification, the material density in the wire hot layers is close to the condensed matter density, and the layers are opaque to probe radiation. Strata become detectable only when the wire core starts expanding. However, as the core expands, the shortwave modes attenuate and modes with wavelengths of several tens of micrometers begin to prevail, which ensures a satisfactory recording of striations 100–200 ns after the onset of current flow. At the same time, according to the model described in Section II-D, the attenuation increment does not depend on the current flowing through the discharge channel after the voltage collapse.

This supposition was completely confirmed by the experiment performed by Rousskikh *et al.* [153]. They investigated the explosion of Al wires of diameter 20, 35, and 50 μm and length 2 cm at $dI/dt_{av} = 10$–15 A/ns; the current density at the time of voltage collapse was $(1$–$1.4) \cdot 10^8$ A/cm^2 for all exploded wires. To observe striation patterns in the wires, the soft X-rays generated at the hot point of an X pinch were used. In the experiment, the wires were exploded in two modes. In the first mode, the duration of the current pulse through the discharge channel was not limited: the current could pass through the channel after the voltage collapse. In the second mode, which we will call below the current-cutoff mode, the current flow through the discharge channel was stopped 10–20 ns before the voltage collapse.

Fig. 22 presents the core diameter and the striation wavelength varying with time for a 35-μm-diameter Al wire; the diameter of the core was measured using radiographs. The data given in Fig. 22 refer to both the no-current-cutoff and the current-cutoff mode. It can be seen that the data on $\lambda(t)$ for both modes fall on one line. Thus, the close agreement between the experimental data on $d(t)$ and $\lambda(t)$ obtained in the no-current-cutoff and in the current-cutoff mode strongly suggests that the striation observed in a WE occurs earlier than the wire is shunted. With the fitting lines $\lambda(t)$, Rousskikh *et al.* [153] determined the initial striation wavelength $\lambda_{collapse}$, that is, the striation wavelength immediately after the development of the shunting discharge, for different wire diameters (see Table V). In Table V, the experimental values of $\lambda_{collapse}$ are compared with the values of $\lambda_{collapse}$ estimated in relation to the energy deposited in the core. In addition, Table V gives data for the current rate,

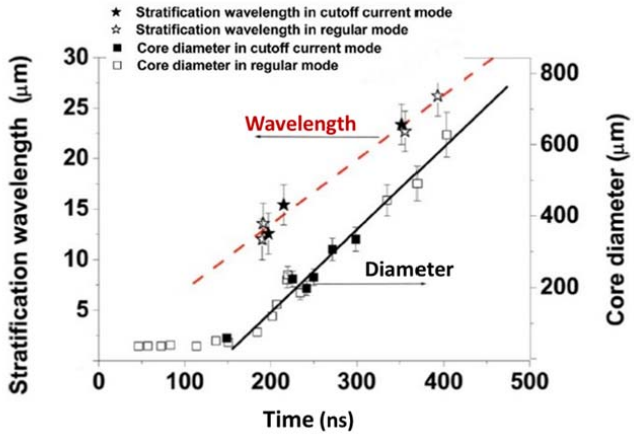

Fig. 22. Explosion of a 35-μm-diameter Al wire: the wire core diameter (boxes) and the average striation wavelength (asterisks) versus time. The solid and the open symbols refer, respectively, to the current-cutoff and the no-current-cutoff mode. Adapted from [153].

the voltage collapse time, the energy deposited in the wire core, and the core expansion velocity, which was estimated as the core radius divided by the interval between the probing time and the voltage collapse time.

As can be seen from Table V, the model wavelengths are close to the experimental ones. At the same time, the experiment clearly revealed a trend toward decreasing $\lambda_{collapse}$ with increasing wire diameter. However, according to the model, this trend should not occur, at least in the ε_{dep} range under investigation.

Wu *et al.* [173] attempted to measure the linear density N_{lin} in the dark and light layers of the wire material that occur during stratification (see Fig. 20). They exploded a 25-μm-diameter, 1-cm-long Ag wire at a high current rate, $(dI/dt)_{av} = 100$ A/ns, and, hence, at a high energy input, $\varepsilon_{dep}/\varepsilon_{atom} \sim 250\%$–$300\%$. Recall that when speaking of strata, we assume *a priori* that dark, opaque to radiation, layers have a higher linear density than light layers [86], [168]. Measurements of N_{lin} were performed using interferometry. The interferometer was adjusted so that the interference fringes were parallel to the wire axis (normal to the striation layers). Due to this arrangement of the interference fringes, Zhao *et al.* [172] could measure N_{lin} both in dark and in light layers. They obtained N_{lin} equal to $2.9 \cdot 10^{17}$ cm^{-1} for dark layers and $2.3 \cdot 10^{17}$ cm^{-1} for light ones, which made, respectively, 86% and 80% of the initial linear density of

the wire material. Thus, the measurement results obtained by Wu *et al.* [173] do not contradict the initial suppositions presented in [86]. It should, however, be noted that, according to the data of [200], the error in measuring N_{lin} using interferometry, which is determined both by the interferogram processing procedure and by the accuracy of the polarization coefficient used in estimating the absolute value of N_{lin}, is $\pm 10\%$.

C. Mechanism of Corona Formation During a WE in Vacuum

The discussion about the composition of the medium in which the core of a wire exploding in vacuum is shunted began in the 60s–70s of the last century (see [201], [202], and references therein). Holmström *et al*. [202] write that the investigation "shows that a discharge exists in a low-pressure metal vapor outside the wire, and that the initial current carriers are thermionic electrons," believing that the core is shunted by this discharge. A similar conclusion was made by the authors of the review [3]. At the same time, Bennett *et al.* [100] arrived at the conclusion that the core is shunted "due to a discharge in released gases initially adsorbed by the wire." The same point of view was expressed by Sinars *et al.* [151] who stated that "a very likely mechanism of corona formation is shunting of the wire by a highly conductive plasma channel, which occurs during the breakdown of gases desorbed by the metal." It seems that the metal vapor can be the main component of the coronal plasma only in some specific cases, for instance, when the wire is completely degassed by heating [82], [126].

Before proceeding to the discussion of the results of experimental studies devoted to the mechanism of corona formation during a WE in vacuum, we consider some general concepts related to the desorption of gas from the surface of a metal heated in vacuum. A more detailed description of the desorption processes is given in Chapter 4 of the book by Roht [124].

In the process of desorption, the gas molecules adsorbed on the surface of a metal and the gas molecules absorbed (dissolved) in the metal bulk are removed. In equilibrium, at pressures of 10^{-3}–10^{-4} Pa, there is a gas monolayer on the surface of a metal, which corresponds to a surface number density of the order of 10^{15} cm^{-2}. For most metals, the concentration of absorbed gas molecules is small, lying within 10^{11}–10^{15} cm^{-3} [192]. The exception is titanium for which it is about 10^{21} cm^{-3} [192]. Therefore, only adsorbed molecules play an essential part in the formation of a gas layer near the wire surface due to desorption under pulsed heating. The desorption rate dN_d/dt depends exponentially on surface temperature T; for the desorption of a monolayer, it is described by the relation [124]

$$\frac{dN_d}{dt} = \frac{N_0\theta}{t^*}\exp\left(-E_{\text{d}}/kT\right) \tag{IV-3}$$

where N_0 is the total number of molecules required to form a complete monolayer, θ is the coverage (i.e., the fraction of possible adsorption sites which are actually occupied with gas molecules), t^* is the period of the molecular oscillation normal to the surface ($\sim 10^{-14}$ s), and E_{d} is the desorption energy ($\sim$1 eV). As follows from (IV-3), the time required for complete desorption of the monolayer at temperatures of 800–1200 K may be 10^{-7}–10^{-9}s.

TABLE VI

EFFECT OF THE EXPOSURE TIME t_{expo} ON THE DURATION OF THE RESISTIVE PHASE t_{res}: p IS THE PRESSURE; THE EXPOSURE TIME WAS MEASURED BETWEEN THE TERMINATION OF THE DEGASSING PROCESS AND THE APPLICATION OF PULSED VOLTAGE TO THE WIRE [197]

t_{expo}, s	t_{res}, ns	p, Torr
45	600 ± 60	$4{\cdot}10^{-8}$
300	400 ± 40	$5{\cdot}10^{-8}$
600	280 ± 28	$5{\cdot}10^{-7}$
900	340 ± 34	$3{\cdot}10^{-8}$
17000	280 ± 28	$6{\cdot}10^{-9}$

The existence of a gas layer on the surface of a metal allowed Karakhanov [197] to experimentally verify the mechanism of gas desorption from wires exploding in vacuum. He exploded 2-cm-long W and Ni wires whose diameters were 94 and 100 μm, respectively. The maximum current amplitude was 5 kA, and the current rate was 15–20 A/ns. The vacuum chamber could be evacuated to $\sim 10^{-9}$ torr (ultrahigh vacuum). The wires were degassed before the application of high voltage to the discharge gap. The degassing was performed by resistively heating the wires with a dc power supply.

Table VI presents the values of t_{res} in relation to t_{expo} measured at different pressures in the vacuum chamber in the W WE experiment [197]. The time t_{res} between the voltage application to the wire and the onset of sharp current rise was measured (the measurement error was about 10%). In the experiment [197], it was taken into account that the adsorbed particle density on the surface of a metal, N_a, depends on the time interval during which the metal is exposed to vacuum, t_{expo}, after degassing. During the exposure time t_{expo}, gas molecules are adsorbed on the wire surface becoming cool. As the adsorption rate dN_a/dt depends on surface temperature as $T^{-0.5}$ [124], the surface density of the gas should increase as the wire metal cools down. If the shunting of the wire occurs in the desorbed gas, the time t_{res} should decrease.

Karakhanov [197] interpreted his experimental results as follows. A certain time after the termination of the degassing process, equilibrium is established between the adsorbed and the desorbed atoms. As mentioned in [197], the surface density of gas molecules adsorbed on a metal surface is rarely greater than the surface density N_0 necessary for a monolayer to form. Karakhanov [197] concluded that when a single gas monolayer completely vaporizes, the discharge that shunts the wire occurs in the gas desorbed from the wire surface.

There is a rather strong objection of fundamental importance against the desorption model for the shunting of the core of a wire exploding in vacuum. The objection is that desorption of one or two gas monolayers is not sufficient to produce a gas with a density at which breakdown over the wire surface is

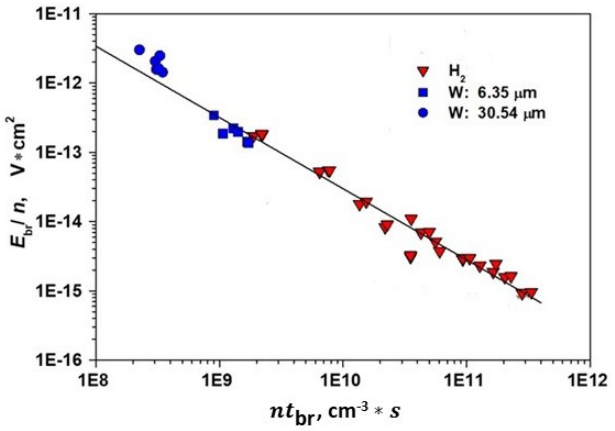

Fig. 23. Data points of $(E_{\rm br}/n)$versus$nt_{\rm br}$ for the breakdown of a 6-mm gap filled with H_2 (red triangles) and for the shunting of 6.35- and 30.54-μm W wires (blue boxes and circles, respectively). Adapted from [123].

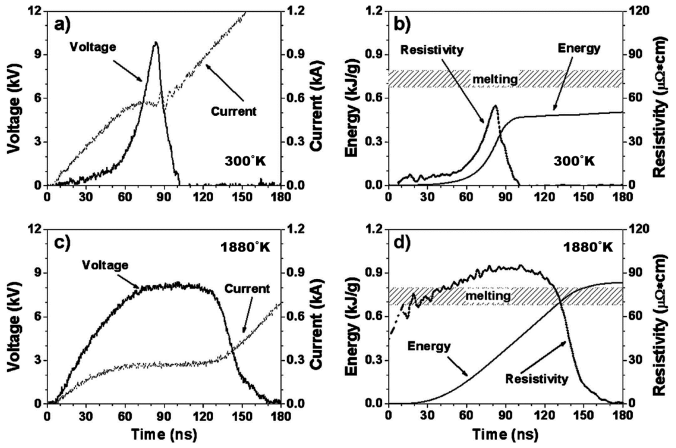

Fig. 24. Current and voltage waveforms for the 2-cm-long, 30.48-μm-diameter W WE, and the time-varying deposited energy and resistivity. (a) and (b) wires were exploded at room temperature (300 K). (c) and (d) wires were preheated (1880 K). The melting range is in accordance with the results of the measurements [204]. Reprinted with permission from [82]. Copyright 2008, AIP Publishing LLC.

possible. Actually, the gas density in a layer which is formed within a time t can be determined as

$$n = \frac{2N_0 r_w}{\upsilon t\,(\upsilon t + 2r_w)} \tag{IV-4}$$

where N_0 is the number of gas particles per unit area, r_w is the wire radius, υ is the velocity of the gas expansion, $\upsilon = \sqrt{kT/m_a}$, T is the gas temperature, and m_a is the atomic mass of the gas particles. According to (IV-4), for a wire with several tens of micrometers in diameter heated to a temperature of 500–1000 K, 20–40 ns after the onset of desorption, the gas density in the layer will be no more than 10^{14}–10^{15} cm^{-3}. At first glance, this density is too low for a breakdown to occur. However, the experiment conducted by Rousskikh *et al.* [123] showed that even at these low densities, the surface breakdown along an exploding wire obeys the laws established for the pulsed breakdown of gases. The main gas that forms the corona is hydrogen, as it is the lightest component of the gases adsorbed on the wire surface. Rousskikh *et al.* [123] compared the characteristics of the breakdown of hydrogen corresponding to the left branch of the Paschen curve with those obtained for exploded W wires. To do this, the relation $(E_{\rm br}/n)$ versus $nt_{\rm br}$, where $E_{\rm br}$ and $t_{\rm br}$ are the breakdown electric field and delay time, respectively, and n is the gas molecule density, was used, which is widely applied in gas breakdown physics (see [203]).

Fig. 23 presents the relation $(E_{\rm br}/n)$ versus $nt_{\rm br}$ plotted for the breakdown of a 6-mm gap filled with H_2 and for the shunting of 6.35-μm-diameter and 30.54-μm-diameter W wires of length 6 mm. The particle density n in the gas layer was estimated by (IV-4) with the temperature of the gas assumed to be equal to the temperature of the wire that was estimated from the energy deposited in the wire as

$$T\,(t) = [m_w c_W\,(t)]^{-1} \int I\,(t)\,V\,(t)\,dt \tag{IV-5}$$

where m_w is the tungsten atom mass and $c_W(t)$ is the heat capacity of tungsten.

It can be seen that the data obtained for the exploded W wires fit well the $(E_{\rm br}/n)$ versus $nt_{\rm br}$ plot obtained for the breakdown of hydrogen. It should be noted that the discharge developing along the wire surface during a WE in vacuum seems to be assisted by an efficiently operating external ionizer. This external ionizer may be the flow of electrons emitted by the rare plasma developed during the breakdown over the cathode surface [193], [194].

Complete degassing of the wire surface (removal of the gas monolayer) leads to a significant increase in $t_{\rm res}$ and, accordingly, to an increase in the energy deposited in the wire exploded in vacuum. A series of experiments [81], [82], [125] was performed in which 2-cm-long, 30.48-μm-diameter W wires having no gas on the surface were exploded at current rates $(dI/dt)_{\rm av}$ = 10–20 A/ns. Each wire was degassed by passing a direct current through it which was not turned off after application of pulsed voltage to the wire. The temperature of the wire, estimated by its resistance, was 1880 ± 100 K. Fig. 24 shows the typical voltage and current waveforms together with the resistivity δ and specific energy $\varepsilon_{\rm dep}$ calculated using the waveforms. In constructing a voltage waveform, the inductive component was subtracted from the voltage divider readings. The values of δ and $\varepsilon_{\rm dep}$ were estimated without regard to the increase in wire diameter during the explosion. The plots in Fig. 24 indicate that $\varepsilon_{\rm dep}$ increased by a factor of 1.8 when the exploded wire was preheated. Note that in the experiment performed by Holmström *et al.* [202], W wires were also heated to high temperatures; however, no effect of the heating on the explosion characteristics was detected. It is possible that Holmström *et al.* [202] turned off the heat source earlier than the wire was exploded, which led to the formation of a gas layer on the wire surface, as observed in the experiment by Karakhanov [197].

The current and voltage waveforms given in Fig. 24(a) and (c) clearly indicate that the preheating of an exploded wire [see Fig. 24(c)] changes not only the energy deposition time and the deposited energy but also the voltage pulse waveform. The difference in current and voltage waveforms between the two explosions can well

be explained in the context of the desorption mechanism of corona formation. When the exploded wire was not degassed [see Fig. 24(a)], its initial temperature was equal to room temperature, its initial resistance was fractions of an ohm, and, within the first 20–40 ns after application of pulsed voltage, the current was determined by the impedance of the driver (3.3 Ω). Both the wire resistance and the voltage across the wire began to rise significantly only when the resistance became greater than the impedance of the driver. The wire resistance reached 5–6 Ω (corresponding to resistivity δ = 15–20 $\mu\Omega \cdot$ cm) in 60–70 ns after the application of voltage to the wire [see Fig. 24(b)]. According to tabular data [205], at these values of δ, the temperature of a W conductor should be 650–900 K, which should provide intense gas desorption from the wire surface. Once a gas layer was formed on the surface of a wire, it started expanding. As follows from the plot given in Fig. 23, when (E_{br}/n) reached 10^{-11}–10^{-13} V $\cdot$ cm^{-2}, breakdown of the gas layer occurred. It seems that the voltage fall time (t_{fall}) [see Fig. 24(a)] is determined by the time delay to the breakdown of the gas layer. According to experimental data [82], [179], t_{fall} does not depend on the material of the exploded wire and equals 10–20 ns. The duration of the resistive phase for the explosion of the nondegassed wire was 95 ns [see Fig. 24(a)] and the specific deposited energy was substantially lower than the melting energy plus the integral of the specific heat from room temperature to melting point [see Fig. 24(b)].

For the exploded degassed (preheated) wires [see Fig. 24(c) and (d)], the current became determined by the wire resistance 20–40 ns after the application of pulsed voltage to the wire: the resistance was 10–12 at t = 30 ns and reached 28 Ω at t = 100 ns. At this time, the resistivity δ was 90–95 $\mu\Omega\cdot$ cm and the surface temperature was 3000–3100 K.

The rate of vaporization F increases with temperature as $F \propto \exp(kT)^{0.5}$ [206]. As the surface temperature of a metal approaches the boiling point (for tungsten T_{boil} = 3695 K), the vaporization of atoms from the metal intensifies. It is very likely that when a preheated W wire explodes, a heterogeneous pinch arises [201] and the corona consists of tungsten atoms. Recall that the corona formed in a WE in vacuum carries the entire current after the plasma channel is formed (at least at $t > t_{\text{res}}$). As the expansion velocity of a plasma in vacuum is determined by the temperature of the plasma and by the atomic mass of its species, it can be supposed that the corona expansion velocity should be different for exploded nondegassed and degassed W wires. This supposition is confirmed by the results of an experiment performed by Rousskikh *et al.* [81] who studied the dynamics of the expanding corona with the help of auxiliary electrodes. The auxiliary electrodes were located at a distance d from the wire axis. They were grounded, and thus they were at a positive potential in relation to the coronal plasma. As soon as the coronal plasma arrived at the auxiliary electrode, a current began to flow through the electrode circuit. The corona expansion velocity was measured 100–200 ns after the onset of current flow through the wire; at the measuring time, the plasma density at the corona boundary was 10^{14} cm^{-3}, according to a rough estimate of

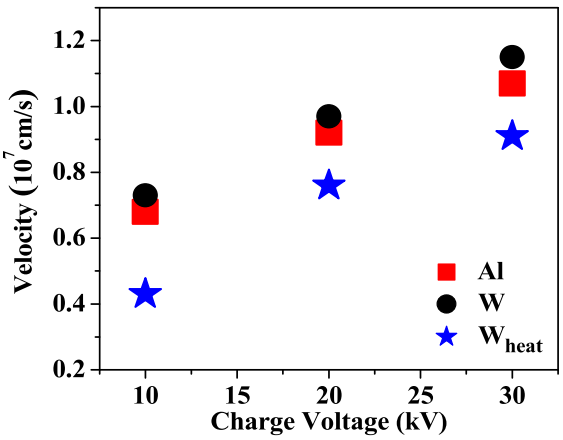

Fig. 25. Plasma corona expansion velocity versus capacitor charge voltage for an Al wire (red boxes), a nonheated W wire (black circles), and a heated W wire (blue asterisks). Reprinted with permission from [81]. Copyright 2008, AIP Publishing LLC.

the plasma density. Three test series were performed: with Al wires 36 μm in diameter, with W wires 30 μm in diameter, and with preheated (1880 K) W wires 30 μm in diameter. All the wires were of the same length equal to 20 ± 0.5 mm. The corona expansion velocity was measured at different current rates $(dI/dt)_{\text{av}}$, which were provided by varying the charge voltage V_{ch} of the driver capacitor: $(dI/dt)_{\text{av}}$ was 10–15 A/ns at V_{ch} = 10 kV, 20–30 A/ns at V_{ch} = 20 kV, and 30–45 A/ns at V_{ch} = 30 kV. The measurement data are presented in Fig. 25.

As expected, the corona expansion velocity v_{corona} increased with capacitor charge voltage V_{ch}, and, hence, with the current flowing through the corona. However, its values at a given V_{ch} were almost the same for the Al wires (red boxes) and nonheated W wires (black circles) and somewhat lower for the W wires heated before the explosion (blue asterisks). This experiment has demonstrated that the expansion velocity of the corona of a wire exploded in vacuum does not depend on the wire material. For both the aluminum and the nonheated tungsten wires, the expansion velocity was $(7 \pm 0.5) \cdot 10^6$ cm/s at V_{ch} = 10 kV, $(9 \pm 0.5) \cdot 10^6$ cm/s at V_{ch} = 20 kV, and $(1.1 \pm 0.6) \cdot 10^7$ cm/s at V_{ch} = 30 kV. Tests with preheated tungsten wires showed that as the desorbed gas was removed, the corona expansion velocity decreased by about 30%. Sarkisov *et al.* [179] measured the expansion velocity of the corona for 25.4-μm Al wires at $(dI/dt)_{\text{av}}$ = 150 A/ns. Based on upstream and downstream current measurements, they obtained the expansion velocity values ranging between $5 \cdot 10^6$ and 10^7 cm/s.

Tkachenko *et al.* [166] measured the corona expansion velocity for Al wires 25 μm in diameter, nonheated W wires 25 μm in diameter, and preheated W wires 25 μm in diameter; the length of all the wires was 12 mm. The current rate in the experiment was 10–20 A/ns. Measurements were performed using framing photography in UV light. The corona expansion velocity was measured 1000–2000 ns after the onset of current flow through the wire. At the measuring time, the plasma density at the boundary was about 10^{16} cm^{-3}. For the aluminum wires and for the nonheated tungsten wires, the expansion

velocity was $2.8 \cdot 10^6$ and $2.7 \cdot 10^6$ cm/s, respectively, whereas for the preheated tungsten wires, it was $1.2 \cdot 10^6$ cm/s. The result obtained in this experiment is qualitatively similar to that reported in [81]: v_{corona} was the same for exploded Al and nonheated W wires, and it decreased substantially when W wires were preheated before the explosion. The difference in absolute values of v_{corona} measured in the experiments [81], [167], [179] is related most likely to different values of the plasma density at the corona boundary at the measuring time. The decrease in v_{corona} is well explained in the context of the desorption model of corona formation. For an exploding nonheated wire, the coronal plasma consists of hydrogen and carbon atoms, whereas for an exploding preheated W wire, it consists of tungsten atoms. It follows that the expansion velocity of a corona consisting of H and C atoms should be greater than that of a corona consisting of W atoms at about the same plasma temperature, and this is observed in the experiment.

At a large value of $(dI/dt)_{\text{av}}$ and a high current, the corona plasma is compressed by the magnetic force of the current flowing through the corona. In the experiment described in [138], 15-μm aluminum wires were exploded at a current amplitude of 100 kA and $(dI/dt)_{\text{av}} = 2$ kA/ns. Chittenden *et al.* [138] observed that the corona was formed 5–6 ns after the onset of current flow, expanded in a short time to 0.5 mm in radius, and 15–20 ns later, its self-pinching began. Within 24 ns from the onset of current flow, the mean radius of the corona decreased to 0.2 mm, and at the vacuum–plasma boundary, $m = 0$ instabilities were detected in both experimental and simulated laser schlieren images. Surprisingly, the core remained opaque to radiation even 85 ns after the onset of current flow (see [138, Fig. 4]). This might indicate that at that time, the total pinch current ($\approx$80 kA) was carried by the corona plasma.

To conclude this section, we refer to several articles that report experimental data which point indirectly to the formation of a corona during a WE in vacuum. A curious fact was observed in the experiment reported in [207] in which Cu and W wires of length 0.5–1.5 cm were exploded at $(dI/dt)_{\text{av}} =$ 400–500 A/ns and a pressure of 10^{-4} torr. It was found that Cu wires of diameter 70 and 300 μm and W wires of diameter 100 μm were not destroyed by a 3 kA current passed through the discharge gap even when the voltage peaked at 200–250 kV at the collapse time. Barakhvostov *et al.* [207] account for this effect by the electrical explosion of the surface layer of the wire metal. However, the gap was most likely short-circuited by the discharge that occurred in the gas of impurities desorbed from the wire surface.

The effect of the gas absorbed by a Pd wire on the collapse voltage V_{col} and deposited energy ε_{dep} was investigated in the experiment described in [208]. It was observed that V_{col} and ε_{dep} for a hydrated Pd wire were lower than those for a nonhydrated wire by 25% and 40%, respectively. Sarkisov [208] believe that their experimental data obtained using electrical and interferometric measuring techniques provide evidence that the gas desorption from the surface of an exploding wire is responsible for the formation of a plasma corona around the wire core.

Thus, no published experimental data contradict the desorption model of the formation of a corona in a WE in vacuum.

D. Radiation From Exploding Wire Plasmas in Vacuum

The evolution of the visible and UV emission from exploding wire plasmas was investigated by Wu *et al.* [175], Sarkisov *et al.* [176], and Tkachenko *et al.* [187]. Let us consider, using the data for exploded 25-μm Al wires [187] as an example, how the emission varies with time. Fig. 26 shows the typical current and voltage waveforms together with the respective waveforms of photocurrents that were obtained by detecting the plasma radiation with a bare diode (BD; unfiltered diode; 10–1000 eV) and a filtered diode (FD; 120–280 and $>$320 eV).

The radiation of intensity J_{BD} [see Fig. 26(b)] was detected by the BD at $t = 80$ ns when the wire became shunted with the coronal plasma, that is, when a voltage collapse occurred ($V(t) = V_{\text{coll}}$). The radiation of intensity J_{FD} [see Fig. 26(b)] was detected by the FD at $t = 140$ ns, that is, 60–80 ns after the termination of the energy deposition into the wire material.

The radiation intensity J_{BD} rapidly increases within a time approximately equal to the voltage fall time t_{fall}. Within the time t_{fall}, a high-conductivity plasma corona is formed around the wire core. The resistive voltage drop across the discharge channel becomes negligible compared with the inductive voltage drop in the discharge circuit, and this is clearly indicated by the waveform $V(t)$ in Fig. 13: $V(t) = L(dI/dt)$ after $t = t_{\text{res}} \sim 80$ ns. Further evolution of the intensity of the radiation from the discharge channel depends on the wire material and on the rate of the current flowing through the wire during the resistive phase. As pointed out in Section II-A, the current rate is determined by the parameters of the generator loaded with the exploding wire and by the wire material and geometric dimensions. In most experiments with wires exploded in vacuum [175], [176], [187], a nonmonotonic increase in radiation intensity $J(t)$ with current was observed [see Fig. 26(b)]: the first short emission spike was followed by a rather long-lasting emission, which intensified as the discharge channel expanded. As can be seen in Fig. 26(b), the amplitude of the second spike of the radiation intensity $J_{\text{BD}}(t)$ is considerably greater than that of the first spike. Note that the second spike was absent in some WE modes, for instance, when $\varepsilon_{\text{dep}}/\varepsilon_{\text{atom}}$ was increased [176] (see Fig. 28).

The experimental data on the plasma emissivity in various spectral ranges obtained by Tkachenko *et al.* [165], [187] (see Fig. 26) allowed them to make some conclusions on the composition of the plasmas produced by WEs in vacuum. Tkachenko *et al.* [187] calculated the photocurrents detected by BD and FD in relation to the source plasma temperature in the range from 0.1 to 60 eV. In the simulation, it was assumed that the radiation was emitted by the plasma layer formed as a result of the explosion of a 1.2-cm long, 25-μm-diameter Al wire. The emission area of the layer was equal to the surface area of the radiating cylinder, $a = \pi dl$, where l is the wire length (1.2 cm) and d is the plasma channel diameter (0.3 cm, which was measured using framing photography at $t \approx 130$–150 ns). The thickness of the radiating layer was assumed to be equal to the diameter of the discharge channel, d. The particle density in the layer was estimated

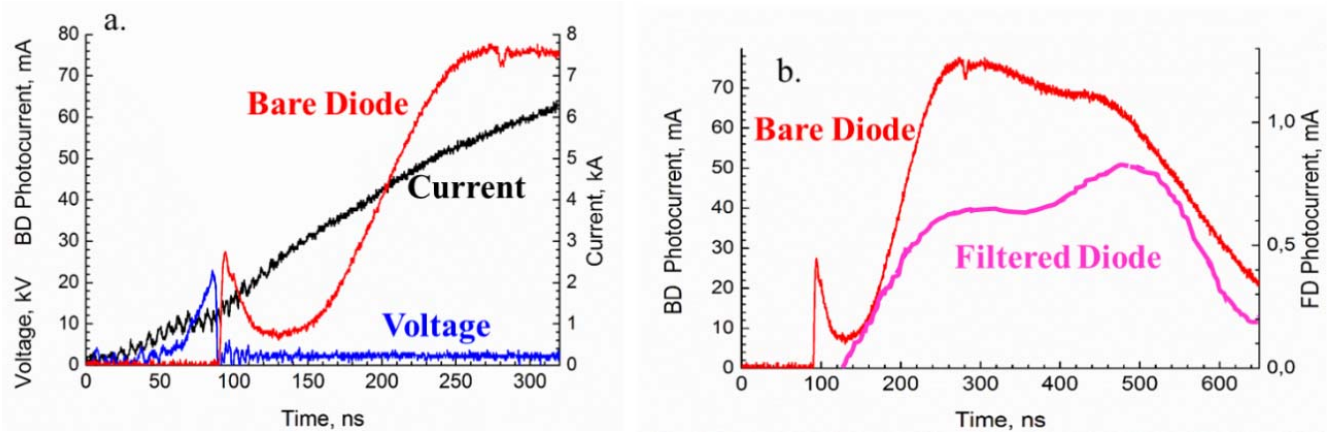

Fig. 26. Explosion of a 1.2-cm-long, 25-μm-diameter Al wire. (a) Waveforms of the wire current and voltage and of the BD photocurrent. (b) Waveforms of the bare (unfiltered diode) and FD photocurrents (J_{BD} and J_{FD}); $t_{res} = 100$ ns. Note that the voltage waveform contains the inductive component: $V(t) = V_{wire} + L(dI/dt)$. Adapted from [187].

as $N = m/\rho l$, where m is the initial mass of the wire (g) and ρ is the density (g/cm^3), and it was obtained that $N = 10^{16}$ cm^{-3}. The simulation was performed in the context of a collision-radiation model for two components of the radiating plasma layer: C plasma and Al plasma. It turned out that if the radiation source is C plasma, the amplitude of the FD signal should not be greater than 10^{-5} A, which is more than an order of magnitude lower than that of the signal detected in the experiment [see Fig. 26(b)].

The simulation has demonstrated that the observed FD signal amplitude could be provided by the radiation of a plasma component at temperature $\leq$ 14 eV. At these temperatures, the radiation of the Al plasma layer was intense enough to provide the observed amplitude of the FD signal (30–40 mA). This result allowed Tkachenko *et al.* [187] to reasonably conclude that the second emission spike occurred due to the radiation from the Al plasma layer whose temperature was 15–20 eV at least after the occurrence of the FD signal, that is, at $t \geq$ 120–140 ns. However, at temperatures below 15 eV, that is, at times less than $t \approx$ 120–140 ns, the calculated radiation intensity of the Al plasma could not provide the experimentally detected first spike in the BD signal. For temperatures below 10 eV, the simulation gave a BD signal amplitude of 10^{-3} A, whereas in the experiment, the first spike amplitude of the BD signal was $2 \cdot 10^{-2}$ A. At the same time, according to the simulation, the C plasma layer could be responsible for the peak amplitude of the BD signal determined experimentally: the BD photocurrent provided by the C plasma layer was in the range $(1–5) \cdot 10^{-2}$ A for the plasma temperature ranged from 3 to 15 eV. Comparing the simulation predictions with the experimental data, Tkachenko *et al.* [187] arrived at the conclusion that the radiation of the C plasma substantially contributed to the amplitude of the first radiation spike detected by the BD.

Thus, the abovementioned experimental results and simulation predictions suggest that the data presented in Fig. 26 can be attributed to the following sequence of events.

1) At $t = 80$ ns after the explosion of a wire, the core is shunted by a discharge that occurs in the desorbed gas; the emissivity of the plasma channel in the time interval 80 ns $\leq t \leq \sim$140 ns is provided by the radiation of carbon and hydrogen plasmas.
2) The amplitude of the first radiation spike reaches a maximum at $t = t_{res} \approx 100$ ns after which the intensity of the carbon and hydrogen plasma radiation decreases due to an increase in current and plasma channel temperature.
3) From $t =$ 120–140 ns on, the Al plasma makes the main contribution to the emissivity of the plasma channel.

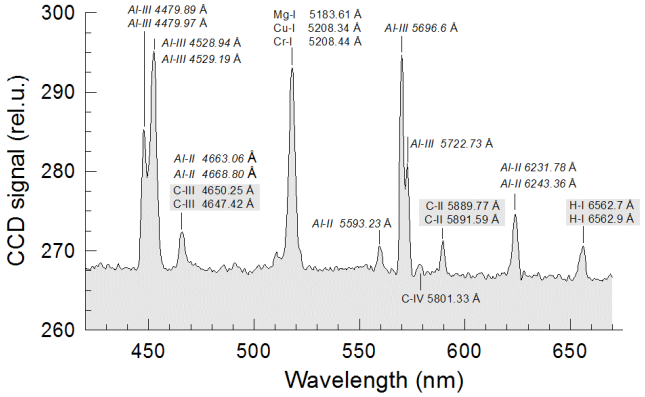

Fig. 27. Time-integrated optical spectrum for the 2-cm-long, 10-μm-diameter Al WE (150 A/ns). Reprinted with permission from [94]. Copyright 2008, AIP Publishing LLC.

Fig. 27 presents the time-integrated optical spectrum obtained by Sarkisov *et al.* [94] for the explosion of a 2-cm-long, 25-μm-diameter Al wire. In the experiment, the total duration of the current flow through the discharge channel was 1.5 μ s [94].

The time-integrated spectrum shown in Fig. 27 does not contradict the results obtained in the experiment discussed earlier [187]. The presence of strong lines of Al ions is completely consistent with the observation that the plasma emissivity during the second (rather long) radiation spike is determined by the wire material. At the same time, the plasma emissivity during the first (short) radiation spike is responsible

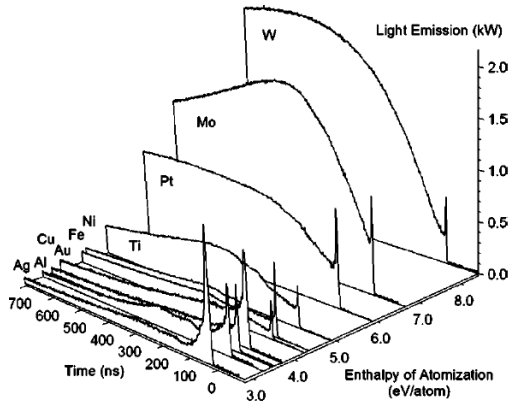

Fig. 28. Waveforms of the light-emission power (200–1100 nm) from a 4π solid angle for 20-μm wires plotted against atomization energy $\varepsilon_{\text{atom}}$. Reprinted with permission from [176]ý. Copyright 2004, AIP Publishing LLC.

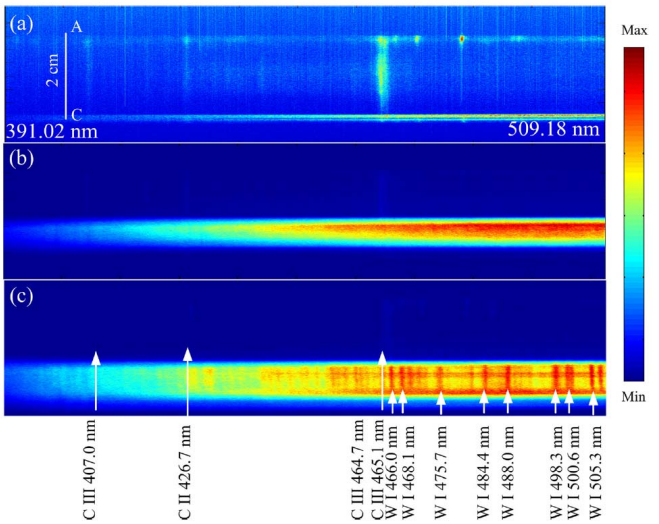

Fig. 29. Optical spectra measured during the explosions of (a) 13-μm bare W wire, (b) 12.5-μm W wire with a 3.5-μm PI coating, and (c) 15-μm W wire with a 2-μm PI coating. Reprinted with permission from [175]. Copyright 2014, AIP Publishing LLC.

for the presence of the carbon and hydrogen lines in the time-integrated spectrum.

It should be noted that, although the sequence of events described by items 1)–3) are in qualitative agreement with the experimental results presented in Fig. 26 [187], the following point remains unclear. As discussed in detail in Section IV-A, for a 25-μm-diameter Al WE driven by a current of rate 10–20 A/ns, identical to that used in the experiment [187], we should have $\varepsilon_{\text{dep}} \ll \varepsilon_{\text{atom}}$. Obviously, when the energy deposited in an exploded wire is low, a considerable portion of the wire material remains in a condensed state. Sarkisov *et al.* [176] showed that the emissivity of the plasma channel in a WE in vacuum may be provided not only by the plasma radiation but also by the radiation of a cloud of microdrops. In the following, we discuss the results reported in [176] in more detail.

The effect of the wire material on the emissivity of the plasma channel formed in a WE in vacuum is illustrated in Fig. 28.

It can be seen that there is a trend for increasing maximum radiation intensity $J(t)$ (measured in the range 200–1100 nm) with atomization enthalpy $\varepsilon_{\text{atom}}$. The trend is due to a decrease in the energy deposited in the wire, ε_{dep}, and to a decrease in ratio $\varepsilon_{\text{dep}}/\varepsilon_{\text{atom}}$ with increasing $\varepsilon_{\text{atom}}$ (see Fig. 17) [176].

As can also be inferred from Fig. 28, the amplitude of the second radiation spike is greater for the wires made of high-melting-point materials (W, Mo, and Pt). According to the model proposed by Sarkisov *et al.* ý [176], the second radiation spike is provided not only by the plasma radiation but also by the radiation of microdrops, which scatter together with the expanding plasma. By the time at which the entire discharge current starts flowing through the corona, that is, at $t = t_{\text{res}}$, the core material is a mixture of microdrops [151] and low-temperature plasma. At a time later than t_{res}, the core starts expanding, and it is during the core expansion that the second radiation spike is detected. The model proposed by Sarkisov *et al.* ý [176] assumes that each microdrop emits radiation like a blackbody at a temperature T, which corresponds to the core temperature at $t = t_{\text{res}}$. Thus, for the maximum radiation intensity in the second spike, we have

$$J_{\text{peak}} \propto N_d T^4 \tag{IV-6}$$

where N_d is the total number of microdrops in the expanding channel. The strong dependence of the radiation intensity on microdrop temperature used in the model [176] yields an increased amplitude of the second radiation spike for high-melting-point metals (3700 K for W, 2896 K for Mo, and 2142 K for Pt) compared with low-melting-point metals.

The time-integrated radiation spectrum measured during a W WE was qualitatively different from that measured during an Al WE. Sarkisov *et al.* [176] ýobserved that the time-integrated spectra of 20-μm W wires did not show individual spectral lines on the background of a very bright continuum. Wu *et al.* [175] were able to detect individual spectral lines for exploded W wires by measuring time-gated spectra. The driver they used provided a current rate of $\sim$100 A/ns in a current pulse of duration 50 ns. Fig. 29 presents the optical spectra measured during the explosions of a 13-μm bare W wire, a 12.5-μm W wire with a 3.5-μm PI coating, and a 15-μm W wire with a 2-μm PI coating [175].

Each spectrum was recorded for a time of 1 μ s. The spectra indicate that for the exploded bare W wire, only one strong line was detected, namely, the line of doubly ionized carbon (C III, 465.1 nm); the lines of neutral tungsten occurred only for the 15-μm W wire coated with a 2-μm PI layer. The presence of carbon lines, which can be seen in Fig. 29(c), allowed Wu *et al.* [175] to suppose a significant part played by the desorbed gas in the shunting of the core of an exploded coated wire as well.

V. In the Future

Since the first publications on the physical phenomena involved in the explosion of thin wires in vacuum, the level of

understanding of these phenomena has increased significantly. It has been established the following.

1) An energy greater than the atomization energy of the material of an exploded bare wire can be deposited into the wire only if the explosion time ($t \sim t_{res}$) is several nanoseconds, which corresponds to a current density of the order of 10^9 A/cm^2 at the onset of the explosion process (see Section IV-A).
2) A wire exploding in vacuum is separated into a core and a corona. The corona formation is largely related to the desorption gases present on the wire surface. Once the corona has formed, the core becomes shunted and not carries current. The coronal plasma expands into vacuum at velocities of up to 10^7 cm/s (see Sections II-D and IV-C).
3) In an exploding wire, ETIs occur due to a strong temperature dependence of metal resistivity; for a wire exploding in vacuum, ETIs start developing earlier than the core becomes shunted by the coronal plasma (see Sections II-E and IV-B).

However, the mechanism of the shunting of a wire exploding in vacuum still remains obscure. The only publication available to us in which some light is shed on the shunting process is the pioneering work by Sarkisov *et al.* [133]. However, an understanding of the details of the shunting process is essential for developing a physical model which could be used in numerical calculations. Apparently, such a model cannot be constructed within the framework of the MHD approximation; it should be based on nonequilibrium kinetic equations describing the dynamics of a plasma.

Currently, there is also absolutely no experimental information about the temperature and density in the hot and cold layers of the wire material in which ETIs occur (see Sections. II-E and IV-B). Besides, the following question is to be resolved experimentally: How much are the current densities at which the ETIs begin to prevail over the sausage MHD instabilities induced by the magnetic force of the current carried by the wire?

It is very likely that during the development of ETIs, the wire material in the hot layers is in a metastable state of superheated (stretched) liquid. In this connection, it is of importance to evaluate the decay time of metastable states and to investigate how it is affected by the thermodynamic parameters of the wire material and by the energy deposited in the wire. Information on the behavior of temperature and density during the decay of a metastable liquid metal will significantly contribute to our knowledge of the phase transformations that occur during the transition of metals from a condensed to a vapor state.

To date, only a few experimental studies of the explosion of wires at current densities of the order of 10^9 A/cm^2 and, accordingly, at nanosecond explosion times have been carried out. However, to study WEs at current densities of 10^9–10^{10} A/cm^2, it is of importance to understand the phenomenon of explosive electron emission that occurs in breakdowns of vacuum gaps exposed to strong electromagnetic fields. This brings up the question of whether equilibrium equations of state apply to such short-term processes as WEs, and if so, whether it is possible to consider the transport coefficients (electrical conductivity and thermal conductivity) to be functions only of the thermodynamic parameters of the material or also to depend on the rate of energy deposition into the exploding wire.

ACKNOWLEDGMENT

This review would not have been possible without the input by many colleagues. In particular, the authors would like to thank Prof. S. I. Tkachenko (MIPT), E. Oreshkin (LPI RAS), A. Rousskikh, A. Zhigalin, T. Cherkashina, and N. Labetskaya (IHCE RAS). They would also like to thank the two reviewers for taking time in reading this long manuscript and for many helpful suggestions.

REFERENCES

[1] W. Muller, *Exploding Wires*, W. G. Chace and H. K. Moor, Eds. New York, NY, USA: Plenum Press, 1959.
[2] V. Burtsev, N. Kalinin, and A. Luchinsky, *Electrical Explosion of Conductors and Its Application in Electrophysical Installations*, Moscow, Russia: Energoatomizdat, 1990.
[3] S. V. Lebedev and A. I. Savvatimskiĭ, "Metals during rapid heating by dense currents," *Sov. Phys. Uspekhi*, vol. 27, no. 10, pp. 749–771, Oct. 1984.
[4] D. A. Hammer and D. B. Sinars, "Single-wire explosion experiments relevant to the initial stages of wire array z pinches," *Laser Part. Beams*, vol. 19, no. 3, pp. 377–391, Jul. 2001.
[5] W. G. Chace, "Exploding wires," *Phys. Today*, vol. 17, no. 8, p. 19, 1964.
[6] A. W. DeSilva and J. D. Katsouros, "Electrical conductivity of dense copper and aluminum plasmas," *Phys. Rev. E, Stat. Phys. Plasmas Fluids Relat. Interdiscip. Top.*, vol. 57, no. 5, pp. 5945–5951, May 1998.
[7] V. E. Fortov and I. T. Iakubov, *The Physics of Non-Ideal Plasma*. Singapore: World Scientific, 2000.
[8] V. N. Korobenko, A. D. Rakhel, A. I. Savvatimski, and V. E. Fortov, "Measurement of the electrical resistivity of hot aluminum passing from the liquid to gaseous state at supercritical pressure," *Phys. Rev. B*, vol. 71, no. 1, Jan. 2005, Art. no. 014208.
[9] V. I. Oreshkin, A. G. Rousskikh, S. A. Chaikovsky, and E. V. Oreshkin, "Investigation of the transport properties of metals in the biphase region," *Phys. Plasmas*, vol. 17, no. 7, Jul. 2010, Art. no. 072703.
[10] A. Grinenko, Y. E. Krasik, S. Efimov, A. Fedotov, V. T. Gurovich, and V. I. Oreshkin, "Nanosecond time scale, high power electrical wire explosion in water," *Phys. Plasmas*, vol. 13, no. 4, Apr. 2006, Art. no. 042701.
[11] T. J. Awe, B. S. Bauer, S. Fuelling, I. R. Lindemuth, and R. E. Siemon, "Experimental investigation of thermal plasma formation from thick aluminum surfaces by pulsed multimegagauss magnetic field," *Phys. Plasmas*, vol. 17, no. 10, Oct. 2010, Art. no. 102507.
[12] T. J. Awe *et al.*, "On the evolution from micrometer-scale inhomogeneity to global overheated structure during the intense joule heating of a z-Pinch rod," *IEEE Trans. Plasma Sci.*, vol. 45, no. 4, pp. 584–589, Apr. 2017.
[13] S. A. Chaikovsky, V. I. Oreshkin, G. A. Mesyats, N. A. Ratakhin, I. M. Datsko, and B. A. Kablambaev, "Electrical explosion of metals in fast-rising megagauss magnetic fields," *Phys. Plasmas*, vol. 16, no. 4, Apr. 2009, Art. no. 042701.
[14] V. I. Oreshkin *et al.*, "MHD instabilities developing in a conductor exploding in the skin effect mode," *Phys. Plasmas*, vol. 23, no. 12, Dec. 2016, Art. no. 122107.
[15] G. S. Sarkisov, P. V. Sasorov, K. W. Struve, D. H. McDaniel, A. N. Gribov, and G. M. Oleinik, "Polarity effect for exploding wires in a vacuum," *Phys. Rev. E, Stat. Phys. Plasmas Fluids Relat. Interdiscip. Top.*, vol. 66, no. 4, Oct. 2002, Art. no. 046413.
[16] R. B. Baksht *et al.*, "Stratification dynamics and the development of electrothermal instability at the wire explosion," *Tech. Phys.*, vol. 58, no. 8, pp. 1129–1137, Aug. 2013.
[17] A. L. Surkaev, "Magnetohydrodynamic perturbations arising in metallic conductors under the action of the discharge current," *Tech. Phys.*, vol. 60, no. 7, pp. 981–988, Jul. 2015.

[18] V. I. Oreshkin, K. V. Khishchenko, P. R. Levashov, A. G. Rousskikh, and S. A. Chaikovskii, "Strata formation at fast electrical explosion of cylindrical conductors," *High Temp.*, vol. 50, no. 5, pp. 584–595, Sep. 2012.

[19] Z. Shi, Y. Shi, K. Wang, and S. Jia, "Experimental investigation on the energy deposition and morphology of the electrical explosion of copper wire in vacuum," *Phys. Plasmas*, vol. 23, no. 3, Mar. 2016, Art. no. 032707.

[20] S. Zakharov, G. Ivanenkov, A. Kolomenskij, S. Pikuz, A. Samokhin, and I. Ulshmid, "Wire X-pinch in a high-current diode," *Sov. Tech. Phys. Lett.*, vol. 8, no. 17, p. 456, 1982.

[21] T. A. Shelkovenko, D. B. Sinars, S. A. Pikuz, K. M. Chandler, and D. A. Hammer, "Point-projection X-ray radiography using an x pinch as the radiation source," *Rev. Sci. Instrum.*, vol. 72, no. 1, pp. 667–670, Jan. 2001.

[22] G. A. Mesyats *et al.*, "X-pinch source of subnanosecond soft X-ray pulses based on small-sized low-inductance current generator," *J. Exp. Theor. Phys.*, vol. 111, no. 3, pp. 363–370, Sep. 2010.

[23] V. Oreshkin, E. Oreshkin, S. Chaikovsky, and A. Artyomov, "Coulomb explosion of 'hot spot,"' *Phys. Plasmas*, vol. 23, no. 9, 2016, Art. no. 092701.

[24] V. I. Oreshkin, A. P. Artyomov, S. A. Chaikovsky, E. V. Oreshkin, and A. G. Rousskikh, "Simulation of the radiation from the hot spot of an X-pinch," *Phys. Plasmas*, vol. 24, no. 1, Jan. 2017, Art. no. 012703.

[25] V. O. Bel'ko and O. A. Emel'yanov, "Nanosecond electric explosion of thin aluminum films," *Tech. Phys. Lett.*, vol. 35, no. 9, pp. 861–864, Sep. 2009.

[26] V. V. Kuznetsov, V. I. Oreshkin, A. S. Zhigalin, I. A. Kozulin, S. A. Chaikovsky, and A. G. Rousskikh, "Metastable states and their disintegration at pulse liquid heating and electrical explosion of conductors," *J. Eng. Thermophys.*, vol. 20, no. 3, pp. 240–248, Sep. 2011.

[27] V. I. Oreshkin, A. S. Zhigalin, A. G. Rousskikh, and V. V. Kuznetsov, "Disintegration of metastable liquid during electrical explosion of aluminum foil," *J. Eng. Thermophys.*, vol. 22, no. 4, pp. 288–297, Oct. 2013.

[28] R. B. Baksht, A. G. Rousskikh, A. S. Zhigalin, V. I. Oreshkin, and A. P. Artyomov, "Stratification in al and cu foils exploded in vacuum," *Phys. Plasmas*, vol. 22, no. 10, Oct. 2015, Art. no. 103521.

[29] T. M. Hutchinson *et al.*, "Experimental observation of the stratified electrothermal instability on aluminum with thickness greater than a skin depth," *Phys. Rev. E, Stat. Phys. Plasmas Fluids Relat. Interdiscip. Top.*, vol. 97, no. 5, May 2018, Art. no. 053208.

[30] W. Stygar *et al.*, "X-ray emission from z pinches at 10^7 A: Current scaling, gap closure, and shot-to-shot fluctuations," *Phys. Rev. E, Stat. Phys. Plasmas Fluids Relat. Interdiscip. Top.*, vol. 69, no. 4, 2004, Art. no. 046403.

[31] E. V. Grabovskii, K. N. Mitrofanov, G. M. Oleinik, and I. Y. Porofeev, "X-ray backlighting of the periphery of an imploding multiwire array in the Angara-5-1 facility," *Plasma Phys. Rep.*, vol. 30, no. 2, pp. 121–127, Feb. 2004.

[32] B. Jones *et al.*, "Planar wire-array Z-pinch implosion dynamics and X-Ray scaling at multiple-MA drive currents for a compact multisource hohlraum configuration," *Phys. Rev. Lett.*, vol. 104, no. 12, 2010, Art. no. 125001.

[33] V. L. Kantsyrev *et al.*, "Radiation sources with planar wire arrays and planar foils for inertial confinement fusion and high energy density physics research," *Phys. Plasmas*, vol. 21, no. 3, Mar. 2014, Art. no. 031204.

[34] S. I. Krivosheev, V. V. Titkov, and G. A. Shneerson, "Two-dimensional field diffusion and magnetohydrodynamic flow in an electric explosion of a miniature single-turn solenoid in a megagauss magnetic field," *Tech. Phys.*, vol. 42, no. 4, pp. 352–366, Apr. 1997.

[35] V. S. Sedoi, G. A. Mesyats, V. I. Oreshkin, V. V. Valevich, and L. I. Chemezova, "The current density and the specific energy input in fast electrical explosion," *IEEE Trans. Plasma Sci.*, vol. 27, no. 4, pp. 845–850, Aug. 1999.

[36] M. I. Lerner *et al.*, "Synthesis of al nanoparticles and Al/AlN composite nanoparticles by electrical explosion of aluminum wires in argon and nitrogen," *Powder Technol.*, vol. 295, pp. 307–314, Jul. 2016.

[37] Y. E. Krasik *et al.*, "Underwater electrical wire explosion and its applications," *IEEE Trans. Plasma Sci.*, vol. 36, no. 2, pp. 423–434, Apr. 2008.

[38] V. I. Oreshkin, S. Chaikovsky, N. A. Ratakhin, A. Grinenko, and Y. E. Krasik, "'Water bath' effect during the electrical underwater wire explosion," *Phys. Plasmas*, vol. 14, no. 10, 2007, Art. no. 102703.

[39] T. J. Awe *et al.*, "Experimental demonstration of the stabilizing effect of dielectric coatings on magnetically accelerated imploding metallic liners," *Phys. Rev. Lett.*, vol. 116, no. 6, Feb. 2016, Art. no. 065001.

[40] G. Mesyats, *Pulsed Power Engineering and Electronics*. Moscow, Russia: Nauka, 2004.

[41] Y. A. Kotov, "Electric explosion of wires as a method for preparation of nanopowders," *J. Nanopart. Res.*, vol. 5, no. 5/6, pp. 539–550, Dec. 2003.

[42] V. S. Sedoi and Y. F. Ivanov, "Particles and crystallites under electrical explosion of wires," *Nanotechnology*, vol. 19, no. 14, Apr. 2008, Art. no. 145710.

[43] N. I. Kuskova *et al.*, "Electroexplosive methods of synthesis of carbon nanomaterials," *Metallofizika I Noveishie Tekhnologii*, vol. 30, no. 6, pp. 833–847, Jun. 2008.

[44] A. Pervikov, E. Glazkova, and M. Lerner, "Energy characteristics of the electrical explosion of two intertwined wires made of dissimilar metals," *Phys. Plasmas*, vol. 25, no. 7, Jul. 2018, Art. no. 070701.

[45] S. A. Pikuz, V. M. Romanova, T. A. Shelkovenko, D. A. Hammer, and A. Y. Faenov, "Spectroscopic investigations of the short wavelength X-ray spectra from X-pinch plasmas," *Phys. Scripta*, vol. 51, no. 4, pp. 517–521, Apr. 1995.

[46] T. J. Awe *et al.*, "Modified helix-like instability structure on imploding z-pinch liners that are pre-imposed with a uniform axial magnetic field," *Phys. Plasmas*, vol. 21, no. 5, May 2014, Art. no. 056303.

[47] S. A. Chaikovsky, V. I. Oreshkin, I. M. Datsko, N. A. Labetskaya, and N. A. Ratakhin, "Skin explosion of double-layer conductors in fast-rising high magnetic fields," *Phys. Plasmas*, vol. 21, no. 4, Apr. 2014, Art. no. 042706.

[48] S. A. Chaikovsky, V. I. Oreshkin, I. M. Datsko, N. A. Labetskaya, D. V. Rybka, and N. A. Ratakhin, "Experimental study of the nonlinear diffusion of a magnetic field and skin explosion of cylindrical conductors," *Phys. Plasmas*, vol. 22, no. 11, Nov. 2015, Art. no. 112704.

[49] C. M. Fowler, W. B. Garn, and R. S. Caird, "Production of very high magnetic fields by implosion," *J. Appl. Phys.*, vol. 31, no. 3, pp. 588–594, Mar. 1960.

[50] A. D. Sakharov, "Magnetoimplosive generators," *Sov. Phys. Uspekhi*, vol. 9, no. 2, pp. 294–299, Feb. 1966.

[51] H. Knoepfel, *Pulsed High Magnetic Fields*. Amsterdam, The Netherlands: North Holland, 1970.

[52] D. H. Parkinson and B. E. Mulhall, *The Generation of High Magnetic Fields*. Berlin, Germany: Springer, 2013.

[53] Y. N. Bocharov, S. Krivosheev, and G. Shneerson, "Delay of a single-coil solenoid failure beginning in a Megagauss magnetic field," *Pis'ma v Zhurnal Tekhnicheskoj Fiziki*, vol. 8, no. 4, pp. 212–216, 1982.

[54] V. I. Oreshkin *et al.*, "Phase transformations of carbon under extreme energy action," *Tech. Phys.*, vol. 57, no. 2, pp. 198–202, Feb. 2012.

[55] M. R. Gomez *et al.*, "Experimental demonstration of fusion-relevant conditions in magnetized liner inertial fusion," *Phys. Rev. Lett.*, vol. 113, no. 15, Oct. 2014, Art. no. 155003.

[56] R. Kinslow, *High-Velocity Impact Phenomena*. New York, NY, USA: Academic, 1970.

[57] V. E. Fortov, "Intense shock waves and extreme states of matter," *Phys.-Uspekhi*, vol. 50, no. 4, pp. 333–353, Apr. 2007.

[58] T. J. Nash *et al.*, "Comparison of a copper foil to a copper wire-array z pinch at 18 MA," *Phys. Plasmas*, vol. 11, no. 10, pp. L65–L68, Oct. 2004.

[59] M. D. Knudson, R. W. Lemke, D. B. Hayes, C. A. Hall, C. Deeney, and J. R. Asay, "Near-absolute hugoniot measurements in aluminum to 500 GPa using a magnetically accelerated flyer plate technique," *J. Appl. Phys.*, vol. 94, no. 7, pp. 4420–4431, Oct. 2003.

[60] R. W. Lemke *et al.*, "Characterization of magnetically accelerated flyer plates," *Phys. Plasmas*, vol. 10, no. 4, pp. 1092–1099, Apr. 2003.

[61] S. A. Slutz, C. L. Olson, and P. Peterson, "Low mass recyclable transmission lines for Z-pinch driven inertial fusion," *Phys. Plasmas*, vol. 10, no. 2, pp. 429–437, Feb. 2003.

[62] E. Azizov *et al.*, "Project 'Baikal'–testing the scheme for electric pulse generation," *Plasma Devices Oper.*, vol. 12, no. 2, pp. 123–132, 2004.

[63] W. A. Stygar *et al.*, "Architecture of petawatt-class z-pinch accelerators," *Phys. Rev. Accel. Beams*, vol. 10, no. 3, 2007, Art. no. 030401.

[64] W. A. Stygar *et al.*, "Conceptual designs of two petawatt-class pulsed-power accelerators for high-energy-density-physics experiments," *Phys. Rev. Special Topics-Accel. Beams*, vol. 18, no. 11, Nov. 2015, Art. no. 110401.

[65] A. A. Kim *et al.*, "Development and tests of fast 1-MA linear transformer driver stages," *Phys. Rev. Special Topics-Accel. Beams*, vol. 12, no. 5, May 2009, Art. no. 050402.

[66] T. W. L. Sanford *et al.*, "Wire number doubling in high-wire-number regime increases Z-accelerator X-ray power," *IEEE Trans. Plasma Sci.*, vol. 26, no. 4, pp. 1086–1093, Aug. 1998.

[67] R. B. Spielman *et al.*, "Tungsten wire-array Z-pinch experiments at 200 TW and 2 MJ," *Phys. Plasmas*, vol. 5, no. 5, pp. 2105–2111, May 1998.

[68] V. V. Alexandrov *et al.*, "Prolonged plasma production at current-driven implosion of wire arrays on Angara-5-1 facility," *IEEE Trans. Plasma Sci.*, vol. 30, no. 2, pp. 559–566, Apr. 2002.

[69] A. V. Shishlov *et al.*, "Gas-puff-on-wire-array Z-pinch experiments on the GIT-12 generator at microsecond implosion times," *IEEE Trans. Plasma Sci.*, vol. 35, no. 3, pp. 592–600, Jun. 2007.

[70] V. V. Aleksandrov *et al.*, "Increase in the energy density of the pinch plasma in 3D implosion of quasi-spherical wire arrays," *Plasma Phys. Rep.*, vol. 40, no. 12, pp. 939–954, Dec. 2014.

[71] V. N. Mokhov *et al.*, "Fusion in the magnetically compressed targets," *Fusion Eng. Des.*, vol. 70, no. 1, pp. 35–43, Jan. 2004.

[72] I. R. Lindemuth, "The ignition design space of magnetized target fusion," *Phys. Plasmas*, vol. 22, no. 12, Dec. 2015, Art. no. 122712.

[73] S. Slutz *et al.*, "Pulsed-power-driven cylindrical liner implosions of laser preheated fuel magnetized with an axial fielda)," *Phys. Plasmas*, vol. 17, no. 5, p. 056303, 2010.

[74] V. I. Oreshkin, S. A. Barengol'ts, and S. A. Chaikovsky, "Numerical calculation of the current specific action integral at the electrical explosion of wires," *Tech. Phys.*, vol. 52, no. 5, pp. 642–650, May 2007.

[75] G. Mesyats, *Cathode Phenomena in a Vacuum Discharge: The Breakdown, the Spark, and the Arc*. Moscow, Russia: Nauka, 2000.

[76] V. P. Skripov, *Metastable Liquids*. Hoboken, NJ, USA: Wiley, 1974.

[77] P. G. Debenedetti, *Metastable Liquids: Concepts and Principles*. Princeton, NJ, USA: Princeton Univ. Press, 1996.

[78] S. V. Lebedev and A. I. Savvatimskii, "Electric metal explosion in experiments for developing superstrong magnetic-fields," *Zhurnal Tekhnicheskoi Fiziki*, vol. 54, no. 9, pp. 1794–1796, 1984.

[79] V. V. Ivanov, "A similarity study of the role of radial inhomogeneities in an exploding wire," *High Temp.*, vol. 21, no. 1, pp. 132–139, 1983.

[80] A. A. Valuev and G. E. Norman, "Nature of the Mesyats effect-pulsed superheating of microscopic spikes on a cathode," *J. Exp. Theor. Phys.*, vol. 89, no. 6, pp. 1180–1183, Dec. 1999.

[81] A. G. Rousskikh, V. I. Oreshkin, A. Zhigalin, I. I. Beilis, and R. B. Baksht, "Expansion of the plasma corona from a wire exploded in vacuum," *Phys. Plasmas*, vol. 17, no. 3, Mar. 2010, Art. no. 033505.

[82] I. I. Beilis *et al.*, "Discharge phenomena associated with a preheated wire explosion in vacuum: Theory and comparison with experiment," *Phys. Plasmas*, vol. 15, no. 1, Jan. 2008, Art. no. 013501.

[83] V. I. Oreshkin, A. S. Zhigalin, A. G. Rousskikh, S. A. Chaikovsky, and R. B. Baksht, "Metastable fluid decay during electric explosion of metallic foils," *Russian Phys. J.*, vol. 60, no. 8, pp. 1400–1407, Dec. 2017.

[84] W. G. Chace and M. A. Levine, "Classification of wire explosions," *J. Appl. Phys.*, vol. 31, no. 7, p. 1298, Jul. 1960.

[85] I. Grigoriev and E. Meylikhov, *Physical Values Handbook*. Moscow, Russia: EnergoAtomIzdat, 1991.

[86] V. I. Oreshkin, "Thermal instability during an electrical wire explosion," *Phys. Plasmas*, vol. 15, no. 9, Sep. 2008, Art. no. 092103.

[87] V. E. Fortov, K. V. Khishchenko, P. R. Levashov, and I. V. Lomonosov, "Wide-range multi-phase equations of state for metals," *Nucl. Instrum. Methods Phys. Res. A, Accel., Spectrometers, Detectors Associated Equip.*, vol. 415, no. 3, pp. 604–608, Oct. 1998.

[88] A. B. Bud'ko, F. S. Felber, A. I. Kleev, M. A. Liberman, and A. L. Velikovich, "Stability analysis of dynamic Z pinches and theta pinches," *Phys. Plasmas*, vol. 1, no. 3, pp. 598–607, Mar. 1989.

[89] K. B. Abramova, N. A. Zlatin, and B. P. Peregud, "Magnetohydrodynamic instability of liquid and solid conductors. Destruction of conductors by an electric current," *Zh. Eksp. Teor. Fiz*, vol. 69, no. 6, pp. 2007–2022, 1975.

[90] L. D. Landau, J. Bell, M. Kearsley, L. Pitaevskii, E. Lifshitz, and J. Sykes, *Electrodynamics of Continuous Media*. Amsterdam, The Netherlands: Elsevier, 1984.

[91] N. Mott, *Metal-Insulator Transitions*. Boca Raton, FL, USA: CRC Press, 1990.

[92] R. Redmer, B. Holst, and F. Hensel, *Metal-to-Nonmetal Transitions*. Berlin, Germany: Springer, 2010.

[93] A. Grinenko, V. T. Gurovich, A. Saypin, S. Efimov, Y. E. Krasik, and V. I. Oreshkin, "Strongly coupled copper plasma generated by underwater electrical wire explosion," *Phys. Rev. E, Stat. Phys. Plasmas Fluids Relat. Interdiscip. Top.*, vol. 72, no. 6, Dec. 2005, Art. no. 066401.

[94] G. S. Sarkisov, S. E. Rosenthal, K. R. Cochrane, K. W. Struve, C. Deeney, and D. H. McDaniel, "Nanosecond electrical explosion of thin aluminum wires in a vacuum: Experimental and computational investigations," *Phys. Rev. E, Stat. Phys. Plasmas Fluids Relat. Interdiscip. Top.*, vol. 71, no. 4, Apr. 2005, Art. no. 046404.

[95] V. Petrosyan and É. Dagman, "Certain peculiarities of electrical explosion of metal and semiconductor specimens in vacuum. II," *Sov. Phys. Tech. Phys.*, vol. 14, p. 1567, May 1970.

[96] Y. Kotov, O. Samatov, V. Sedoi, L. Chemezova, and A. Chertov, "Heating of conductors by high-density current," in *Megagauss Fields and Pulsed Power Systems*. New York, NY, USA: Nova, 1990, pp. 497–502.

[97] C. Stallings, K. Nielsen, and R. Schneider, "Multiple-wire array load for high-power pulsed generators," *Appl. Phys. Lett.*, vol. 29, no. 7, pp. 404–406, 1976.

[98] V. I. Oreshkin *et al.*, "Study of metal conductivity near the critical point using a microwire electrical explosion in water," *Tech. Phys.*, vol. 49, no. 7, pp. 843–848, Jul. 2004.

[99] N. I. Kuskova, S. I. Tkachenko, and S. V. Koval, "Investigation of liquid metallic wire heating dynamics," *J. Phys., Condens. Matter*, vol. 9, no. 29, pp. 6175–6184, Jul. 1997.

[100] F. D. Bennett, H. S. Burden, and D. D. Shear, "Correlated electrical and optical measurements of exploding wires," *Phys. Fluids*, vol. 5, no. 1, p. 102, 1962.

[101] E. Oktay, "Effect of wire cross section on the first pulse of an exploding wire," *Rev. Scientific Instrum.*, vol. 36, no. 9, pp. 1327–1328, Sep. 1965.

[102] S. A. Khainatskii, "Conditions for realization of an optimum regime of the electric explosion of conductors in liquid media," *Tech. Phys. Lett.*, vol. 35, no. 4, pp. 299–301, Apr. 2009.

[103] O. Antonov, S. Efimov, D. Yanuka, M. Kozlov, V. T. Gurovich, and Y. E. Krasik, "Generation of converging strong shock wave formed by microsecond timescale underwater electrical explosion of spherical wire array," *Appl. Phys. Lett.*, vol. 102, no. 12, Mar. 2013, Art. no. 124104.

[104] D. Shafer *et al.*, "Generation of fast cumulative water jets by underwater electrical explosion of conical wire arrays," *J. Appl. Phys.*, vol. 117, no. 1, Jan. 2015, Art. no. 015901.

[105] S. P. Lyon, "Sesame: The Los Alamos National Laboratory equation of state database," Los Alamos Nat. Lab., Los Alamos, NM USA, Tech. Rep. LA-UR-92-3407, 1992.

[106] K. V. Khishchenko, S. I. Tkachenko, P. R. Levashov, I. V. Lomonosov, and V. S. Vorob'ev, "Metastable states of liquid tungsten under subsecond wire explosion," *Int. J. Thermophys.*, vol. 23, no. 5, pp. 1359–1367, Sep. 2002.

[107] R. Trunin, L. Gudarenko, M. Zhernokletov, and G. Simakov, *Experimental Data on Shock Wave Compression and Adiabatic Expansion of Condensed Matter*. Sarov, Russia: RFNC-VNIIEF Publ, 2006.

[108] A. Sapozhnikov, G. Kovalenko, P. Greshuk, and E. Mironova, "Wide-range tabular equation of water state," *Voprosy Atomnoi Nauki i Tekhniki*, no. 2, p. 15, 1991.

[109] Y. B. Zel'dovich, and Y. P. Raizer, *Physics of Shock Waves and High-Temperature Hydrodynamic Phenomena*. Chelmsford, MA USA: Courier Corporation, 2012.

[110] D. V. Minakov, M. A. Paramonov, and P. R. Levashov, "Consistent interpretation of experimental data for expanded liquid tungsten near the liquid-gas coexistence curve," *Phys. Rev. B, Condens. Matter*, vol. 97, no. 2, Jan. 2018, Art. no. 024205.

[111] M. P. Desjarlais, "Practical improvements to the lee-more conductivity near the metal-insulator transition," *Contrib. Plasma Phys.*, vol. 41, nos. 2–3, pp. 267–270, Mar. 2001.

[112] Y. T. Lee and R. M. More, "An electron conductivity model for dense plasmas," *Phys. Fluids*, vol. 27, no. 5, p. 1273, 1984.

[113] I. D. Bakulin, V. Kuropatenko, and A. Luchinskii, "Magnetohydrodynamic computation of exploding conductors," *Zhurnal Tekhnicheskoi Fiziki*, vol. 46, pp. 1963–1969, Sep. 1976.

[114] N. Volkov, "Plasma model of conductivity of metals," *Zhurnal Tekhnicheskoi Fiziki*, vol. 49, no. 9, pp. 2000–2002, 1979.

[115] J. Stephens and A. Neuber, "Exploding-wire experiments and theory for metal conductivity evaluation in the sub-eV regime," *Phys. Rev. E, Stat. Phys. Plasmas Fluids Relat. Interdiscip. Top.*, vol. 86, no. 6, Dec. 2012, Art. no. 066409.

[116] J. Stephens, J. Dickens, and A. Neuber, "Semiempirical wide-range conductivity model with exploding wire verification," *Phys. Rev. E, Stat. Phys. Plasmas Fluids Relat. Interdiscip. Top.*, vol. 89, no. 5, May 2014, Art. no. 053102.

[117] K. Wang, Z. Shi, Y. Shi, J. Bai, J. Wu, and S. Jia, "The equation of state and ionization equilibrium of dense aluminum plasma with conductivity verification," *Phys. Plasmas*, vol. 22, no. 6, Jun. 2015, Art. no. 062709.
[118] L. Spitzer and R. Härm, "Transport phenomena in a completely ionized gas," *Phys. Rev.*, vol. 89, no. 5, pp. 977–981, Mar. 1953.
[119] S. Braginskii, "Transport phenomena in a completely ionized two-temperature plasma," *Sov. Phys. JETP*, vol. 6, no. 33, pp. 358–369, 1958.
[120] V. Gantmakher, *Electrons in Disordered Media*. Moscow, Russia: Fizmatlit, 2003.
[121] G. Mierdel, *Elektrophysik*. Berlin, Germany: VEB Verlag Technik, 1970.
[122] A. Ioffe, and A. Regel, *Non-Crystalline, Amorphous and Liquid Electronic Semiconductors*. London, U.K.: Heywood and Company ltd, 1960.
[123] A. G. Rousskikh, R. B. Baksht, A. Y. Labetskii, V. I. Oreshkin, A. V. Shishlov, and S. A. Chaikovskii, "Electric explosion of fine tungsten wires in vacuum," *Plasma Phys. Rep.*, vol. 30, no. 11, pp. 944–952, Nov. 2004.
[124] A. Roth, *Vacuum Technology*. New York, NY, USA: North Holland, 2012.
[125] A. G. Rousskikh *et al.*, "The effects of preheating of a fine tungsten wire and the polarity of a high-voltage electrode on the energy characteristics of an electrically exploded wire in vacuum," *IEEE Trans. Plasma Sci.*, vol. 34, no. 5, pp. 2232–2238, Oct. 2006.
[126] S. A. Pikuz, T. A. Shelkovenko, D. B. Sinars, J. B. Greenly, Y. S. Dimant, and D. A. Hammer, "Multiphase foamlike structure of exploding wire cores," *Phys. Rev. Lett.*, vol. 83, no. 21, pp. 4313–4316, Nov. 1999.
[127] A. D. Rakhel, "Metal evaporation via electrical high-density current," *Zhurnal Tekhnicheskoi Fiziki*, vol. 65, no. 12, pp. 27–38, Dec. 1995.
[128] V. S. Vorobev, "Dynamics of conductor heating and evaporation by high-density pulse current," *Zhurnal Tekhnicheskoi Fiziki*, vol. 66, no. 1, pp. 35–48, Jan. 1996.
[129] S. Anisimov, Y. A. Imas, G. Romanov, and Y. V. Khodyko, *Action of High-Power Radiation on Metals*. Moscow, Russia: Nauka, 1970.
[130] V. V. Aleksandrov *et al.*, "Dynamics of heterogeneous liners with prolonged plasma creation," *Plasma Phys. Rep.*, vol. 27, no. 2, pp. 89–109, Feb. 2001.
[131] S. V. Lebedev *et al.*, "Effect of discrete wires on the implosion dynamics of wire array Z pinches," *Phys. Plasmas*, vol. 8, no. 8, pp. 3734–3747, Aug. 2001.
[132] S. I. Tkachenko, K. V. Khishchenko, V. S. Vorob'ev, P. R. Levashov, I. V. Lomonosov, and V. E. Fortov, "Metastable states of liquid metal under conditions of electric explosion," *High Temp.*, vol. 39, no. 5, pp. 674–687, Sep-Oct. 2001.
[133] G. S. Sarkisov, J. Caplinger, F. Parada, and V. I. Sotnikov, "Breakdown dynamics of electrically exploding thin metal wires in vacuum," *J. Appl. Phys.*, vol. 120, no. 15, Oct. 2016, Art. no. 153301.
[134] Y. D. Korolev and G. A. Mesyats, *Physics of Pulsed Breakdown in Gases*. Moscow, Russia: Nauka, 1991.
[135] A. V. Gurevich *et al.*, "Observation of the avalanche of runaway electrons in air in a strong electric field," *Phys. Rev. Lett.*, vol. 109, no. 8, Aug. 2012, Art. no. 085002.
[136] E. V. Oreshkin, S. A. Barengolts, S. A. Chaikovsky, and V. I. Oreshkin, "Simulation of a runaway electron avalanche developing in an atmospheric pressure air discharge," *Phys. Plasmas*, vol. 22, no. 12, Dec. 2015, Art. no. 123505.
[137] K. J. Peterson *et al.*, "Simulations of electrothermal instability growth in solid aluminum rods," *Phys. Plasmas*, vol. 20, no. 5, 2013, Art. no. 056305.
[138] J. P. Chittenden *et al.*, "Plasma formation in metallic wire Z pinches," *Phys. Rev. E, Stat. Phys. Plasmas Fluids Relat. Interdiscip. Top.*, vol. 61, no. 4, pp. 4370–4380, Apr. 2000.
[139] G. V. Ivanenkov and W. Stepniewski, "Radiative dynamics of imploded wires with a two-phase dense core," *Plasma Phys. Rep.*, vol. 28, no. 6, pp. 457–471, Jun. 2002.
[140] K. Wang, Z. Shi, and Y. Shi, "The formation and evolution of the core-corona structure in the electrical explosion of aluminum wire in vacuum: Experimental and numerical investigations," *J. Phys. D, Appl. Phys.*, vol. 50, no. 31, Aug. 2017, Art. no. 315201.
[141] G. A. Mesyats, S. P. Bugaev, and D. I. Proskurovskiĭ, "Explosive emission of electrons from metallic needles," *Sov. Phys. Uspekhi*, vol. 14, no. 4, pp. 536–537, Apr. 1972.
[142] G. A. Mesyats, "Ecton mechanism of the vacuum arc cathode spot," *IEEE Trans. Plasma Sci.*, vol. 23, no. 6, pp. 879–883, Dec. 1995.
[143] D. L. Shmelev and E. A. Litvinov, "Computer simulation of ecton in a vacuum arc," *IEEE Trans. Dielectr. Electr. Insul.*, vol. 6, no. 4, pp. 441–444, Aug. 1999.
[144] S. P. Bugaev, E. A. Litvinov, G. A. Mesyats, and D. I. Proskurovskiĭ, "Explosive emission of electrons," *Sov. Phys. Uspekhi*, vol. 18, no. 1, pp. 51–61, Jan. 1975.
[145] A. A. Samokhin, "Numerical investigation of the physical model of a high-power electromagnetic wave in a magnetically insulated transmission line," *Plasma Phys. Rep.*, vol. 36, no. 2, pp. 149–163, Feb. 2010.
[146] V. V. Loskutov, A. V. Luchinskii, and G. A. Mesiats, "MGD processes at the initial stage of the explosive emission," *Doklady Akademii Nauk SSSR*, vol. 271, no. 5, pp. 1120–1122, 1983.
[147] S. A. Barengolts *et al.*, "Mechanism of vacuum breakdown in radio-frequency accelerating structures," *Phys. Rev. A, Gen. Phys.ccelerators Beams*, vol. 21, no. 6, Jun. 2018, Art. no. 061004.
[148] S. A. Barengolts, E. V. Oreshkin, V. I. Oreshkin, and K. V. Khishchenko, "Simulation of the explosion of a surface microprotrusion during a radio frequency breakdown," *IEEE Trans. Plasma Sci.*, vol. 47, no. 8, pp. 3406–3411, Aug. 2019.
[149] G. Fursey, V. Zhukov, and I. Baskin, "Limiting densities of FEE current and pre-explosive effects," in *Emission Electronics*. Novosibirsk, Russia: Nauka 1984, pp. 21–41.
[150] D. B. Sinars *et al.*, "The effect of insulating coatings on exploding wire plasma formation," *Phys. Plasmas*, vol. 7, no. 2, pp. 429–432, Feb. 2000.
[151] D. B. Sinars *et al.*, "Experiments measuring the initial energy deposition, expansion rates and morphology of exploding wires with about 1 kA/wire," *Phys. Plasmas*, vol. 8, no. 1, pp. 216–230, Jan. 2001.
[152] G. S. Sarkisov, K. W. Struve, and D. H. McDaniel, "Effect of current rate on energy deposition into exploding metal wires in vacuum," *Phys. Plasmas*, vol. 11, no. 10, pp. 4573–4581, Oct. 2004.
[153] A. G. Rousskikh *et al.*, "Study of the strata formation during the explosion of a wire in vacuum," *Phys. Plasmas*, vol. 15, no. 10, Oct. 2008, Art. no. 102706.
[154] D. Yanuka *et al.*, "X-ray radiography of the overheating instability in underwater electrical explosions of wires," *Phys. Plasmas*, vol. 26, no. 5, May 2019, Art. no. 050703.
[155] A. Valuev, I. I. Dikhter, and V. Zeigarnik, "Striations arising in the explosion of cesium wires at supercritical pressures," *Zhurnal Tekhnicheskoi Fiziki*, vol. 48, pp. 2088–2096, 1978.
[156] V. I. Oreshkin *et al.*, "Wire explosion in vacuum: Simulation of a striation appearance," *Phys. Plasmas*, vol. 11, no. 10, pp. 4771–4776, Oct. 2004.
[157] V. I. Oreshkin, "Overheat instabilities in the electric explosion of wires," *Tech. Phys. Lett.*, vol. 35, no. 1, pp. 36–39, Jan. 2009.
[158] V. I. Oreshkin, "The development of overheat instabilities in a metastable metal," *Tech. Phys. Lett.*, vol. 44, no. 10, pp. 930–933, Oct. 2018.
[159] R. Franz and G. Wiedemann, "Ueber die Wärme-Leitungsfähigkeit der Metalle," *Annalen der Phys.*, vol. 165, no. 8, pp. 497–531, 1853.
[160] A. M. Steiner *et al.*, "The electro-thermal stability of tantalum relative to aluminum and titanium in cylindrical liner ablation experiments at 550 kA," *Phys. Plasmas*, vol. 25, no. 3, Mar. 2018, Art. no. 032701.
[161] V. I. Oreshkin, K. V. Khishenko, E. V. Oreshkin, and A. G. Rousskikh, "The effect of the metal phase state on the growth of thermal instabilities in an electrically exploding conductor," *Plasma Res. Exp.*, vol. 1, no. 3, 2019, Art. no. 035006.
[162] H. Bluhm, *Pulsed Power Systems*. Berlin, Germany: Springer-Verlag, 2006.
[163] P. U. Duselis, J. A. Vaughan, and B. R. Kusse, "Factors affecting energy deposition and expansion in single wire low current experiments," *Phys. Plasmas*, vol. 11, no. 8, pp. 4025–4031, Aug. 2004.
[164] K. M. Chandler, D. A. Hammer, D. B. Sinars, S. A. Pikuz, and T. A. Shelkovenko, "The relationship between exploding wire expansion rates and wire material properties near the boiling temperature," *IEEE Trans. Plasma Sci.*, vol. 30, no. 2, pp. 577–587, Apr. 2002.
[165] S. I. Tkachenko, V. M. Romanova, A. R. Mingaleev, A. E. Ter-Oganesyan, T. A. Shelkovenko, and S. A. Pikuz, "Study of plasma parameter's distribution upon electrical wire explosion," *Eur. Phys. J. D*, vol. 54, no. 2, pp. 335–341, Aug. 2009.
[166] S. I. Tkachenko *et al.*, "Analysis of the discharge channel structure upon nanosecond electrical explosion of wires," *Phys. Plasmas*, vol. 14, no. 12, Dec. 2007, Art. no. 123502.
[167] S. I. Tkachenko, A. R. Mingaleev, V. M. Romanova, A. E. Ter-Oganes'yan, T. A. Shelkovenko, and S. A. Pikuz, "Distribution of matter in the current-carrying plasma and dense core of the discharge channel formed upon electrical wire explosion," *Plasma Phys. Rep.*, vol. 35, no. 9, pp. 734–753, Sep. 2009.

[168] S. A. Pikuz, T. A. Shelkovenko, A. R. Mingaleev, D. A. Hammer, and H. P. Neves, "Density measurements in exploding wire-initiated plasmas using tungsten wires," *Phys. Plasmas*, vol. 6, no. 11, pp. 4272–4283, Nov. 1999.
[169] D. B. Sinars, T. A. Shelkovenko, S. A. Pikuz, J. B. Greenly, and D. A. Hammer, "Exploding aluminum wire expansion rate with 1–4.5 kA per wire," *Phys. Plasmas*, vol. 7, no. 5, pp. 1555–1563, May 2000.
[170] D. A. Chalenski, B. R. Kusse, and J. B. Greenly, "Soldered contact and current risetime effects on negative polarity wire array z pinches," *Phys. Plasmas*, vol. 16, no. 8, Aug. 2009, Art. no. 082707.
[171] M. R. Gomez, J. C. Zier, R. M. Gilgenbach, D. M. French, W. Tang, and Y. Y. Lau, "Effect of soft metal gasket contacts on contact resistance, energy deposition, and plasma expansion profile in a wire array z pinch," *Rev. Sci. Instrum.*, vol. 79, no. 9, 2008, Art. no. 093512.
[172] J. Zhao *et al.*, "Expansion characteristics of plasma generated by electrically exploding single aluminum wire in high vacuum," *IEEE Trans. Plasma Sci.*, vol. 41, no. 8, pp. 2214–2220, Aug. 2013.
[173] J. Wu, Y. Lu, X. Li, D. Zhang, and A. Qiu, "Investigations on stratification structure parameters formed from electrical exploding wires in vacuum," *Phys. Plasmas*, vol. 24, no. 11, Nov. 2017, Art. no. 112701.
[174] J. Wu *et al.*, "Atomization and merging of two al and w wires driven by a 1 kA, 10 ns current pulse," *Phys. Plasmas*, vol. 23, no. 11, Nov. 2016, Art. no. 112703.
[175] J. Wu *et al.*, "Transforming dielectric coated tungsten and platinum wires to gaseous state using negative nanosecond-pulsed-current in vacuum," *Phys. Plasmas*, vol. 21, no. 11, Nov. 2014, Art. no. 112708.
[176] G. S. Sarkisov, P. V. Sasorov, K. W. Struve, and D. H. McDaniel, "State of the metal core in nanosecond exploding wires and related phenomena," *J. Appl. Phys.*, vol. 96, no. 3, pp. 1674–1686, Aug. 2004.
[177] G. S. Sarkisov, B. S. Bauer, and J. S. De Groot, "Homogeneous electrical explosion of tungsten wire in vacuum," *J. Exp. Theor. Phys. Lett.*, vol. 73, no. 2, pp. 69–74, Jan. 2001.
[178] G. S. Sarkisov and D. McCrorey, "Imaging of exploding wire phenomena," *IEEE Trans. Plasma Sci.*, vol. 30, no. 1, pp. 98–99, Feb. 2002.
[179] G. S. Sarkisov, K. W. Struve, and D. H. McDaniel, "Effect of deposited energy on the structure of an exploding tungsten wire core in a vacuum," *Phys. Plasmas*, vol. 12, no. 5, May 2005, Art. no. 052702.
[180] T. C. Wagoner *et al.*, "Differential-output B-dot and D-dot monitors for current and voltage measurements on a 20-MA, 3-MV pulsed-power accelerator," *Phys. Rev. Accel. Beams*, vol. 11, no. 10, Oct. 2008, Art. no. 100401.
[181] A. Klimov, *Experimental Methods in High-Current Electronics*. Tomsk, Russia: TPU, 2013.
[182] T. Huiskamp, F. J. C. M. Beckers, E. J. M. van Heesch, and A. J. M. Pemen, "B-dot and D-Dot sensors for (Sub)Nanosecond high-voltage and high-current pulse measurements," *IEEE Sensors J.*, vol. 16, no. 10, pp. 3792–3801, May 2016.
[183] R. Fletcher, "Production and measurement of ultra-high speed impulses," *Rev. Sci. Instrum.*, vol. 20, no. 12, pp. 861–869, 1949.
[184] Y. Li *et al.*, "Influence of insulating coating on aluminum wire explosions," *Phys. Plasmas*, vol. 21, no. 10, Oct. 2014, Art. no. 102513.
[185] S. Voeten, Matching high voltage pulsed power technologies," Ph.D. dissertation, Eindhoven Univ. Technol., Eindhoven, The Netherlands, 2013.
[186] W. Stygar and G. Gerdin, "High frequency Rogowski coil response characteristics," *IEEE Trans. Plasma Sci.*, vol. 10, no. 1, pp. 40–44, Mar. 1982.
[187] S. I. Tkachenko *et al.*, "Study of the core-corona structure formed during the explosion of an aluminum wire in vacuum," *Plasma Phys. Rep.*, vol. 38, no. 1, pp. 1–11, Jan. 2012.
[188] Y. Shi, Z. Shi, K. Wang, Z. Wu, and S. Jia, "Factors affecting the exploding characteristics of tungsten wires with negative-polarity current," *Phys. Plasmas*, vol. 24, no. 1, Jan. 2017, Art. no. 012706.
[189] Z. Shi, K. Wang, Y. Shi, J. Wu, and R. Han, "Experimental investigation on the energy deposition and expansion rate under the electrical explosion of aluminum wire in vacuum," *J. Appl. Phys.*, vol. 118, no. 24, Dec. 2015, Art. no. 243302.
[190] *NIST Chemistry WebBook, SRD 69*. [Online]. Available: https://webbook.nist.gov/
[191] I. S. Grigoriev and E. Z. Meilikhov, *Handbook of Physical Quantities*. Boca Raton, FL, USA: CRC Press, 1997.
[192] Y. Fukai, *The Metal-Hydrogen System: Basic Bulk Properties*. Berlin, Germany: Springer, 2006.
[193] A. G. Rousskikh, D. Pil'tikhina, R. B. Baksht, I. I. Beilis, and S. A. Chaikovsky, "Effect of electrode polarity on wire explosion in vacuum," *J. Appl. Phys.*, vol. 104, no. 1, Jul. 2008, Art. no. 013306.
[194] S. A. Pikuz *et al.*, "Studying of explosive electron emission from 'Whisker' cathode using X-Ray point-projection radiography," *IEEE Trans. Plasma Sci.*, vol. 46, no. 11, pp. 3815–3819, Nov. 2018.
[195] A. Hamilton, V. I. Sotnikov, and G. S. Sarkisov, "Vaporization energy and expansion velocity of electrically exploding aluminum and copper fine wires in vacuum," *J. Appl. Phys.*, vol. 124, no. 12, Sep. 2018, Art. no. 123302.
[196] V. M. Romanova *et al.*, "On the phase state of thin silver wire cores during a fast electric explosion," *Phys. Plasmas*, vol. 25, no. 11, Nov. 2018, Art. no. 112704.
[197] S. Karakhanov, "Pulsed heating of conductors in ultrahigh vacuum-'Anomalous' electron emission," *Zhurnal Tekhnicheskoi Fiziki*, vol. 48, pp. 1474–1481, Jul. 1978.
[198] V. S. Vorob'ev, S. P. Malyshenko, S. I. Tkachenko, and V. E. Fortov, "What initiates the explosion of a current-carrying conductor?" *J. Exp. Theor. Phys. Lett.*, vol. 75, no. 8, pp. 373–377, Apr. 2002.
[199] S. I. Tkachenko, V. S. Vorob'ev, and S. P. Malyshenko, "The nucleation mechanism of wire explosion," *J. Phys. D, Appl. Phys.*, vol. 37, no. 3, pp. 495–500, Feb. 2004.
[200] G. S. Sarkisov, I. L. Beigman, V. P. Shevelko, and K. W. Struve, "Interferometric measurements of dynamic polarizabilities for metal atoms using electrically exploding wires in vacuum," *Phys. Rev. A, Gen. Phys.*, vol. 73, no. 4, Apr. 2006, Art. no. 042501.
[201] N. Bobrova, T. Razinkova, and P. Sasorov, "Heterogeneous equilibrium states of radiating Z-pinches," *Fizika Plazmy*, vol. 14, no. 9, pp. 1053–1060, 1988.
[202] I. Holmström, S. K. Händel, and B. Stenerhag, "Undegassed and degassed exploding tungsten wires in vacuum," *J. Appl. Phys.*, vol. 39, no. 7, pp. 2998–3002, Jun. 1968.
[203] P. Felsenthal and J. M. Proud, "Nanosecond-pulse breakdown in gases," *Phys. Rev.*, vol. 139, no. 6A, pp. A1796–A1804, Sep. 1965.
[204] R. S. Hixson and M. A. Winkler, "Thermophysical properties of solid and liquid tungsten," *Int. J. Thermophys.*, vol. 11, no. 4, pp. 709–718, Jul. 1990.
[205] P. Tolias *et al.*, "Analytical expressions for thermophysical properties of solid and liquid tungsten relevant for fusion applications," *Nucl. Mater. Energy*, vol. 13, pp. 42–57, Dec. 2017.
[206] A. W. Searcy and D. Beruto, "Kinetics of endothermic decomposition reactions. I. steady-state chemical steps," *J. Phys. Chem.*, vol. 80, no. 4, pp. 425–429, Feb. 1976.
[207] S. V. Barakhvostov *et al.*, "Mechanisms of the destruction of micron conductors by an electromagnetic pulse with a subnanosecond front," *JETP Lett.*, vol. 94, no. 7, pp. 549–555, Dec. 2011.
[208] G. S. Sarkisov, "Effect of hydration on the electrical explosion of a fine palladium wire in a vacuum," *Phys. Plasmas*, vol. 24, no. 11, Nov. 2017, Art. no. 110701.

Vladimir I. Oreshkin received the M.S. degree in physics from the Physics and Technology Department, Tomsk Polytechnic Institute, Tomsk, Russia, in 1983, and the Ph.D. and D.Sci. degrees from Tomsk State University, Tomsk, in 1993 and 2005, respectively.

Since 1987, he has been with the Institute of High Current Electronics SB RAS, Tomsk. The main areas of his scientific activity are numerical modeling of processes occurring in imploding light liners and emission of radiation by high-temperature dense plasmas and studying the transport properties of nonideal dense plasmas.

Rina B. Baksht (Member, IEEE) received the Ph.D. degree in electrical engineering from the Tomsk Polytechnic Institute, Tomsk, Russia, in 1967.

From 1982 to 2000, she worked as a Professor of plasma physics (diagnostics and experimental equipment) with Tomsk State University, Tomsk. From 2002 to 2010, she was a Researcher with the Propulsion Physics Laboratory, Soreq Nuclear Research Center (NRC), Yavne, Israel. From 2006 to 2011, she was a Consulting Researcher with Tel Aviv University, Tel Aviv, Israel. She is currently a part-time Researcher with the Institute of High Current Electronics (IHCE) SB RAS, Tomsk. Since 1968, she has been with the IHCE SB RAS, where she was involved in vacuum discharges, Z-pinch plasma radiation sources, and wire explosions.